ANALYSIS OF A RAPID SOIL EROSION ASSESSMENT TOOL

by

PATRICK BUSSEN

A THESIS

submitted in partial fulfillment of the requirements for the degree

MASTER OF SCIENCE

Department of Biological and Agricultural Engineering
College of Engineering

KANSAS STATE UNIVERSITY
Manhattan, Kansas

2009

Approved by:

Major Professor
Stacy Lewis Hutchinson

Abstract

Soil erosion is a serious problem resulting in degradation of soil systems and nonpoint source (NPS) pollution of water resources. Concentrated overland flow is the primary transport mechanism for many NPS pollutants including soil, and locating areas where sheet flow transitions into concentrated flow is useful for assessing the potential for soil erosion. The ability to predict areas where overland flow transitions to concentrated flow and soil erosion potential is high assists land managers in implementing best management practices (BMPs) to reduce soil erosion and NPS.

An erosion model, called the nLS model, was developed to identify transitional overland flow regions. The model is based on the kinematic wave overland flow theory and uses Manning's n values, flow length, and slope as inputs to determine where overland flow transitions to sheet flow and soil erosion potential increases. Currently, the model has only been tested and validated for watersheds within Kansas. In order to assess model uncertainties and evaluate the model's applicability to other regions, a sensitivity analysis on key input parameters was conducted.

To assess model operations, several sensitivity analyses were performed on model inputs, including digital elevation models (DEMs) and landuse/landcover data (LULC). The impact of slope was assessed using two methods. First, by modifying the DEMs in a stepwise fashion from flatter to steeper terrains, and second, by modifying the elevation of each DEM cell based on the associated elevation error. To assess difficulties that might arise from the parameterization of surface roughness, LULC classes were assigned Manning's n values within the suggested range

using a Monte Carlo simulation. In addition, the critical threshold value used for locating erosion potential sites was modified, and alternative model calculations were used to assess the potential for improving model accuracy. Finally, the model was run using data from multiple sites, including two study areas in Hawaii and two in Kansas. The outputs for each site were analyzed in an attempt to identify any trends caused by site characteristics.

Results from this study showed that the nLS model was sensitive to all of the inputs. Modifying the Manning's roughness coefficient significantly altered the final nLS values and shifted the critical threshold points, especially in areas of the upper watershed. Changes in the slope value modified the nLS model outputs in a predictable manner, but there was some variability, especially in areas with lower slope values. In addition, discrepancies in the DEM, which may be present due to measurement or processing error, were shown to significantly alter the flow paths of a watershed. These findings suggest that accurate roughness coefficients and LULC data are especially important for regions with a steeper topography, and accurate elevation data is important for regions with lower slope values. The results also suggest that the threshold value for the model plays a vital role in locating potential soil erosion sites, and adjustments to this value could possibly be used as a method for calibrating the nLS model. Finally, the alternative model calculations used in this study did not significantly improve the accuracy of the nLS model, so the existing model is sufficient for obtaining accurate nLS estimates. The information gained from this study can improve the assessment of soil erosion processes due to concentrated overland flow. By successfully implementing a land management program that makes use of the nLS models, it should be possible to improve BMP placement and design, helping to improve water and soil quality.

Table of Contents

List of Figures

List of Tables

Acknowledgements

The guidance provided by my faculty advisor, Dr. Stacy Hutchinson, was extremely helpful and vital to the completion of this work. My committee members also provided important assistance during this project. The knowledge provided by Dr. Shawn Hutchinson on the subject of geographic information systems was crucial, and the assistance of Dr. Phil Barnes was especially helpful in completing this work. Previous work performed by Ik-Jae Kim at Kansas State University was also important for this project. Finally, the cooperation of the ITAM offices at Fort Riley, Schofield Barracks, and Pohakuloa Training Area throughout the duration of this research was greatly appreciated.

This study was funded by the Environmental Security Technology Certification Program (ESTCP), 'Validating the Kinematic Wave Approach for Rapid Soil Erosion Assessment and Improved BMP Site Selection to Enhance Training Land Sustainability' (Project Number 08 EB-SI2-017).

CHAPTER 1 - Introduction

To determine areas of high erosion potential on military training lands, the nLS model (Kim, 2006) was developed as part of a Strategic Environmental Research Development Program (SERDP), 'Assessing the Impact of Maneuver Training on NPS Pollution and Water Quality' (Project number SI-1339). This model utilizes readily available elevation and landuse/landcover (LULC) data in a Geographic Information System (GIS) to apply the kinematic wave theory for predicting where overland flow transitions to concentrated flow and soil erosion potential increases. The nLS model requires less data and is less labor-intensive than other pollution models (i.e. WEPP, RUSLE, KINEROS, EUROSEM, and SWAT), making it ideal for military land managers who must evaluate the environmental impacts of training exercises in a rapid manner.

The elevation and LULC input parameters of the nLS model are used to estimate Manning's roughness coefficient (n), flow length (L), and slope (S) for a study area. From these values, the model determines areas of transitional flow regimes based on the nLS equation, $nL/S^{0.5}$, as described by McCuen and Spiess (1995). Soil erosion is closely associated with areas where water runoff transitions from overland flow to concentrated flow. By predicting areas where water runoff makes this transition, sites with higher potential for soil erosion can be located.

While the nLS model has been tested with field data and proven successful for two watersheds in Kansas (Kim, 2006), it has yet to be tested in ecoregions outside of this area. Varying conditions that exist at a site, including topography, LULC, soil types, and precipitation levels, may have an effect on the accuracy of the model. By using a sensitivity analysis to

examine the impacts of individual model inputs, as well as field parameter estimation and calculations used on the model, the importance of each component was determined.

To quantify variations that may occur in the nLS model outputs, the input parameters were modified using several methods. To analyze the effects of slope, the elevation data was modified in a stepwise fashion, from flatter to steeper terrains. To examine the potential for DEM error to effect model calculations, the elevation values were modified based on an appropriate error range. The LULC was also examined by randomly distributing the individual LULC classes across the study area multiple times and comparing the results. To analyze the effects of estimating the Manning's roughness coefficient, the LULC classes were assigned random Manning's n values within a preset range during a Monte Carlo simulation. To study the effects of the threshold value used for locating erosion potential sites, multiple values were used in the model. To examine the accuracy of the model calculations, alternative model processes were implemented and evaluated. Finally, the model was applied to four distinct study sites to identify trends in the model outputs caused by site characteristics. By identifying limitations that may exist within the model, it is possible to improve the accuracy of the model outputs. In this way, the model calculations can be assessed and properly utilized at multiple sites with varying conditions.

CHAPTER 2 - Literature Review

Soil Erosion and Nonpoint Source Pollution

Reducing soil erosion and surface runoff are major concerns across the country. Soil erosion can lead to a variety of problems, including the pollution and sedimentation of various water bodies. This type of pollution is described as diffuse pollution, or nonpoint source (NPS) pollution, that can come from a variety of sources, including agriculture, urban runoff, construction, and forestry (USEPA, 2003). NPS pollution is the leading cause of degradation throughout the nation's surface water (USEPA, 2003). It occurs when water runoff transports and deposits natural and man-made pollutants. According to the 2004 National Water Quality Inventory (USEPA, 2004), 44% of the assessed streams, 64% of the assessed lake areas, and 30% of the assessed bay and estuarine areas do not meet the national water quality standards, including 246,002 miles of river, 10,451,402 acres of lake, and 7,641 square miles of estuary (USEPA, 2004). According to the report, agriculture, including NPS pollution from cropland and grazing, is the leading cause of pollution in rivers and streams, and it is the third largest source of pollution for lakes, ponds, and reservoirs. In addition, atmospheric deposition, including NPS pollution from contaminated air, is the leading cause of pollution in estuaries and lakes (USEPA, 2004).

There are many negative impacts that result from NPS pollution. Nutrients, sediments, and pathogens are all major problems associated with NPS pollution (Baker, 1992). Sedimentation caused by excess erosion can alter aquatic habitat, suffocate fish eggs and bottom-dwelling organisms, and interfere with drinking water treatment processes and recreational use

(USEPA, 2002). Excess nutrients from NPS pollution can cause nuisance overgrowth of algae, depleting the dissolved oxygen and disrupting the existing ecosystem of a water body (USEPA, 2002). Other pollutants carried by runoff can contaminate both surface and groundwater sources of drinking water (Baker, 1992).

Environmental Issues on Military Installations

Much focus is placed on water and soil management in agricultural and urban environments for handling the problems associated with NPS pollution. Military training lands can also experience significant amounts of soil erosion leading to NPS pollution. Military training exercises can cause significant land degradation, leading to adverse environmental impacts, particularly soil erosion. The military has been required to minimize these impacts since the passage of the National Environmental Policy Act of 1969 (NEPA) and the publication of U.S. Army Regulation 200-2 (Department of Army, 1988). To optimize the sustainable use of training land, the Army has initiated the Integrated Training and Management (ITAM) program. The ITAM program allows the military to manage and maintain training lands while still supporting military readiness.

A management program for military installations requires unique considerations. The military must maintain high-quality training to remain prepared for their mission, so land management practices must be flexible with minimal impacts on training exercises. In addition, the various factors effecting soil erosion must be considered. Military training exercises often include many military vehicles that are large, heavy, and have the capability of covering considerable areas of land (Quist *et al*., 2003). The movement of these vehicles can cause significant land degradation, compacting the soil and removing the vegetative cover (Milchunas *et al*., 1999). The extent of the degradation depends on the vehicles involved, their operating

characteristics, and the existing soil conditions within the training area (Ayers *et al*., 2005). Most military vehicles are heavy, and the small turning radii associated with tracked vehicles have been shown to cause severe rutting and compaction (Liu *et al*., 2007). The path taken by these vehicles is typically determined by military doctrine, so certain areas, like stream crossings, will have significantly higher traffic. In addition, climate plays a significant role in soil erosion. Temperature, rainfall, and storm frequency can have significant impacts on land degradation (Lal, 1994). Because of these various factors, military training exercises can lead to significant land degradation.

Best Management Practices

To alleviate runoff problems and reduce NPS pollution, various Best Management Practices (BMPs) can be implemented. BMPs can be structural, which use physical formations to alter hydrologic pathways; vegetative, which use plants with root systems that stabilize the soil as well as absorb and store water; or management techniques that reduce negative impacts (Novotny, 2003). Many of these BMPs focus on agricultural and urban applications. While many of them can be applied in different ways, there are some significant differences between these practices and those needed for military installations.

For urban areas, typical BMPs include surface basins, infiltration and exfiltration trenches, pervious pavement, and swales (Livingston, 2000). Unlike BMPs suitable for the rangeland of military installations, these practices focus on the limited space and impervious surfaces of an urban environment. Nearly all BMPs focus on reducing water runoff and increasing soil infiltration. However, BMPs for application outside of urban areas are typically more expansive in a spatial context.

For agricultural areas, there are various BMPs that can be applied. These practices come in various forms, but the overall goal is to reduce the negative impacts of agricultural activities, while retaining the productive capacity of the land (Mostaghimi *et al.*, 1997). Typical BMPs include terracing, contour farming, cover crops, stream fencing, buffer strips, brush management, and various management techniques (NRCS, 2001; 2002; 2003; 2007; 2008). While a majority of these practices focus on agricultural land, many of them can be applied toward military rangeland.

To employ these techniques on military installations, the major differences between military and agricultural practices must be considered. While agricultural areas experience significant erosion due to farming and ranching practices, the majority of environmental problems on military installations is due to training exercises. Military vehicles can be significantly heavier than farming equipment, and tracked vehicles can cause significant damage to vegetation and soil (Liu *et al*., 2007). These vehicles, with a turning radius that is much tighter than agricultural equipment, form deep ruts and have a much larger cumulative impact width (Liu *et al*., 2007; Ayers *et al*., 2005). In addition, the movement of military vehicles and personnel is governed by military doctrine. On the other hand, the movement of agricultural equipment is often uniform across entire fields. This results in unique erosion patterns between the two landuse types.

Due to the different conditions found on military installations, the implementation of BMPs within these areas is unique. One notable practice for military installations is the appropriate timing of training exercises. By avoiding times when the land is especially vulnerable, like after a precipitation event, land degradation can be reduced.

To direct hydrologic flow, terraces, diversions, and dikes can be used to decrease erosion. These land-forming techniques can reduce soil erosion and NPS pollution while occupying a minimal amount of the training area. Terraces, which are earth embankments constructed across the slope, can reduce erosion by decreasing slope length and reducing water runoff (NRCS, 2008). Diversions, which are channels constructed across the slope, can be used to break up water concentrations and divert surface flow from eroding areas (NRCS, 2001). Dikes, which are earthen barriers, can be used to protect sensitive areas from excessive water flows and control water levels (NRCS, 2002). On military installations, any of these structures could be applied around areas with high traffic flow, where soil compaction is greatest. Compacted ruts formed by military vehicles will cause water runoff to concentrate, increasing the sediment transport capacity (Gatto, 2001). By redirecting the hydrologic flow path, runoff concentration can be reduced and erosion can be prevented.

Maintaining vegetative cover is also important for preventing excessive erosion. One method that can be applied to rangeland is the use of vegetative barriers. Strips of stiff, dense vegetation are planted along the overall contour of the terrain or across concentrated flow areas to manage water problems (NRCS, 2003). This practice can be used to reduce sheet, rill, and ephemeral gully erosion, trap sediment, and stabilize steep slopes. On military installations vegetative barriers can be placed alongside streams to minimize the loss of valuable training lands. Critical Area Planting is another vegetative BMP that can help reduce erosion. By establishing permanent vegetation, this practice can stabilize areas with high rates of soil erosion (NRCS, 2007). This practice is useful for areas that have had significant land degradation from military training exercises. By restoring the vegetation at vital locations within a training area, environmental impacts can be reduced.

All of these BMPs are important, and their proper implementation across the landscape can help reduce runoff and soil erosion. Most importantly, maintaining vegetation across susceptible areas will have significant positive impacts. By dissipating the erosive force of water runoff, vegetation can significantly decrease NPS pollution. In addition, the root structure can help increase infiltration into the soil. Also important for areas that are susceptible to erosion is the placement of appropriate structures, including terraces, diversions, and dikes, that can improve hydrologic flow. While the timing of training exercises can aid in improving the conditions of vegetation and soil, the need for quality training may make it difficult to avoid military exercises at times when the land is more susceptible to degradation.

Predicting and Modeling Soil Erosion

To maximize the effectiveness of a land management program, it is necessary to determine ideal locations for BMPs. Extensive, widespread BMPs would be cost-intensive and inefficient (Veith, 2003). Improper placement of BMPs can make them less effective and reduce the availability of land for other purposes. A predictive model could be used to assist in the placement of BMPs. In addition, the model could aid military officers in selecting the best time and location for a particular training exercise.

Existing Models

Various models have been developed to estimate soil erosion, but the majority of these models focus on agricultural applications (Fiener *et al*., 2008). Such models include the Water Erosion Prediction Project (WEPP), the Revised Ephemeral Gully Erosion Model (REGEM), the European Soil Erosion Model (EUROSEM), the kinematic runoff and erosion (KINEROS) model, the Agricultural Non-Point Source Pollution (AGNPS) model, the Revised Universal Soil

Loss Equation (RUSLE), the Soil and Water Assessment Tool (SWAT), and many others. WEPP is a model developed for the USDA that predicts soil loss and sediment deposition (Flanagan and Nearing, 1995). REGEM was developed to model water runoff after a rainfall event (Gordon *et al*., 2006). EUROSEM was developed to predict sediment transport, erosion, and deposition by rill and interill flow for single storm events (Morgan *et al*., 1998). KINEROS was developed to describe the process of interception, infiltration, surface runoff, and erosion in agricultural and urban watersheds using one-dimensional kinematic equations (Smith *et al*., 1995). SWAT was developed by the USDA to quantify the impact of land management practices in large watersheds (Gassman *et al*., 2007). This model is the most comprehensive, incorporating eight factors including hydrology, weather, sedimentation, soil temperature, crop growth, nutrients, pesticides, and agricultural management (Neitsch *et al*., 2002). However, it is also the most difficult to use because it requires the most data and time to obtain results.

All of these models address soil erosion. However, they may not be the best applications for military installations. While both WEPP and REGEM can be used to address the growth of gullies caused by erosion (Gordon *et al*., 2006), none of the models predict initiation points of soil erosion. This ability would be useful for determining potential gully sites for military land managers. WEPP and REGEM are also limited for military applications because they were specifically designed for agriculture and forestry purposes (Flanagan and Nearing, 1995). EUROSEM was designed only to predict erosion for single fields or small catchments (Morgan *et al*., 1998). KINEROS is also limited to small watersheds (Smith *et al*., 1995).

Many of these models, including SWAT, AGNPS, and RUSLE, require a large amount of input data. The acquisition of the initial input data can be very time-intensive (Jetten *et al*., 1996). For agricultural purposes, these models are sufficient, since the agricultural processes

occur on a slower timescale. However, military training exercises are very dynamic, and a management program set around these exercises would require a predictive model that takes less time to run. Because of this, a rapid assessment tool would be ideal for land managers on military installations.

Simpler models often lump parameters into over simplified generalities, which has the potential to make them less accurate (Merritt *et al*., 2003). However, there are several advantages to a rapid-assessment model that can assist in a land management plan for military training. More complex models that require large amounts of data can lead to increased input errors, making simpler models more desirable (Jetten *et al*., 2003). In addition, a rapid-assessment model supplies faster results, which would give the military more flexibility in planning their training exercises. For military land managers, such a tool can help determine the environmental cost of training exercises and prioritize areas for BMP implementation and more intensive management practices. In this way, environmental impacts can be reduced without compromising the quality of military training.

Kinematic Wave Approach

The kinematic wave theory has proven to be useful for assessing certain aspects of overland flow transport at varying flow regimes (Laguna and Giraldez, 1993; Wong and Chen, 1999; Singh, 2001). The initial purpose behind the development of the kinematic theory was to explain the movement of flood waves (Singh, 2001). The uses of the kinematic wave theory have been expanded to additional uses. For example, it is often used to calculate time of concentration within a drainage area as a shock wave runoff hydrograph (McCuen and Spiess, 1995; Willgoose and Kucera, 1994; Jaber and Mohtar, 2002). The kinematic wave model used to calculate the time of concentration for overland flow is commonly combined with Manning's

surface roughness coefficients (Ragan and Duru, 1972; McCuen and Spiess, 1995; Wong, 2005). The equation for this model is

$$t_c = \frac{a}{i^{0.4}} \left(\frac{nL}{\sqrt{S}} \right)^{0.6} \quad [1]$$

where t_c is the time of concentration for sheet flow (minutes); i is the rainfall intensity (millimeters per hour); n is the Manning's coefficient (unitless measure of surface roughness for overland flow); L is the length of sheet flow (meters); S is the slope (meters per meter); and a is a constant.

To implement the kinematic wave equation, there are several assumptions that must be made. First, momentum and pressure forces are neglected. Second, there is no local inflow that occurs within a given area. Third, there are no backwater effects. Fourth, detention storage is negligible. Fifth, discharge is a function of depth only. And sixth, the equation is only applicable for non-concentrated flow (McCuen and Spiess, 1995). Because of these assumptions, which are unrealistic in most cases, additional information is required for the accurate application of the kinematic wave model under different flow regimes in varying drainage areas. To address this problem, McCuen and Spiess (1995) determined that the value of $nL/S^{0.5}$ could be used to determine when the model could accurately calculate times of concentration for sheet flow. In the study, it was found that a value of just over 100 could be used to as a threshold value for determining where sheet flow transitions into concentrated flow (McCuen and Spiess, 1995). In a study of more complex watersheds, Kim (2006) determined that a value of around 131 could be used as a threshold value for sheet flow. Areas in the watershed that have a value near this threshold value can be described as transitional areas between sheet flow and concentrated flow.

The nLS Model

To assist in reducing environmental impacts on military bases, a predictive model was developed for Fort Riley, Kansas based on the kinematic wave theory. This model, referred to as the nLS model, was used to predict gully formations in two watersheds within Kansas, and was shown to have an overall model accuracy as high as 89% (Kim, 2006). The model requires few input requirements, which are relatively easy to obtain. This reduces the time needed to acquire data. The inputs include digital elevation models (DEMs) and landuse/landcover data (LULC), which are then integrated into a geographic information system (GIS).

As water moves down a watershed, it transitions from overland sheet flow into concentrated flow. The concentration of this overland flow is a primary cause of soil erosion (Abrahams and Atkinson, 1993). As the flow concentrates, its erosive energy increases. Due to this increase in energy, concentrated flow is closely associated with increased soil erosion, and determining where water begins to transition from overland flow into concentrated flow can be used to find areas with higher erosion potential, where gullies are likely to begin (Kim, 2006; Bennett *et al*., 2000). By locating the points at which this event occurs in a watershed, the best placement for BMPs can be determined.

The nLS equation is used to determine the transition point of overland flow from sheet to concentrated flow. The equation, as used in the model, is

$$nLS\ \ Value = \frac{nL}{\sqrt{S}} \qquad [2]$$

where n is the Manning's coefficient (unitless measure of surface roughness for overland flow); L is the length of sheet flow (feet); and S is the slope (feet per feet).

Input data for the nLS model was derived from LULC data and DEMs. Manning's coefficients were obtained from LULC data. This value accounts for vegetation, soil, and land-

use properties that may have an impact on water movement (Ward and Trimble, 2003). To determine the slope, flow length, and flow path, topographic information from a DEM was used. Once the values were inputted into the model and the nLS values were calculated, any areas that had nLS values within the threshold range of 131 ± 22.6, were described as areas with a higher erosion potential (Kim, 2006). By locating the sites with nLS values close to the given threshold value, it was possible to predict the future formation of gullies from soil erosion.

To successfully implement the nLS model, a GIS was used. GIS technology allows data to be preprocessed from large stores into suitable forms, analyzed for modeling, and processed after the results have been obtained (Goodchild *et al*., 1993). The ability to handle large quantities of data makes GIS ideal for integrating elevation and LULC data into an environmental model. However, there are also limitations to using GIS with the nLS model. The potential for errors in the calculations of surface properties may exist due to the misrepresentation of spatial variability caused by data resolution that is too coarse (Corwin and Vaughan, 1997; Verro *et al*., 2002). Zhang and Montgomery (1994) reported that 10-m DEMs offered more reliable hydrologic assessments than 30-meter DEMs. Similarly, Kim (2006) found that the accuracy of the nLS model increased as the data was improved from a resolution of 30 meters to 10 meters and up to 3 meters.

Model Sensitivity Approaches

While the nLS model has been tested with field data from the Cheney Reservoir watershed and the Fort Riley study area, model errors related to input parameters and model calibration could make it more difficult to obtain accurate results for other sites. Locations with different precipitation regimes, LULC conditions, topographic characteristics, and soil types may not be as well-represented by the model. For example, the Manning's n coefficient, which has

proven effective for grasslands, may be less helpful for predicting erosion in forested, volcanic, or desert areas. Model limitations need to be identified to ensure that the model can be effectively implemented at other sites. A sensitivity analysis assists with analyzing uncertainties in the output caused by variations in input parameters (Tiscareno-Lopez *et al*., 1993). This type of analysis can help assess the mathematical simulations of the model, increasing its accuracy. In addition, the most sensitive variables in the model prediction can be identified, allowing the less sensitive variables to be generalized or omitted, and potentially simplifying the model (Zerihun *et al*., 1996). A sensitivity analysis can also help detect errors resulting from nonlinear equations and numerical solution methods, complicated computer programming, and the theoretical approaches used to model natural phenomena (Ferreira *et al*., 1995).

Quantifying model simulation error can be done using various methods of sensitivity testing. The most common method is the independent parameter perturbation (IPP), which is based on a linear system where parameters are individually varied by a fixed percentage from a given base value (Ferreira *et al*., 1995). This method has been used with various NPS pollution models. For example, the WEPP model was analyzed by Nearing *et al*. (1990) and Tiscareno-Lopez *et al*. (1993) to determine the average model response of selected output variables. This study was based on a linear regression analysis, as well as a Monte Carlo simulation. In erosion modeling, the high spatial and temporal variability associated with the model parameters makes it difficult to select an initial value for each parameter (Quinton, 1997). To address this, Monte Carlo techniques involve repeated numerical samplings for sets of parameters based on postulated distributions, creating many samples of varying values (Veihe and Quinton, 2000). Ma *et al*. (2000) used similar analysis techniques to determine uncertainties of the Root Zone Water Quality Model (RZWQM), and Wedwick *et al*. (2001) used a Monte Carlo simulation to

analyze the Groundwater Loading Effects of Agricultural Management Systems (GLEAMS-IR) model.

Research Objectives

The nLS model was developed as a tool for predicting locations with high soil erosion potential. The ability of the model to accurately and rapidly predict areas with high soil erosion potential makes it ideal for land management programs on military installations. Currently, the model has been tested and validated for the Cheney Reservoir watershed, as well as a study area located in Fort Riley Kansas. In these areas, the model has proven very effective at locating potential soil erosion sites (Kim, 2006). However, the accuracy of the model has not been tested in areas outside of Kansas.

The potential for input parameters to affect the accuracy of the model must be analyzed before the nLS model can be implemented effectively. Therefore, the objective of this study is to determine the sensitivity of the model to the different parameters. This will be done by evaluating model uncertainties that result from changing the input data during IPP and Monte Carlo simulations. In addition, the effects of modifying the nLS threshold value used for identifying soil erosion potential sites will be evaluated. Finally, the model will be modified using alternative calculation methods to determine the validity of the current model's calculations. By successfully implementing the nLS model for a military installation, erosion problems can be predicted. This allows land managers to assess environmental impacts of training exercises and take the proper steps to alleviate the problems. BMPs can be better implemented for repairing and preventing excess soil erosion. There is also potential for the nLS model to be expanded to help land managers in forestry or agriculture.

CHAPTER 3 - Study areas

Four study areas, two located in Kansas and two in Hawaii, were selected for analysis (Figure 3.1). Each study area has unique climatic, topographic, and vegetative conditions (Table 3.1). Three of the sites are located on U.S. Army military installations, making them different from the surrounding areas because of the potential for maneuvering activities that can induce the transport of sediment and other pollutants. The fourth study site was a much larger area that includes the contributing watershed of a large municipal water supply reservoir in south-central Kansas. By selecting a variety of diverse locations for this study, the impacts of site-specific characteristics on the nLS model were examined.

Figure 3.1 Locations of the four study areas within the United States, including two in Kansas and two in Hawaii, overlaid over a precipitation map.

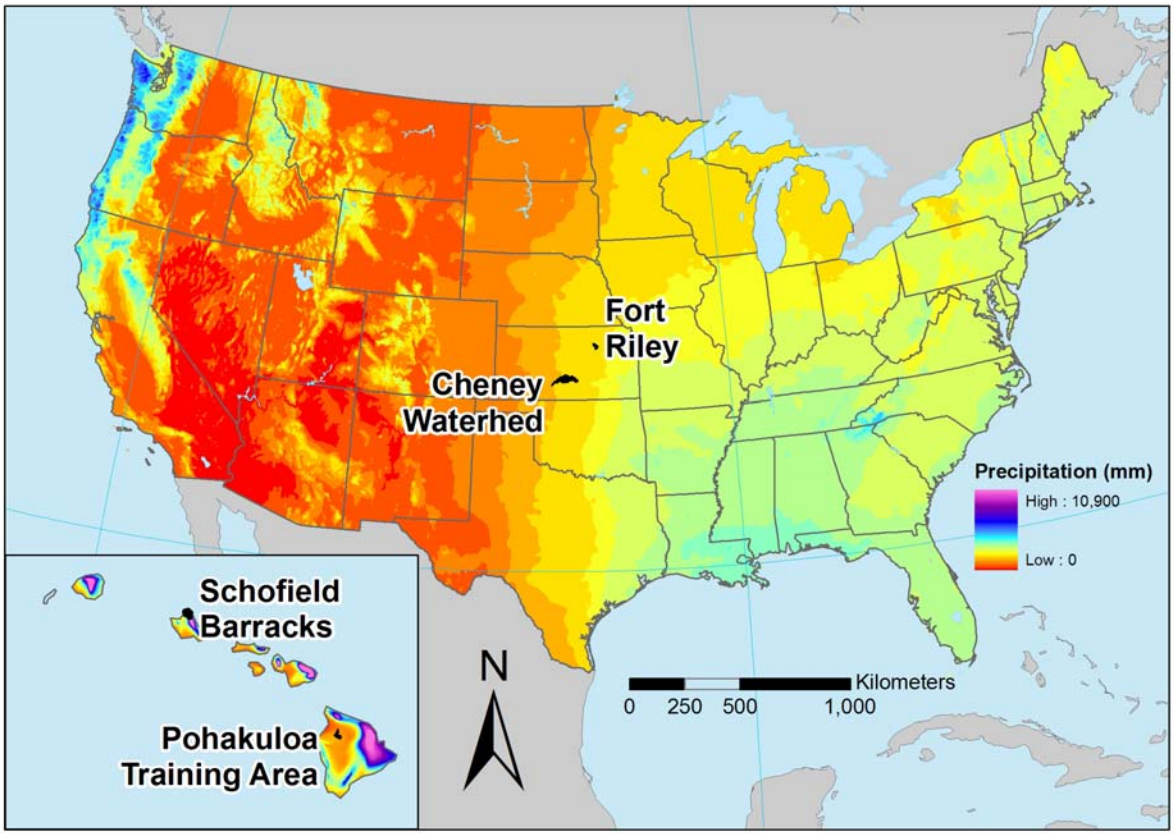

Table 3.1 Summary of site characteristics at the four study areas.

Study Area	Size (km^2)	Ecoregion	Annual Precipitation (mm)	Temperature (°C)	Elevation Range (m)	Average Slope (%)
Fort Riley, KS	411	Flint Hills[1]	850[3]	6 – 19[3]	312 - 420	6.84
Cheney Watershed, KS	2,564	Central Great Plains[1]	673 (West) 798 (East)[3]	5 – 21[3]	433 - 669	1.44
Keamuku Parcel, HI	93	Tropical Dry Forest[2]	640[4]	16 – 21[4]	806 - 1866	34.49
Kahuku Training Area, HI	38	Tropical Moist & Dry Forest[2]	1020 (North) 3810 (South)[5]	20 – 25[4]	16 - 647	38.14

1 – Omernik, 1995
2 – Ricketts *et al*., 1999
3 – Daly *et al*., 2002
4 – NOAA/NCDC, 2009
5 – U.S. Army, Hawaii and 25th Infantry Division, 2001

The datasets from each site were used as model inputs to calculate nLS values and potential erosion areas for each study area. To incorporate any run-on from the surrounding area, model inputs included the area covered by all watersheds overlapping the study sites. Watersheds for the Kansas sites were based on the available 14-digit Hydrologic Unit Code (HUC 14) delineations (http://water.usgs.gov/GIS). For Hawaii, watersheds were derived from USGS DEM data (GDSI, 1995). Transitional flow areas were defined as those pixels with a critical nLS threshold value of 131 ± 22.6, based on the findings of Kim (2006). Although the entire area of contributing watersheds was used as input, the analysis of model outputs was limited to the area within each study site. Data for the Kahuku Training Area was used for various sensitivity analyses of the nLS model. Comparisons of the predicted erosion areas were then made between each site. Model outputs were examined as functions of overall slope, Manning's roughness coefficient, and drainage density. By analyzing the relationship between site characteristics and model predictions, generalizations could be made on the expected model performance within specific ecoregions.

Fort Riley, Kansas

Fort Riley is a U.S. Army training installation located in northeastern Kansas (Figure 3.2). The base covers more than 410 km^2 and is located just west of the city of Manhattan. The military units stationed at the installation employ large numbers of tracked and wheeled vehicles. Fort Riley is located within the Flint Hills ecoregion, which spans the area from northeastern Kansas to the Oklahoma border, and contains the largest remnant of uncultivated tallgrass prairie in the U.S. (Omernik, 1995).

Figure 3.2 Aerial view of the Fort Riley Army installation, located in northeast Kansas.

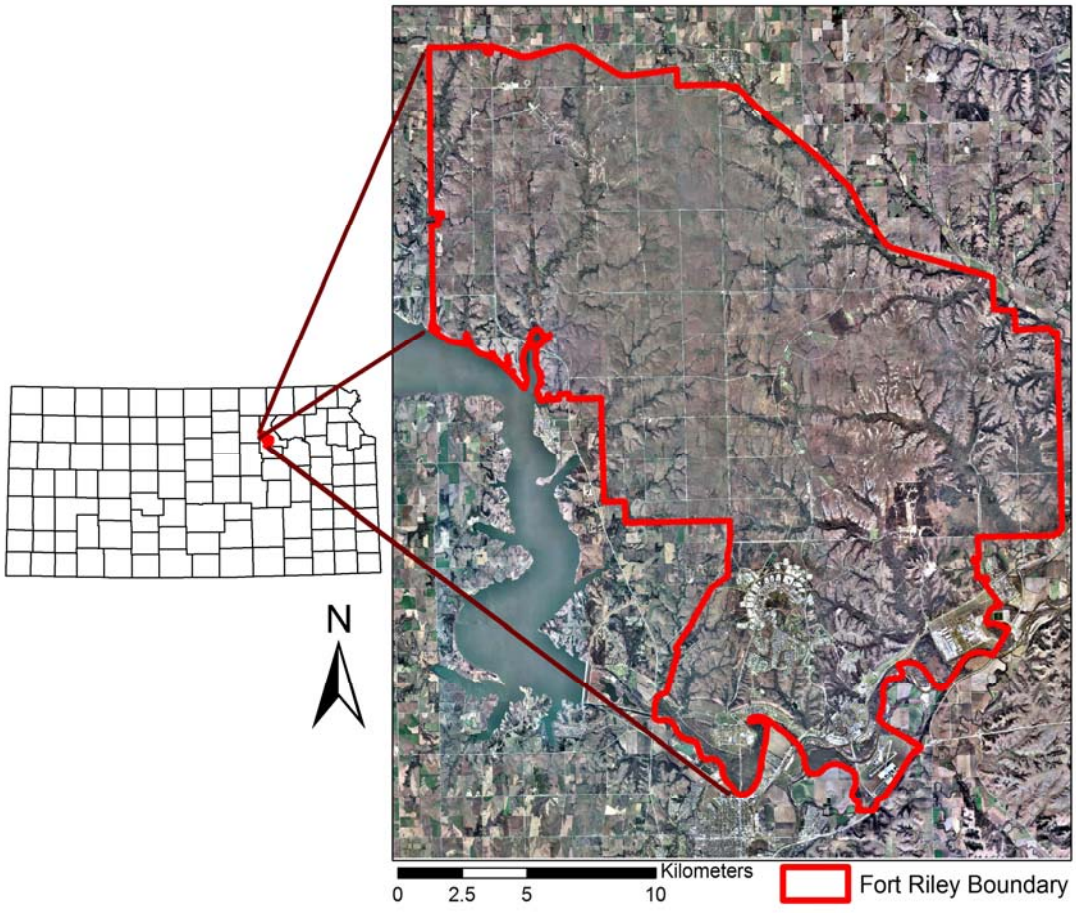

Elevations on Fort Riley range from 312 and 419 m above sea level, based on the 10-meter USGS National Elevation Data. By overlapping the installation boundaries with the HUC

14 watershed boundaries, it was determined that the study area contains 10 watersheds which empty to the Kansas River. The drainage density (total length of streams per total drainage area) on Fort Riley is 1.80 (km/km^2) as calculated using surface hydrography data from the National Hydrography Dataset (NHD, http://nhd.usgs.gov). Mean annual precipitation is 850 mm, and maximum and minimum temperatures are 19 °C and 6 °C, based on weather data from 1971 to 2000 (Daly *et al*., 2002). The majority of the soils on Fort Riley are silty clay loams and silty loams, which tend to have moderate permeability (Jantz *et al*., 1975). The three major LULC groups on Ft. Riley are wide hillslope grasslands, shrublands, and woodlands (Egbert *et al*., 2001). The study area includes 15 distinctive vegetative classes as well as urban areas and water bodies.

Cheney Reservoir Watershed, Kansas

The Cheney Reservoir watershed is located in south central Kansas near the city of Wichita (Figure 3.3). The reservoir comprises an area of 40 km^2 with a contributing drainage area of approximately 2,524 km^2, comprised primarily of agricultural land. The Cheney Reservoir has been the primary drinking water source (60-70% daily basis) for the city of Wichita, Kansas and the surrounding area since construction in 1965 (Pope and Milligan, 2002). The entire area is considered to be part of the Central Great Plains ecoregion, which includes parts of Nebraska, Kansas, Oklahoma, and Texas (Omernik, 1995).

Figure 3.3 Cheney Reservoir watershed, located in south-central Kansas.

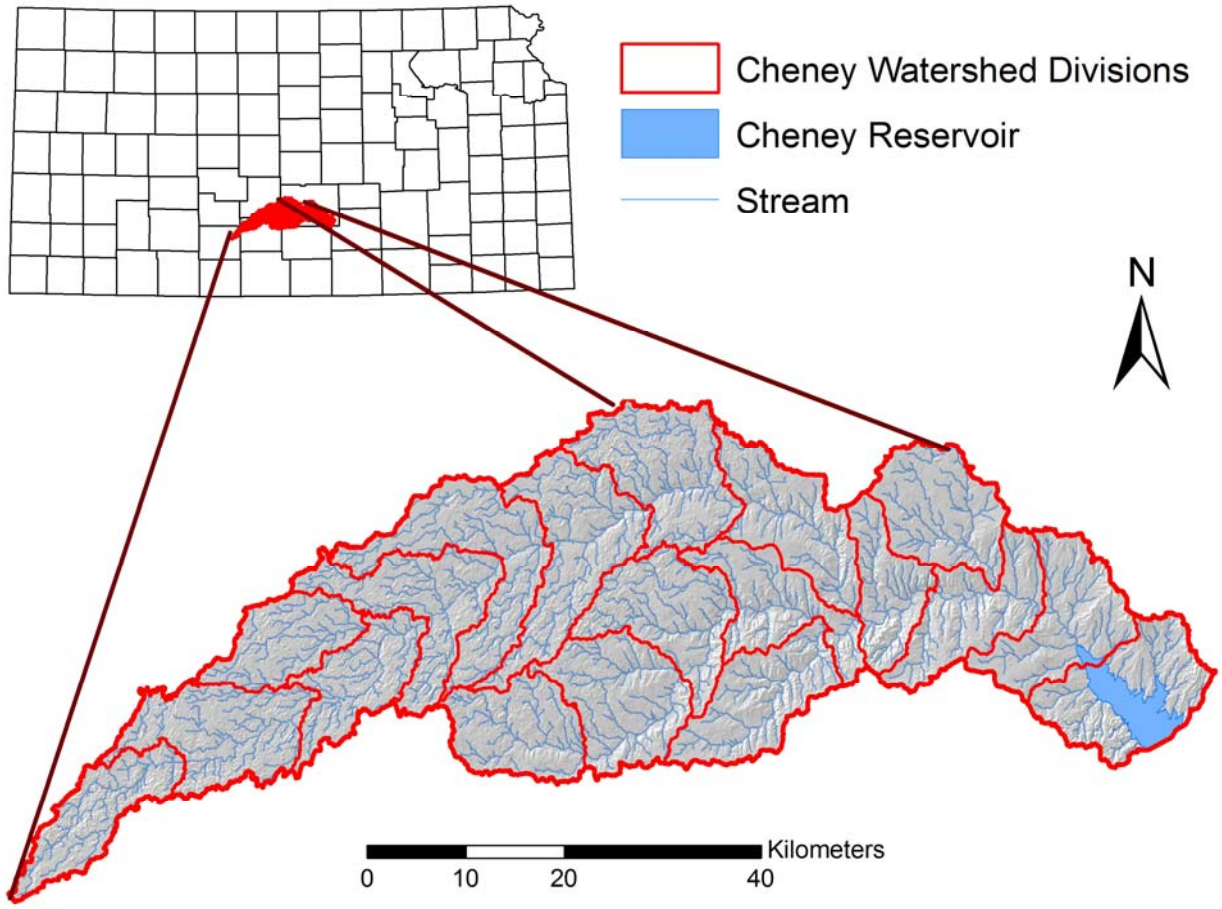

Elevations in the watershed vary from 433 m to 669 m above sea level with an average slope of 1.44%, based on the USGS 10-meter DEM. Mean annual precipitation increases from west to east with an average of 673 mm at the west end of the watershed and 798 mm at the east end of the watershed (Daly *et al*., 2002). Mean annual temperatures range from 5.9 °C to 20.8 °C (Daly *et al*., 2002). According to local county soil survey (Rockers *et al*., 1966), soils in the watershed mainly consist of sandy loam, loamy fine sand, and fine sandy loam. Nineteen HUC 14 subwatersheds comprise the study area. The drainage density for Cheney is 0.76 km/km^2, based on NHD high-resolution data.

There are 25 LULC classifications within the watershed based on Kansas GAP landcover data. Land in the watershed is typically used for agricultural production (54%), and areas of CRP (Conservation Reserve Program) are also fairly common throughout the watershed. The major crops grown within the watershed are wheat (63%), sorghum (24%), corn (10%), and soybeans (3%) (Mau, 2001).

Keamuku Training Area, Hawaii

The Keamuku Parcel (KP) is part of Pohakuloa Training Area, an Army Installation located on the island of Hawaii. The study area covers 93.3 km^2 and is located on the northwest section of the installation (Figure 3.4). The area was used primarily as pasture land from the middle 1800s until very recently, but was purchased by the U.S. Army to serve as additional training land. The study area is located within the Hawaiian Dry Forest ecoregion (Rickets *et al*., 1999) and receives much less rainfall than the majority of the Hawaiian Islands.

Figure 3.4 Aerial view of the Keamuku Training Area, part of Pohakuloa Training Area on western portion of the Big Island, Hawaii.

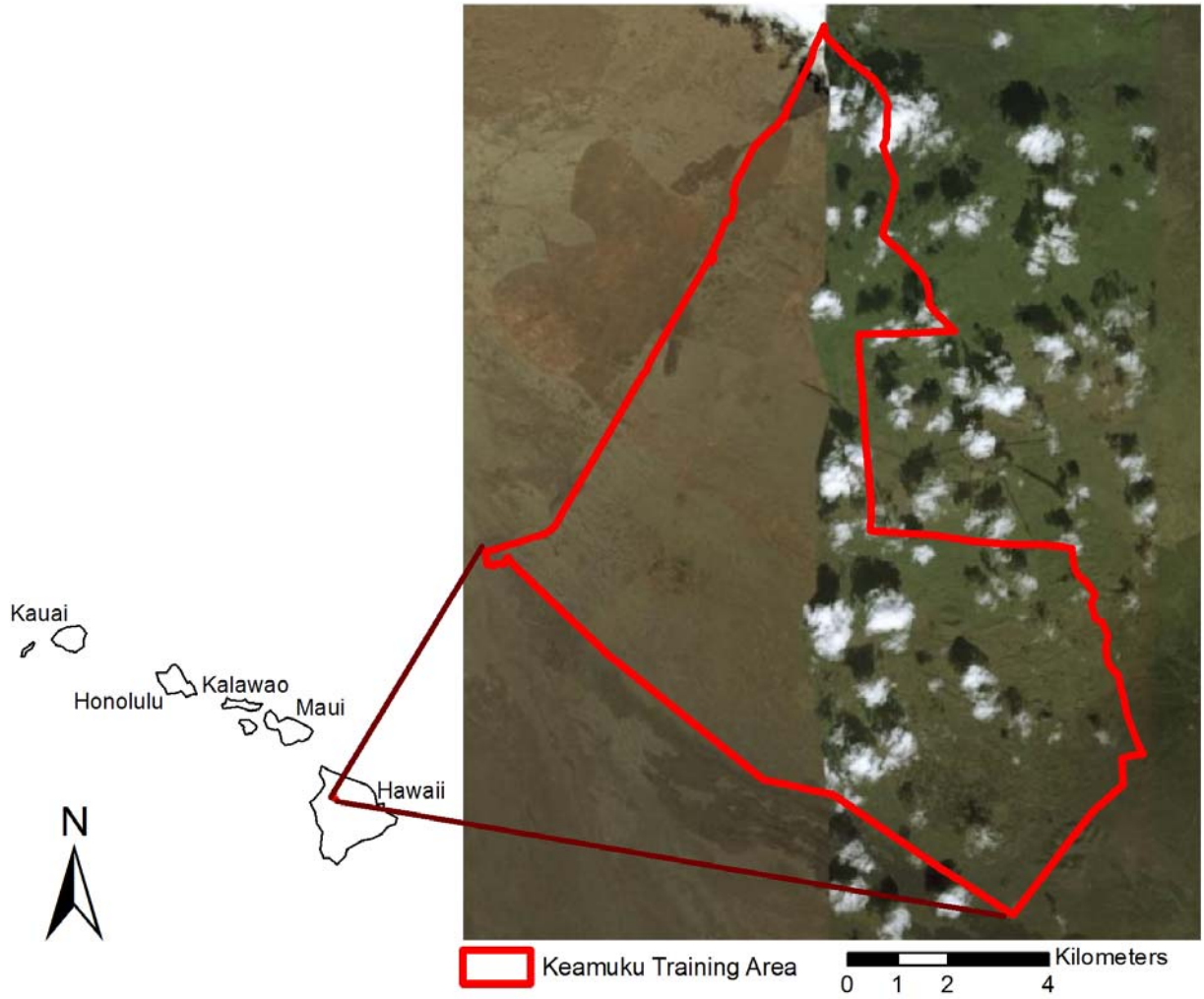

Elevations for KP range from 806 m to 1,866 m above sea level, based on the USGS 10-meter DEM. Annual precipitation across KP varies from 250 to 750 mm across the landscape, and average temperature ranges from 15 to 21°C (NOAA/NCDC, 2009). The island of Hawaii is the youngest island of the Hawaiian island chain, and was formed as the Pacific Plate passed over a hotspot in the earth's mantle (Chytka *et al.*, 2008). The soils of this area are relatively young and poorly developed, being formed from past lava flows (Chytka *et al.*, 2008). The Natural Resources Conservation Service (NRCS) Soil Survey identifies several soil types within

the Keamuku Parcel. The majority of these soils are stony sand, stony peat, and loamy sands. The entire training area is located within a single watershed, based on the GDSI (1995) delineations, which flows directly into the Pacific Ocean. Using the NHD high resolution data, the drainage density for Keamuku is 0.77 km/km^2.

Due to the training area's ranching history, the majority of the native vegetation has been replaced by non-native species (TTI, 2004). Within Keamuku, the majority of the area is comprised of either herbaceous grasslands or shrublands, and there are several trails that cross the site. In the surrounding watershed, there are large portions of barren land formed by lava flows, as well as grasslands and shrublands. In all, there are 16 distinct LULC classes in the surrounding watershed based on Hawaii GAP data, with 12 of those classes falling within the study area.

Kahuku Training Area, Hawaii

The Kahuku Training Area (KTA) is part of Schofield Barracks, a U.S. Army installation on the Island of Oahu, Hawaii (Figure 3.5). The area has held a military presence since 1944 (US Army and 25th Infantry Division, 2001). The training area covers 38.3 km^2 of leased and federally owned land at the northern tip of the Koʻolau mountain range. The Army conducts various military training exercises in the area, and activities taking place on adjacent and surrounding properties include cattle ranching along the north and northeast property boundaries, diversified agriculture, and recreation (SRGI, 2009). Due to site's location and the significant change in elevation, the area is actually located in two different ecoregions. To the south, the mountainous forests of are considered part of the Hawaiian Moist Forest, while a small portion of the north end of the installation is located in a Hawaiian Dry Forest (Rickets *et al*., 1999).

Figure 3.5 Aerial view of the Kahuku Training Area, part of Schofield Barracks on the northern edge of the island of Oahu, Hawaii.

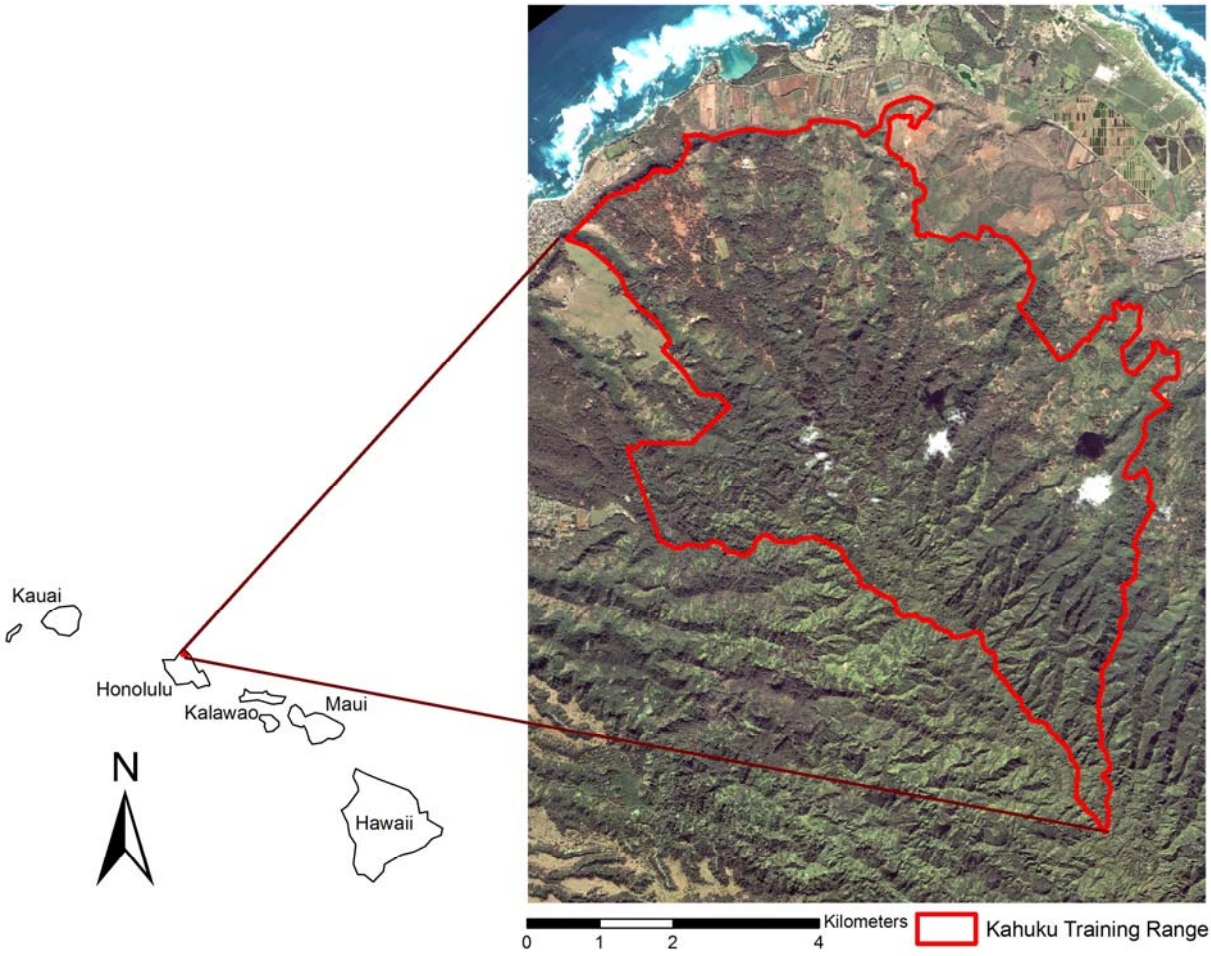

The elevations across KTA range from 16 meters up to 647 m along the Koʻolau mountains, based on the 10-meter National Elevation Data. A large percentage of the area is dominated by extremely rugged terrain and steep slopes. Annual average rainfall ranges between 3810 mm at the Koʻolau summit to 1020 mm near the coast (US Army and 25th Infantry Division, 2001). Average annual temperatures range from 20 to 25°C (NOAA/NCDC, 2009). The Island of Oahu lies within the tropical latitudes and is periodically subjected to storms with high rainfall magnitudes (SRGI, 2009). Because Oahu is older than the island of Hawaii, the soils are more developed. The NRCS Soil Survey identifies five soil series within KTA, all of

which are considered to be either well-drained silty clays or rock land, developed from weathered basalt lavas. Based on the GDSI (1995) boundaries, four subwatersheds are delineated across the boundaries of KTA, all of which drain into the Pacific Ocean. Based on NHD high resolution flow lines, the drainage density of the area is 1.95km/km^2.

Vegetation communities within KTA include upland tree-shrubs, shrub-grasses and mixed grasses, all of which are dominated by plant species that are non-native and several that are invasive (SRGI, 2009). Native species exist in scattered locations throughout the training area, however they are primarily found in small patches at higher elevations. Native vegetation communities found within KTA include the *Aleurites moluccana* (Kukui), *Metrosideros polymorpha* (Ohia), *Acacia koa*, and *Dicranopteris linearis* (Uluhe) forest species, and the remaining area is made up of non-native mixed vegetation communities including species of *Brothriochloa ischaemum* (Yellow Bluestem), *Andropogon virginicus* (Broomsedge Bluestem) *Panicum maximum* (Guinea Grass), *Lycium carolinanum* (Christmas berry), species of *Eucalyptus*, and species of *Eusideroxylon* (Ironwood) (SRGI, 2009). In all, there are a total of 25 distinctive landcover and landuse classifications, including various classifications for crop and urban areas.

KTA experiences several unique land-use activities that affect its susceptibility to soil erosion. Military training on the area involves the use of vehicles on roads and trails and, to a lesser extent, off road areas. Other military activities that impact soils include foot traffic and military air operations, which include the use of terrestrial landing areas and drop zones (SRGI, 2009). Civilian off-road vehicles are also an issue within the training area (SRGI, 2009). As part of their shared lease agreement with the State of Hawaii, the Army is permitted use of a 180-hectare training area during the weekdays, while a civilian off-road vehicle organization, the

Hawai‘i Motor Sports Association, is allowed access during the weekends and federal holidays (US Army and Infantry Division, 2001). Off-road vehicle damage to soil resources is widespread and significant across KTA. In addition, animal impacts caused by both feral pigs and domesticated cattle are common. These hoofed animals often turn up soils during foraging and movement. The damage caused by feral pigs to Hawaii watersheds has been well documented (Diong, 1982; Miller and Holt, 1992).

It was observed that the military training, off-road vehicles, and animal activity each have a significant impact on the vegetative cover and soil erosion at KTA. All of these activities can cause significant vegetation removal and soil compaction, increasing the potential for water runoff, soil erosion, and resulting in increased NPS pollution. These activities, especially animal impacts, may be difficult to control, and consequently it may be more difficult to predict areas that are more susceptible to land degradation.

CHAPTER 4 - Materials and Methods

Model Description

To locate areas with higher erosion potential, the nLS model was developed to determine where water transitions from overland flow to concentrated flow (Kim, 2006). To do this, the model makes use of the nLS equation, as developed by McCuen and Spiess (1995), within a GIS environment. The equation, restated here, is

$$nLS\ \ Value = \frac{nL}{\sqrt{S}} \qquad [2]$$

where n is the Manning's roughness coefficient; L is the length of sheet flow (feet); and S is slope (feet per feet).

To calculate the nLS values, the model required only elevation data and LULC data, which were used to acquire the necessary values for the calculations. From the LULC data, a Manning's n value was determined based on a lookup table that was located within the model. From the elevation data, slope was obtained using the deterministic eight-direction (D8) method (O'Callaghan and Mark, 1984), which finds the rate of maximum change in elevation for each cell by examining the eight surrounding cells. In addition, flow direction and flow accumulation were both obtained from the elevation data using GIS tools that also made use of the D8 method. Flow direction determines the direction to each raster cell's steepest downslope neighbor and assigns a value that is associated with that direction (Figure 4.1). Flow accumulation uses the information from flow direction to create output that represents accumulated flow to each cell (Figure 4.2). See Appendix B - for detailed tool descriptions.

Figure 4.1 Values associated with the direction of flow from each raster cell. Values range from one for the East and increase by powers of two clockwise to 128 for the Northeast.

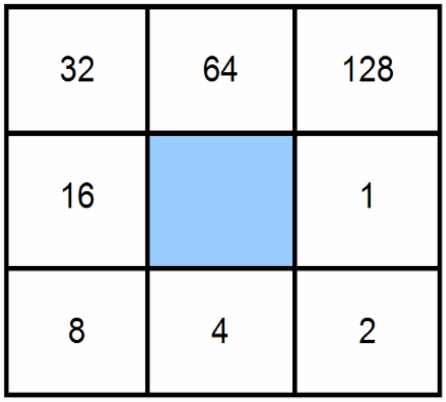

Figure 4.2 Demonstration of the flow accumulation tool. Flow direction data shown on the left is used to determine the total accumulated flow into each output raster cell.

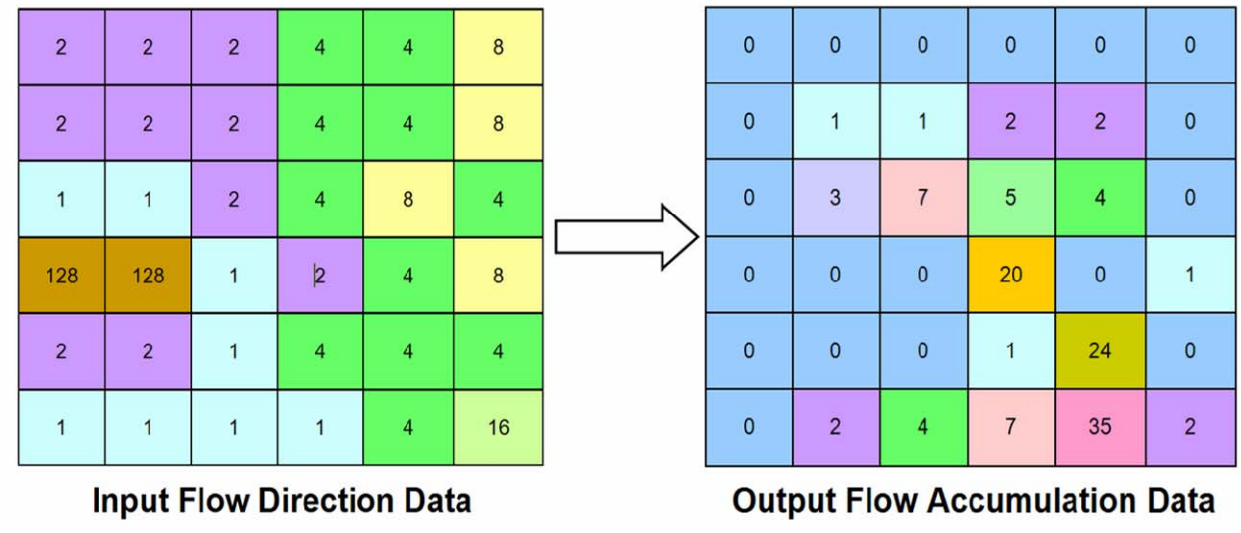

The process of pit removal was not applied to the elevation data. Pits are defined as local sinks in the topography that interrupt the flow networks. The pits may be present due to DEM error, but they can also exist in the actual topography of an area. To create continuous flow networks, artificial adjustments to the elevation are often used to smooth over potential pits. However, continuous flow networks are not vital to the operation of the nLS model, since the analysis is primarily concerned with potential erosion areas located in the uppermost regions of a

watershed. In addition, this method may remove important erosion features, and so it was not implemented in the nLS model.

Once the initial model parameters were obtained, the nLS values were calculated for an entire study area. From these calculations, any areas with nLS values near a given threshold value were extracted. These sites were described as areas where water flow transitions from overland flow to concentrated flow. By determining where flow transition occurs, areas of higher soil erosion potential are also found. In this way, the model can assist land managers in determining ideal locations for implementing best management practices.

Data Acquisition and Description

The data for this study was obtained either through nationally available datasets or through the Integrated Training Area Management (ITAM) offices of the military installations. The spatial data includes elevation and LULC information for each of the sites. The elevation data was comprised of 10-meter DEMs that were taken from the National Elevation Dataset. While data with finer resolution has been shown to produce more reliable results, a 3-meter DEM was only available for one study site. To obtain comparable results, 10-meter data was used at all four sites. The LULC data was comprised of United States Geological Survey (USGS) Gap Analysis Program (GAP), National Landcover Data, or more detailed data taken from the ITAM offices (Table 4.1).

Table 4.1 Elevation and landuse/landcover data description and source.

Site	Elevation Data			Landuse/Landcover Data		
	Dataset	Spatial Resolution	Source	Dataset	Spatial Resolution	Source
Fort Riley, KS	National Elevation Dataset (NED)	10 meters	USGS[3]	Kansas GAP	30 meters	KARS[4]
Cheney Reservoir Watershed, KS						
Keamuku Training Area, HI[1]				Hawaii GAP	30 meters	GAP[5]
Kahuku Training Area[2]						ITAM

1 – Part of Pohakuloa Training Area, Hawaii, Hawaii
2 – Part of Schofield Barracks, Oahu, Hawaii
3 – U.S. Geological Survey (http://ned.usgs.gov/)
4 – Kansas Applied Remote Sensing Program (http://www.KansasGIS.org)
5 – Gap Analysis Program (http://gapanalysis.nbii.gov)

Input data for Fort Riley include a 10-meter DEM obtained from USGS National Elevation Data (Figure 4.3) and LULC classifications obtained from Kansas GAP (Figure 4.4). To capture accurate hydrologic flow, all watersheds that intersect Fort Riley were included, based on HUC 14 delineations. DEM values range from 300 m to 433 m above mean sea level for the entire watershed area. LULC data includes 17 separate LULC classifications across the study area.

Figure 4.3 Elevation and hydrologic data for Fort Riley, Kansas.

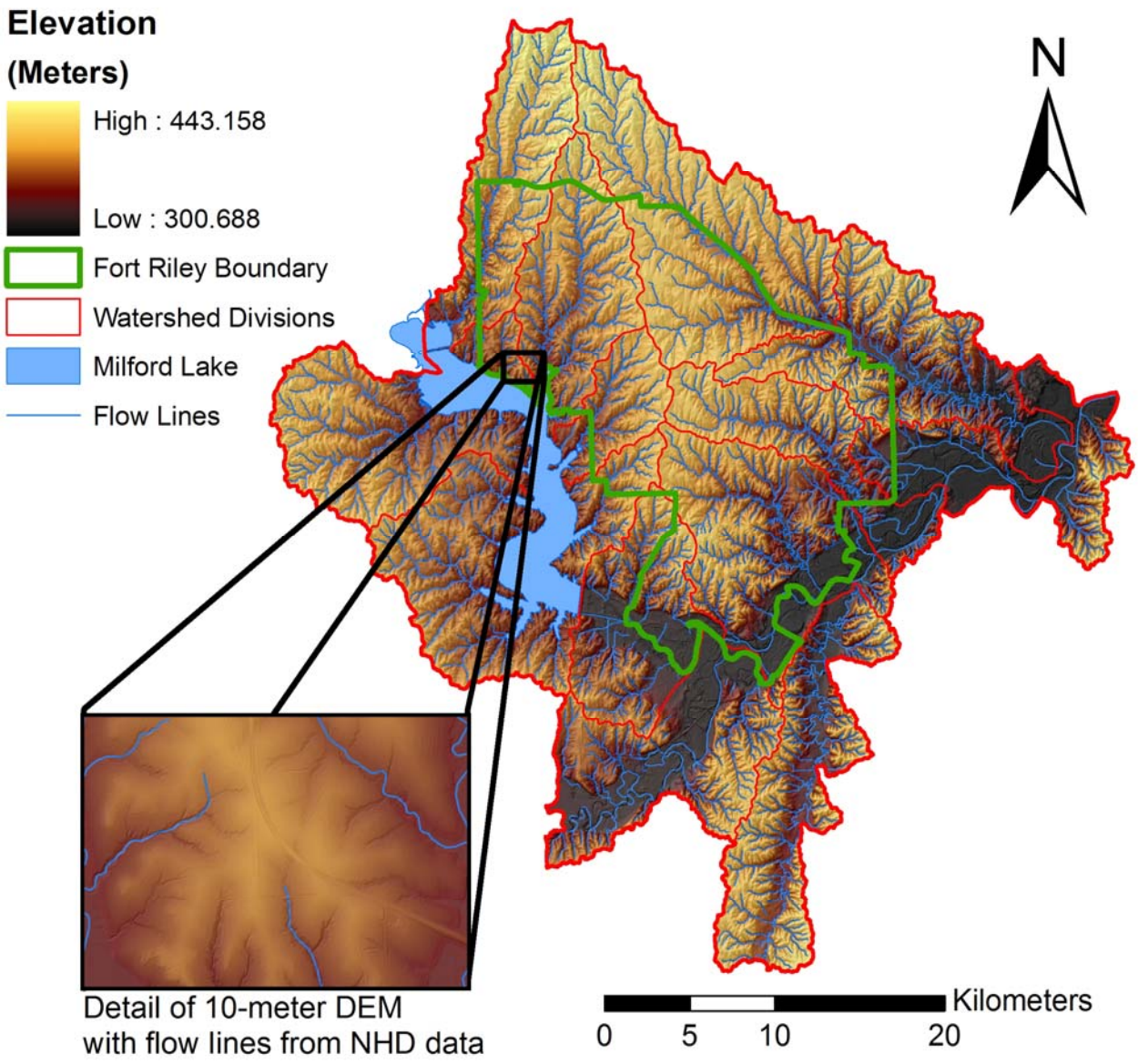

Figure 4.4 Landuse/landcover data for Fort Riley, Kansas.

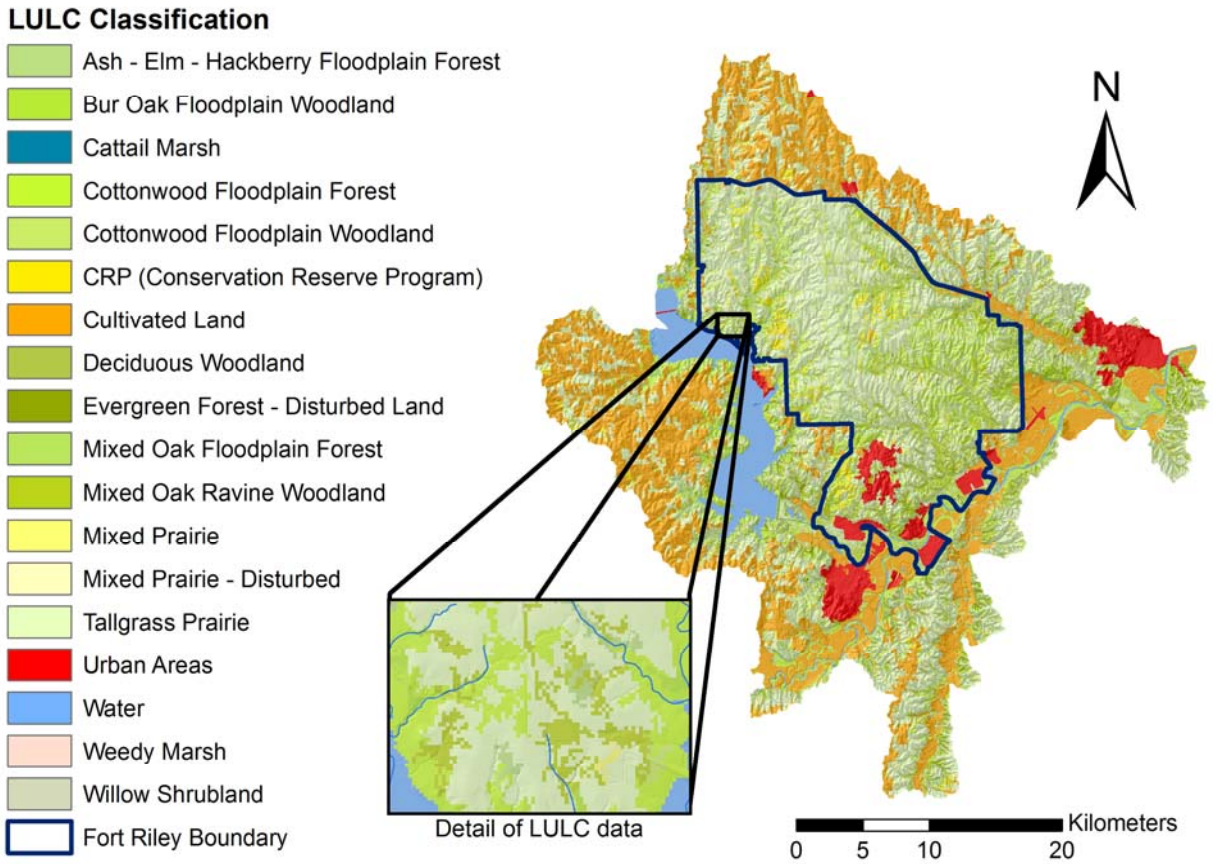

Input data for Cheney watershed include a 10-meter DEM taken from the USGS National Elevation Data (Figure 4.5) and LULC classifications obtained from Kansas GAP data (Figure 4.6). DEM values range from 433 m to 669 m in elevation for the study area. LULC data includes 25 separate LULC classifications for the study area. The Cheney watershed is divided into subwatersheds, based on HUC 14 delineations.

Figure 4.5 Elevation and hydrologic data for the Cheney watershed, Kansas.

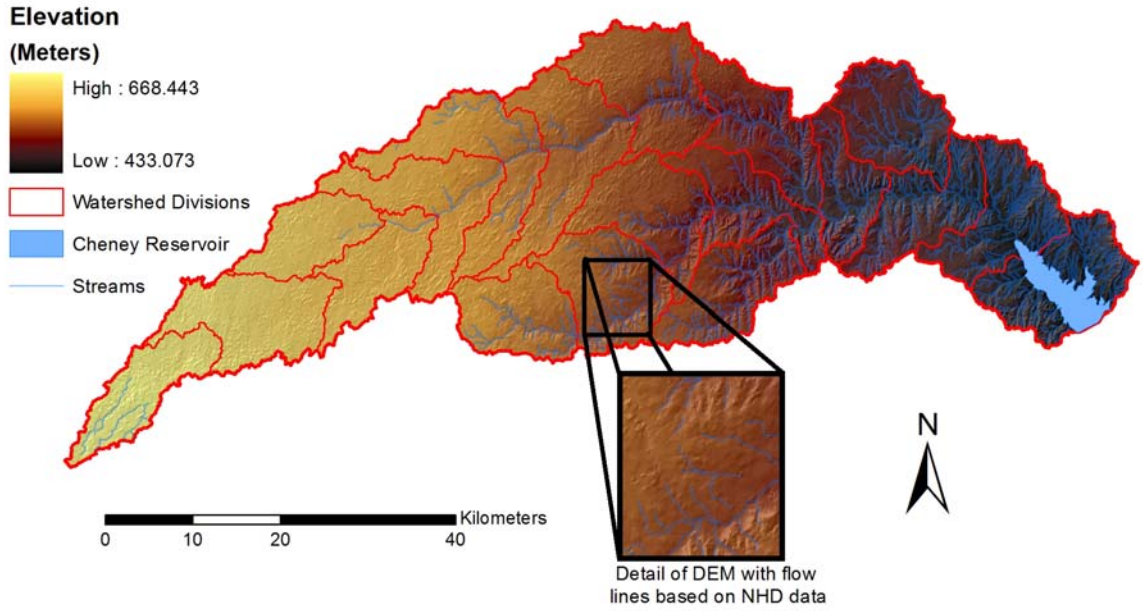

Figure 4.6 Landuse/landcover data for Cheney Watershed, Kansas.

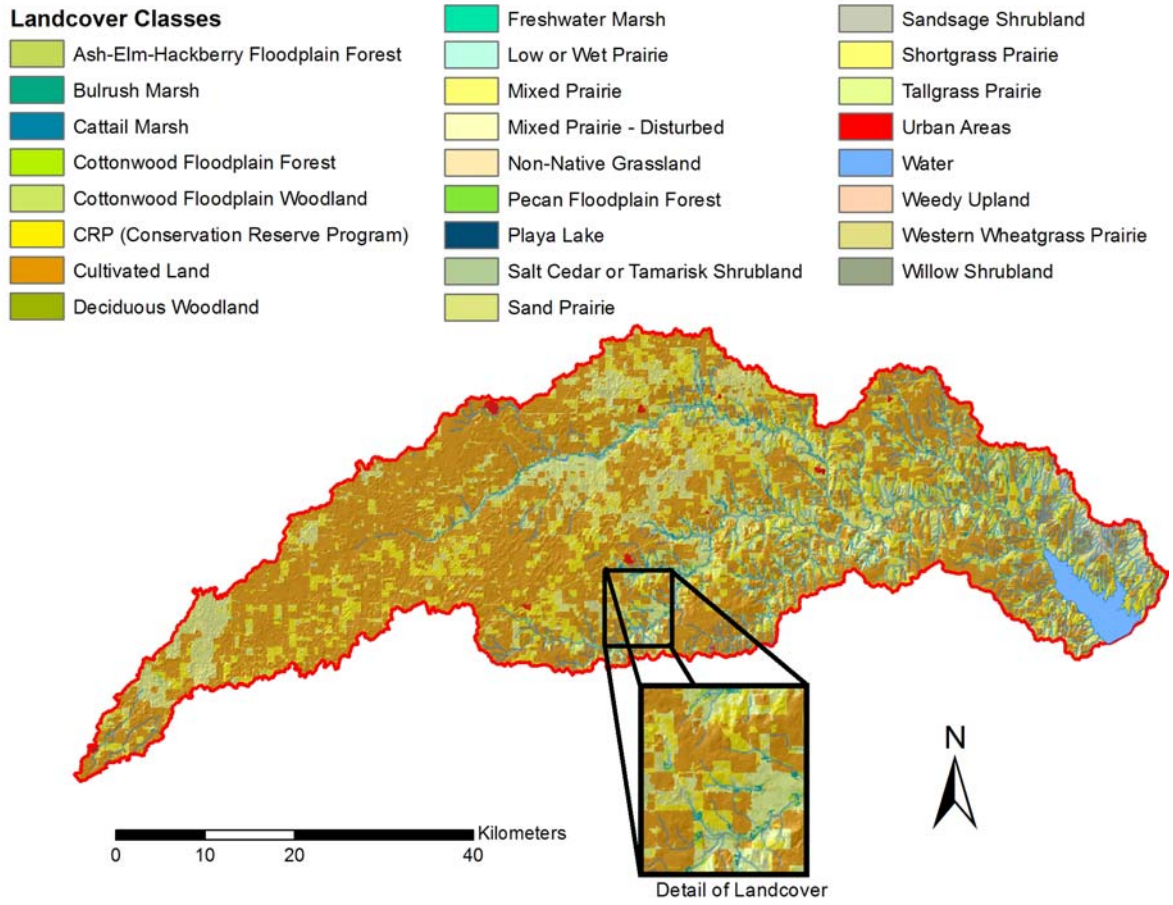

Input data for KP includes a 10-meter DEM obtained from USGS National Elevation Data (Figure 4.7) and LULC classifications obtained from the Hawaii GAP data (Figure 4.8). DEM values range from Sea level to 1866 m in elevation for the study area. LULC data includes 10 separate LULC classifications for the entire watershed. Watersheds that intersect KP were included, based on GDSI (1995) delineations.

Figure 4.7 Elevation and hydrologic data for Keamuku Parcel, located on the Big Island of Hawaii.

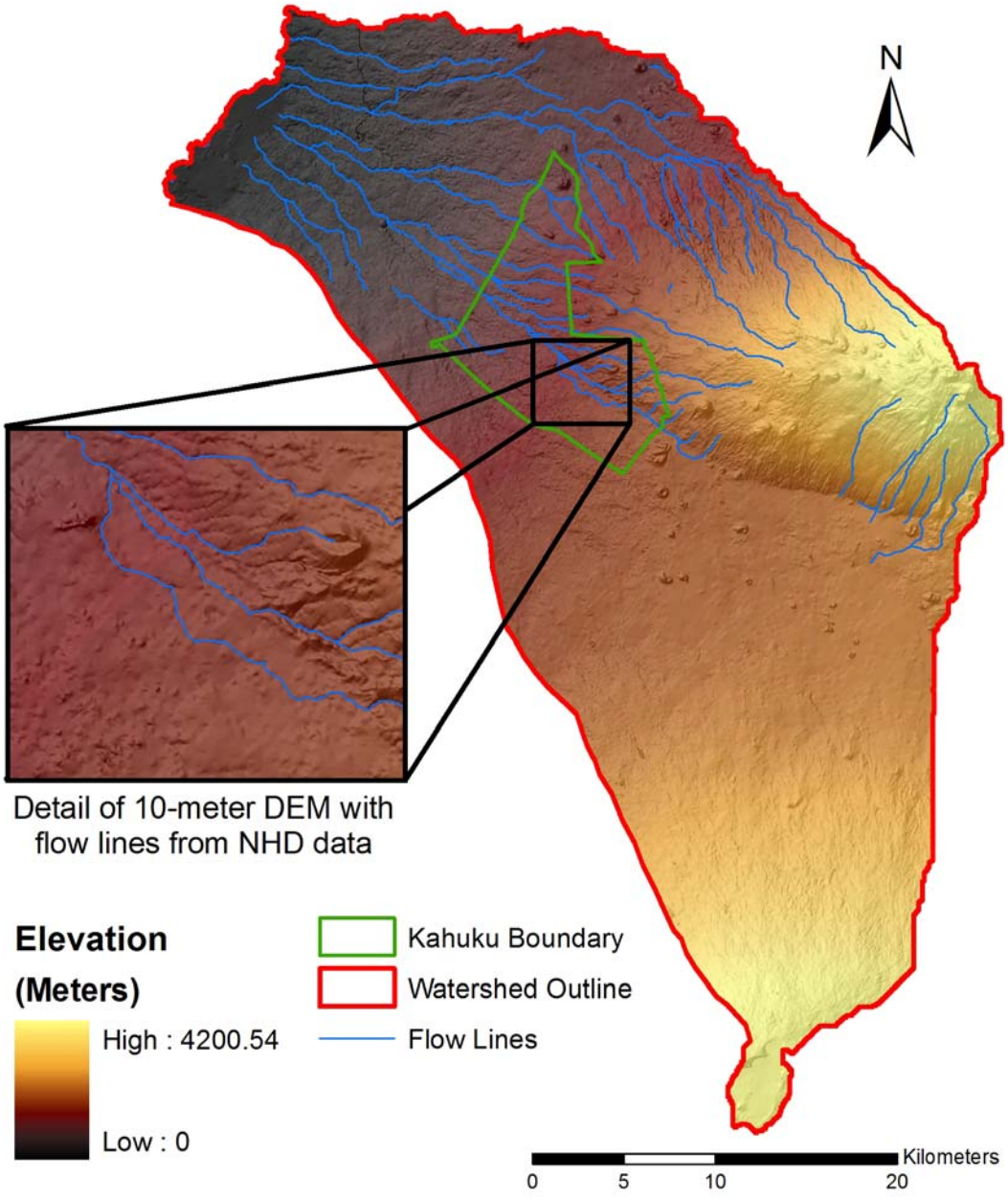

Figure 4.8 Landuse/landcover data for Keamuku Parcel, on the Big Island of Hawaii.

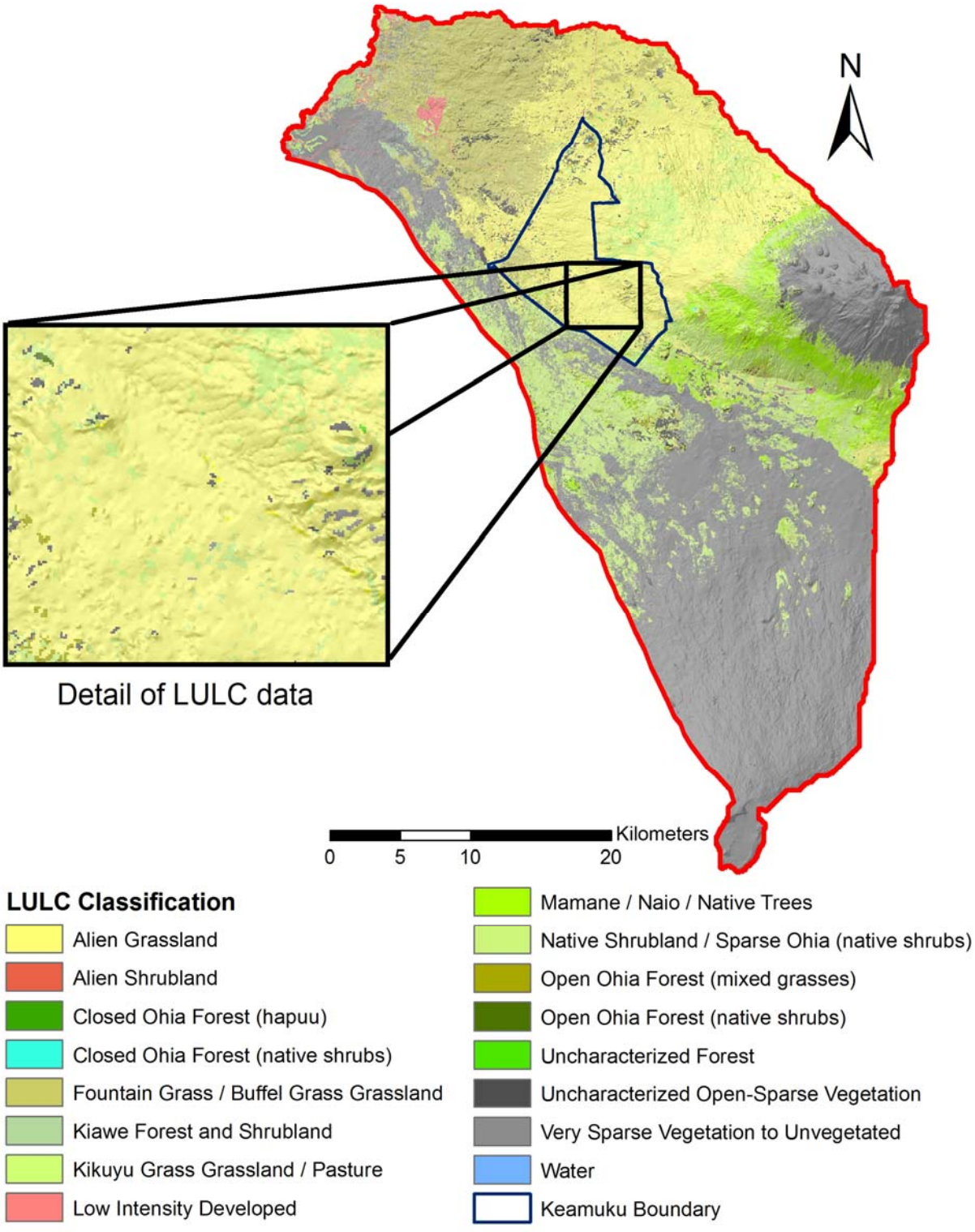

Input data for KTA include a 10-meter DEM taken from the USGS National Elevation Dataset (Figure 4.9). LULC classifications were obtained from the ITAM office for areas in and around the installation boundaries, and from Hawaii NLCD data for the remaining areas (Figure 4.10). DEM values range from sea level to 709 m in elevation for the entire watershed. LULC data includes 25 separate LULC classifications for the entire watershed area. Watersheds that intersect KTA were included in the analysis of the study area, based on GDSI (1995) delineations.

Figure 4.9 Elevation and hydrologic data for Kahuku Training Area, Hawaii.

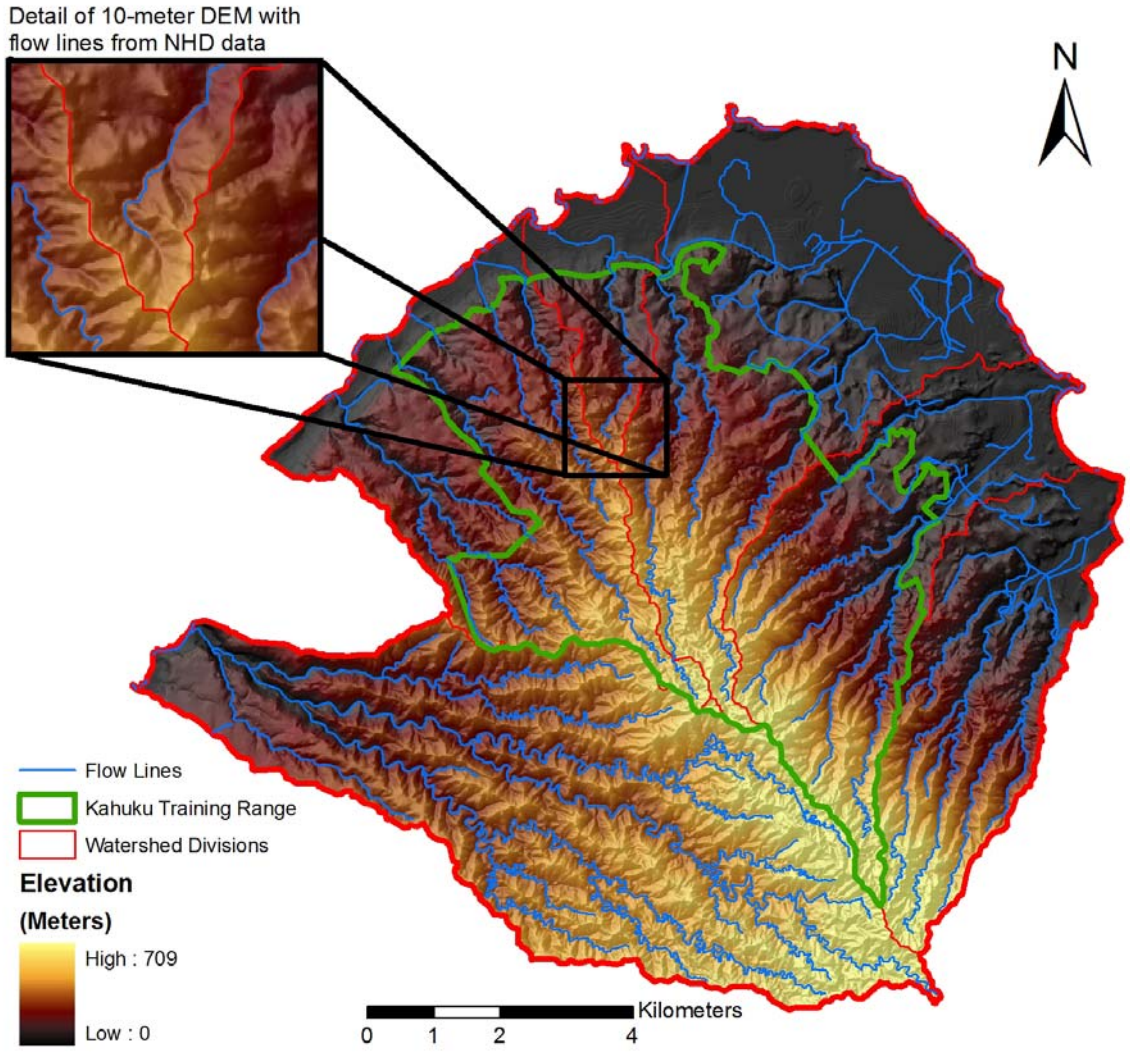

Figure 4.10 Landuse/landcover data for Kahuku Training Area, Hawaii.

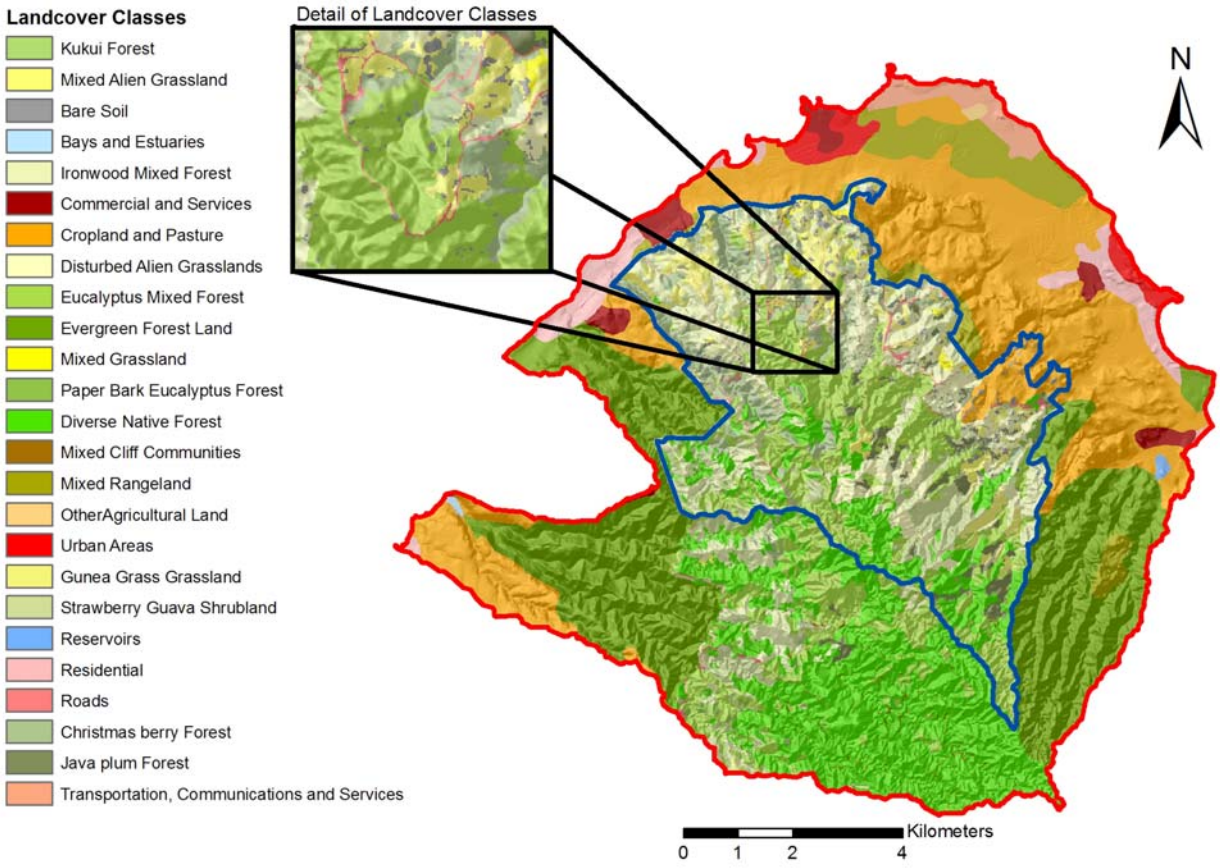

Within the GIS environment, the elevation data was used with the "slope" tool to calculate percent slope, which was then converted into slope grade, in feet per feet. In addition, the elevation data was also used to calculate flow accumulation within the study area using the "flow direction" and "flow accumulation" tools. The LULC data was used to estimate Manning's surface roughness coefficients. As the vegetative cover for a given LULC increases, the surface roughness increases as well. Chow (1959) determined a range of Manning's coefficients associated with a variety of LULC classifications (Table 4.2). Based on these associations, the table of Manning's roughness coefficients was related to the LULC divisions using a "reclassify" tool within the GIS environment.

Table 4.2 Reference table of Manning's roughness coefficients for general landcover/landuse classification (Chow, 1959).

Landuse/Landcover Description	Minimum n	Normal n	Maximum n
Pasture, no brush			
1.short grass	0.025	0.03	0.035
2. high grass	0.03	0.035	0.05
Cultivated areas			
1. no crop	0.02	0.03	0.04
2. mature row crops	0.025	0.035	0.045
3. mature field crops	0.03	0.04	0.05
Brush			
1. scattered brush, heavy weeds	0.035	0.05	0.07
2. light brush and trees, in winter	0.035	0.05	0.06
3. light brush and trees, in summer	0.04	0.06	0.08
4. medium to dense brush, in winter	0.045	0.07	0.11
5. medium to dense brush, in summer	0.07	0.1	0.16
Trees			
1. dense willows, summer, straight	0.11	0.15	0.2
2. cleared land with tree stumps, no sprouts	0.03	0.04	0.05
3. same as above, but with heavy growth of sprouts	0.05	0.06	0.08
4. heavy stand of timber, a few down trees, little undergrowth, flood stage below branches	0.08	0.1	0.12
5. same as 4. with flood stage reaching branches	0.1	0.12	0.16

Model Implementation

The nLS model was implemented in the ArcGIS 9.3.1 GIS program developed by the Environment System Research Institute (ESRI, Redlands, CA). By integrating the DEMs and LULC spatial data into a GIS-based algorithm, large amounts of data can be processed to calculate the soil erosion potential for a study area. The ESRI ModelBuilder was used in the ArcGIS system to develop and refine the nLS model for analysis.

To prepare the input parameters for data processing, several steps were taken. First, the data was project to the appropriate coordinate system for each site. The LULC data and DEMs were clipped to match the boundaries of the contributing watersheds for each study area. In addition, the LULC data was converted from a shapefile format to a raster dataset in order to

make use of ArcGIS's raster calculator functions. Once the inputs were prepared, they were introduced into the model.

ArcGIS provides users with a variety of tools that can be utilized to calculate the properties of a surface represented by raster datasets. In the most basic model, the DEM was used to obtain slope values, length, flow direction, and flow accumulation. The LULC raster was used to derive corresponding Manning's roughness coefficients. Once these values were obtained, raster calculations can be used to obtain the nLS value. The fundamental version of the model is represented as a diagram (Figure 4.11), with model inputs represented as blue circles, ArcGIS tool functions represented as yellow squares, and derived datasets represented as green circles.

Figure 4.11 Illustration of the basic nLS model, divided into five processing steps: Manning's n reclassification, slope calculation, flow direction determination, individual nLS calculations, and output nLS accumulation.

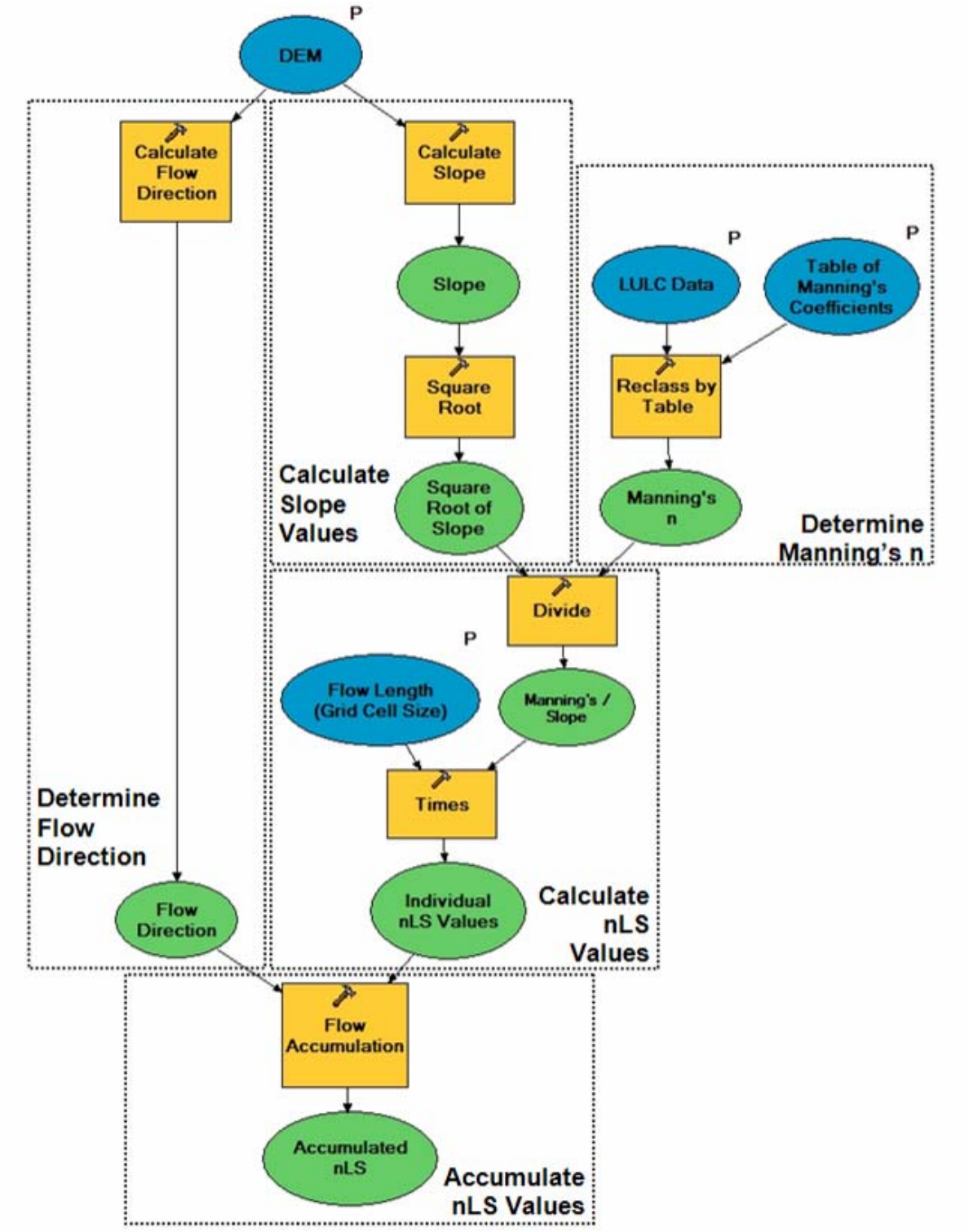

Sensitivity Analysis

To test the impacts of the model parameters on the overall model performance, sensitivity analyses were run on several components of the model (Table 4.3). Input parameters, including elevation and LULC data, were modified to determine the effects of these values on the model. In addition, adjustments of the nLS threshold value were investigated. Finally, the model operations were revised to examine the impacts on model efficiency and accuracy.

Table 4.3 Summary of parameters used for sensitivity analyses performed on nLS model.

Analysis	Model Parameters			
	Input DEM	*Input LULC*	*Derived Manning's n*	*Model Calculations*
Slope Sensitivity	Modified by intervals of 10%	Original LULC Data	Normal Manning's n	Original Model
LULC Distribution	Original DEM	Modified Spatial Distribution	Normal Manning's n	Original Model
Manning's n Classification	Original DEM	Original LULC Data	Range of Manning's n	Original Model
Modified Model Processes	Original DEM	Original LULC Data	Normal Manning's n	Alternative Calculations

Input Slope Parameter

An IPP analysis on the slope input parameter was completed using data from KTA on the island of Oahu. The original LULC data was used to determine the Manning's n value, while the DEM was adjusted from 10% of the original elevation up to 200% using intervals of 10%. Modifying the DEM in this way effectively changed the slope for the study area. The model used for the analysis is illustrated in Appendix A -. For each modified DEM, the response of the nLS model was evaluated by examining points with an nLS value of 100 for the original slope

values. By analyzing the change in nLS values at these points, the impacts of steeper slopes could be compared to those of flatter slopes.

Elevation Data Error

In addition to the effects of a uniform modification of slope, the model's sensitivity to DEM error was analyzed. According to the USGS, national elevation data can vary as much as 15 meters from the published value. The actual accuracy depends on the original DEM source and the resolution level. For the 10-meter resolution data, the vertical accuracy was estimated to be plus or minus 7 meters (http://seamless.usgs.gov). To determine the effects of this potential error, the original DEM was modified based on this range of error. A model was developed that would alter the DEM by randomly assigning new elevation values within ± 7 meters of the original value. A Monte Carlo simulation was completed by repeating the random assignment of elevation values 20 times. Once the simulation was complete the model outputs were examined. By analyzing the impacts of randomly assigning DEM values within a given range, the importance of accurate elevation data can be assessed.

Input Landuse and Landcover Distribution

Sensitivity analyses were performed on the LULC input parameter at KTA. The original 10-meter DEM was used to determine slope and flow length values for the model. For LULC parameters, two analyses were done. The first analyzed the spatial arrangement of the individual LULC classes with the study area watershed. For the current nLS model, it is unclear how the location and spatial arrangement of LULC classes within a watershed impacts the resulting "downstream" nLS values. To examine this problem, new and different LULC maps were created using a random raster creation function in the GIS environment. A Monte Carlo analysis

was performed on the LULC distribution by repeating the random LULC creation several times to create ten LULC layers. Each of these LULC layers had similar total areas for each LULC class but different spatial arrangements of individual LULC pixels. The model was run and the nLS values at fixed locations were analyzed, in addition to the contributing LULC for those points. By changing the arrangement of the LULC pixels while keeping the same total area for each LULC class, it was possible to observe the effects of the spatial location of a LULC class on resulting nLS values.

Manning's n Parameter

The second analysis of nLS model sensitivity to the LULC input parameter examined the impacts of selecting an appropriate Manning's n value for a given LULC class. For each LULC class present at the KTA study area, a range of Manning's roughness coefficient values was determined. In the original nLS model, design a single Manning's n to all raster cells of each LULC class. Here, the nLS model was changed so that each raster cell was randomly assigned one Manning's n value from the predetermined range of values appropriate for a given LULC class at KTA (Table 4.4). These values were based on the reference values previously discussed (Table 4.2). Once the Manning's n values were assigned, the nLS model was run and the potential erosion areas were obtained using a threshold value of 100. A Monte Carlo simulation was performed by repeating this process 100 times, thereby allowing the model output to be analyzed for sensitivity to the Manning's n roughness coefficient input. By analyzing the impacts of randomly assigning Manning's n values within a given range, the importance of an accurate Manning's n value was assessed.

Table 4.4 Manning's n values associated with landuse/landcover classifications for Kahuku Training Area (Chow, 1959).

Landuse/Landcover Description	Manning's n Values		
	Minimum	Normal	Maximum
Bare Soil	0.02	0.03	0.04
Kukui Forest	0.11	0.15	0.2
Mixed Alien Grassland	0.03	0.035	0.05
Bays and estuaries*	0.075	0.1	0.15
Ironwood Mixed Forest	0.08	0.1	0.12
Commercial and Services*	0.01	0.015	0.02
Cropland and pasture*	0.02	0.03	0.04
Disturbed Alien Grasslands	0.025	0.03	0.035
Eucalyptus Mixed Forest	0.11	0.15	0.2
Evergreen forest land*	0.11	0.15	0.2
Haole koa / Guinea grass Mixed Grassland	0.03	0.035	0.05
Paper bark eucalyptus Forest	0.11	0.15	0.2
Ohi'a / Acacia koa / Uluhe Diverse Native Forest	0.1	0.12	0.16
Mixed Cliff Communities	0.03	0.04	0.05
Mixed Rangeland*	0.04	0.06	0.08
Other agricultural land*	0.02	0.03	0.04
Other urban or built-up land*	0.04	0.08	0.12
Guinea grass Grassland	0.03	0.035	0.05
Strawberry guava Shrubland	0.07	0.1	0.12
Reservoirs*	0.075	0.1	0.15
Residential*	0.04	0.08	0.12
Roads	0.01	0.015	0.02
Christmas berry Forest	0.04	0.06	0.08
Java plum Forest	0.04	0.06	0.08
Transportation, communications and services*	0.03	0.05	0.07

*LULC taken from National Landcover Dataset (NLCD). These areas are located within the surrounding watershed, but outside of base's more detailed vegetative classification.

Output Threshold Value

In addition to analyzing the input parameters, the magnitude of the critical threshold value was also examined using a simple IPP analysis. Adjusting the threshold value has no impact on the calculation of the nLS values, but the location of the resulting threshold points, where the critical value is realized, will shift up- or downslope according to the adjusted threshold value. To test the impacts of this parameter, the model was run two separate times and the output grid queried to identify where each threshold value was located. For the first run, a

threshold value of 100 was used, as suggested by McCuen and Spiess (1995). For the second run, a threshold value of 131 was used, as suggested by Kim (2006). The results were then compared to evaluate how the choice of a threshold value influences the resulting prediction of potential soil erosion.

Variation in Model Calculations

The calculation of nLS values within the model were also examined in this study. To test alternative methods of calculating nLS values, the input parameters were utilized in several different ways within the model. To test these variations, it is important to understand the mathematics of the nLS model itself. The model, as previously described, can be summarized by the equation:

$$(nLS)_{Existing} = Accumulated\left[\frac{(Cell\ n) * (Cell\ Length)}{\sqrt{Cell\ Slope}}\right] = \sum \frac{n_i L_i}{\sqrt{S_i}} \qquad [3]$$

where $(nLS)_{Existing}$ is the nLS value obtained using the original nLS model, n is the Manning's n coefficient, L is the flow length (feet), S is the slope for an individual grid cell (feet per feet), and i is a variable used to index the grid cells in a contributing watershed.

Through the use of the model (Figure 4.11) Equation 3 was implemented for every point across a landscape, creating an output raster layer of nLS values for an entire study area. This method provides a reasonable estimate that can be used to find areas where water transitions from overland flow to concentrated flow (Kim, 2006). However, the model required noticeable adjustment of the threshold value from just over 100 (McCuen and Spiess, 1995) in the original study to 131 in the original Kansas study site (Kim, 2006). It may be possible to reduce the magnitude of this adjustment by using a model that more closely resembles the original nLS calculations presented in Equation 2.

To investigate the possibility of generating more accurate results, an alternative version of the nLS model was developed that used available GIS tools to calculate average Manning's n and average slope for the upstream watershed of a given cell. The values from this modification may represent Equation 2 more accurately than the existing nLS model. The calculations in this modified version of the model are shown in Equation 4 below.

$$(nLS)_{Alt.} = \frac{(Average\ n) * Total\ L}{\sqrt{Average\ S}} = \frac{\left(\sum n \Big/ Total\ number\ of\ cells\right) * \sum L}{\sqrt{\sum S \Big/ Total\ number\ of\ cells}} \qquad [4]$$

where $(nLS)_{Alt.}$ is the nLS value obtained using the alternative nLS model, and the term "*Total number of cells*" refers to the total number of grid cells in the contributing watershed of a given point in the study area.

Because the accumulation of a given value is equal to the summation of that value with respect to flow direction in ArcGIS (Equation 5), it can be summarized as shown in Equation 6.

$$(nLS)_{Alt.} = \frac{\left(Accumulated\ n \Big/ Accumulated\ Cells\right) * (Accumulated\ L)}{\sqrt{(Accumulated\ S \Big/ Accumulated\ Cells)}}$$

$$= \frac{(Accumulated\ n) * (Accumulated\ L)}{\sqrt{(Accumulated\ S) * (Accumulated\ Cells)}} \qquad [5]$$

$$\left(\frac{nL}{\sqrt{S}}\right)_{Alt.} = \frac{\sum n_i * \sum L_i}{\sqrt{\sum S_i * i}} \qquad [6]$$

Using the same input data as the original nLS model, Equation 6 can be applied to derive an accumulated nLS value everywhere across a study area. This alternative method provides an

nLS value that is derived from the average Manning's n, average slope, and total flow length of the contributing watershed, in contrast to the original model (Equation 3). The magnitude, range, and location of specific nLS threshold values were then compared.

CHAPTER 5 - Results and Discussion

Sensitivity Analysis

Overall, the analyses performed in this study revealed that each of the model input parameters had a significant impact on model outputs. Accurate elevation and LULC data is required to ensure reliable results. Varying slope, elevation, and LULC data can dramatically change the output nLS values, and the Manning's roughness coefficient must be carefully selected for each LULC type. Similarly, the model was highly sensitive to adjustments of the critical nLS threshold value used for identifying areas of transitional flow. In addition, variations in the model calculations used with the model did not indicate any potential to improve model accuracy. The results from each of the four study sites suggest that the model will need to be calibrated for each location to ensure accurate predictions of transitional flow locations.

Input Slope Parameter

The response of the model output to changing elevation inputs clearly follows a power trend (Figure 5.1). The relationship between slope and the nLS output, as determined by the input elevation data, can be described by the equation below:

$$(nLS)_{\text{mod}} = \frac{100}{\sqrt{S_{ratio}}} \quad (R^2 = 0.9999) \qquad [7]$$

where $(nLS)_{\text{mod}}$ is the nLS value obtained using the modified elevations and S_{ratio} is the ratio of the modified slope to the original slope (S_{mod}/S_0), which was varied from 0.10 to 2.00.

Figure 5.1 Graph of the nLS model response to changing slope values during the slope sensitivity analysis.

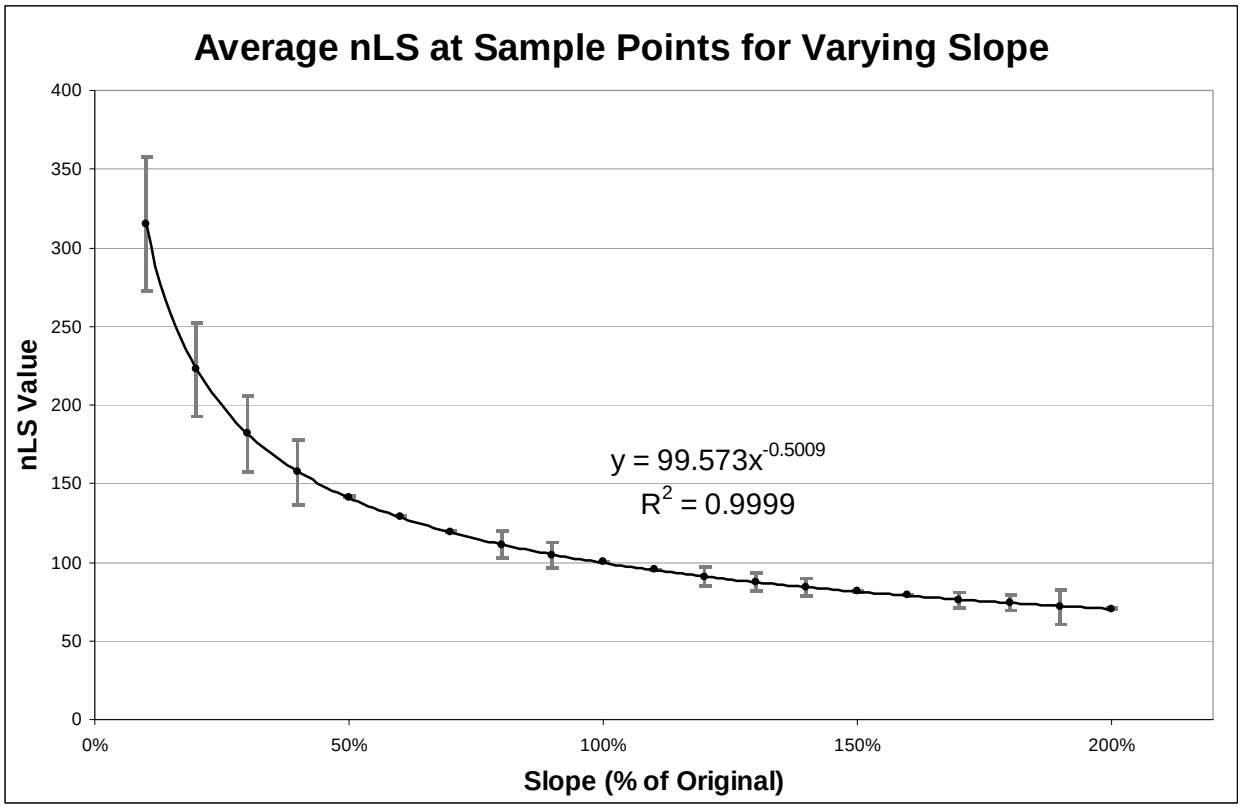

This result was expected due to the way slope was implemented in the model (Equation 2). The value of 100 corresponds to the initial nLS value of 100 for the observed points with the original DEM data. By back calculating, it is possible to derive the original nLS equation. Since Manning's n and flow length values were not changed, and since 100 was the original nLS value,

$$(nLS)_0 = \frac{nL}{\sqrt{S_0}} = 100 \qquad [8].$$

where $(nLS)_0$ is the nLS value obtained using the original elevation, n is the Manning's roughness coefficient, L is the flow length, and S_0 is the slope obtained using the original DEM.

Substituting Equation 8 into Equation 7 yields

$$(nLS)_{\text{mod}} = \frac{100}{\sqrt{S_{ratio}}} = \frac{nL/\sqrt{S_0}}{\sqrt{S_{ratio}}} \qquad [9].$$

Replacing S_{ratio} with the slope values S_{mod} and S_0, Equation 9 becomes:

$$(nLS)_{\text{mod}} = \frac{nL / \sqrt{S_0}}{\sqrt{S_{\text{mod}} / S_0}} = \frac{nL}{\sqrt{S_{\text{mod}}}} \quad [10].$$

where S_{mod} is the slope obtained using the modified DEM. This result is equivalent to Equation 2 using an alternative value for slope.

From this derivation, it becomes apparent that adjusting the slope across a watershed will modify the nLS value in a way that directly corresponds to the slope value in Equation 2. This suggests that the nLS model implements slope in a way that correctly corresponds to the nLS equation. While the overall trends for nLS outputs caused by a changing slope value can be easily predicted, there were several values from the sample points that were well outside the expected value. Nearly all of the standard deviation (Figure 5.1) can be explained by these outlying points. The points seem to be clustered in the lower watersheds of the study site, away from the more mountainous areas (Figure 5.2). This suggests that the model is especially sensitive to areas with lower slope values, where the nLS outputs are more variable. Because of this, study areas located in areas with a flatter topography, like Kansas, may experience more variability in the nLS outputs, so the input LULC data will play a large role in the output nLS values. Steeper areas, like the volcanic terrain of Hawaii, will have less variability, and LULC will play a smaller role because slope is the driving factor for the nLS output.

Figure 5.2 Location of the observation points used for the slope sensitivity analysis. Red points indicate observation points with nLS values that did not follow the nLS equation.

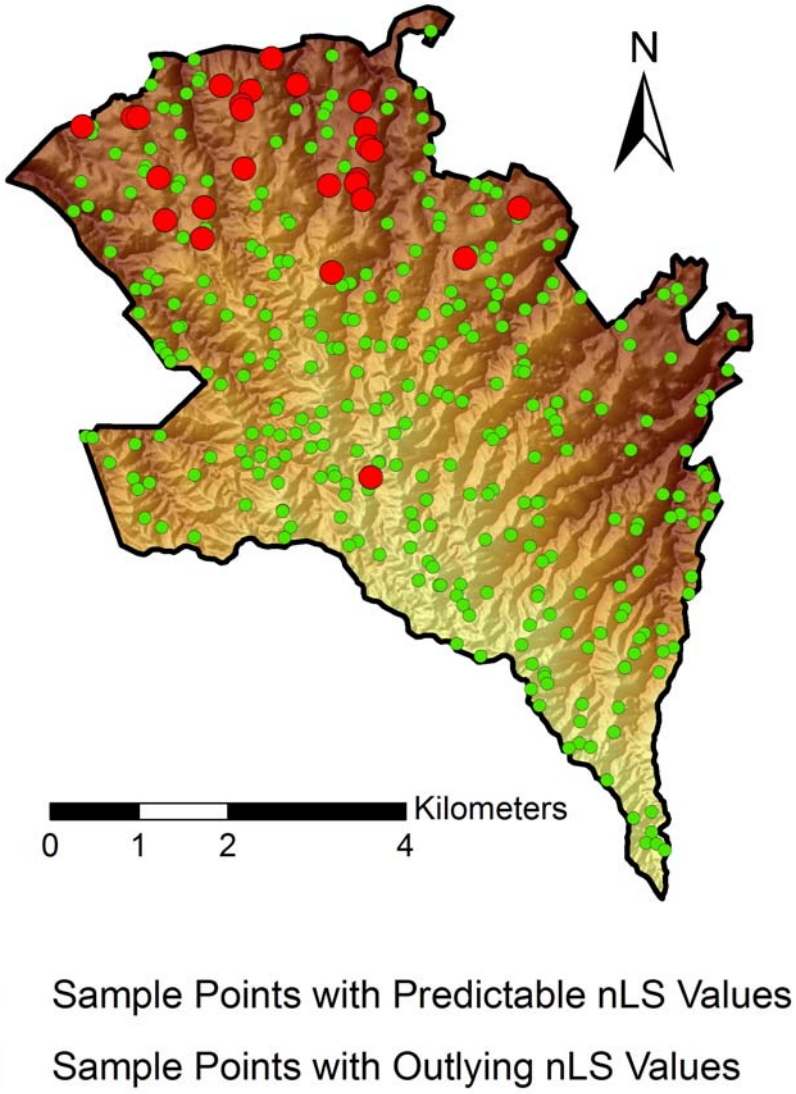

Upon examination, it was determined that the outlying points were located in smaller reaches of the watersheds in the lowland areas of the study site. These areas were typified by lower slope values. To evaluate the cause for the unusual nLS values, the flow was analyzed across each of the modified DEMs. By implementing flow analysis tools in ArcGIS, the flow paths for each DEM were determined using a 1000 m^2 watershed for initial flow. While certain areas had consistent flow, other areas had fluctuating flow tendencies (Figure 5.3). In the image,

blue areas represent locations that were consistent flow paths for all modified DEMs, white areas represent consistent sheet flow, while yellow and red areas represent fluctuating flow paths. Observation points analyzed in the study are displayed as green circles. The analysis showed that modifying the DEM caused changes in flow paths, which was an unexpected effect. In addition, the observation points that experienced unusual nLS values were consistently located in reaches that have fluctuating flow paths. This trend suggests that the unexpected nLS values of the analysis were a result of variations in the surface modifications, and do not reflect any errors in the model calculations. It also illustrates that change in elevation values in areas of lower slope, whether purposely manipulated or caused by DEM error, have a greater impact on the resulting flow paths.

Figure 5.3 Variations in the flow network caused by uniform DEM modifications. The majority of the area is either consistent flow (blue) or lack of flow (white). A small portion experienced fluctuating flow paths (yellow to red).

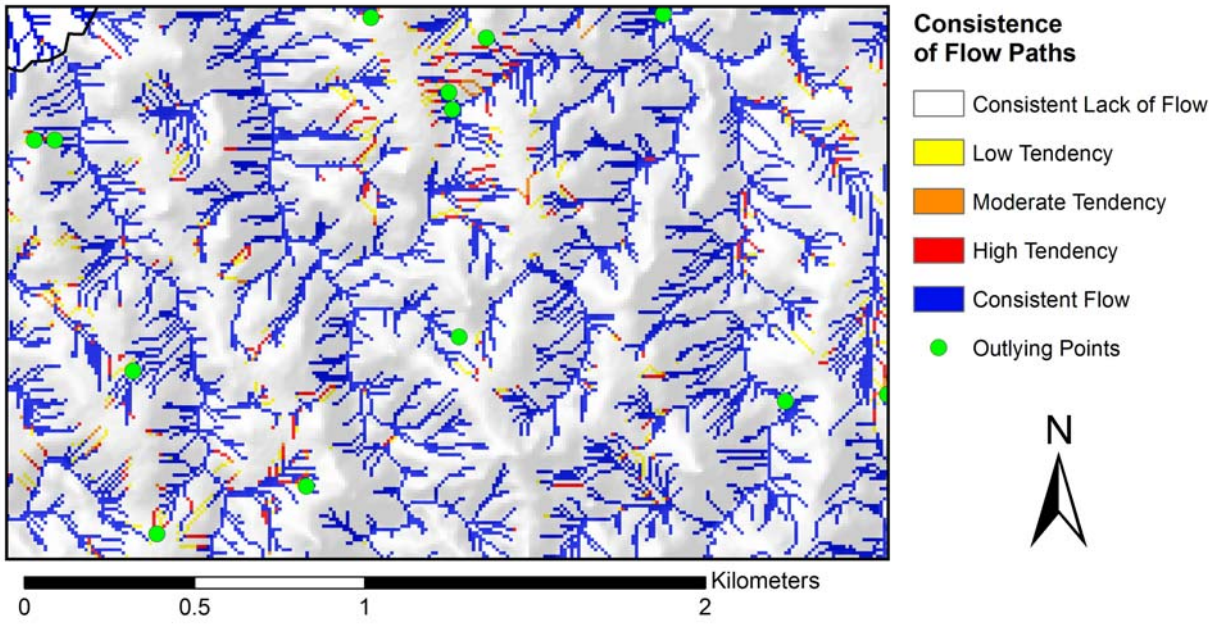

For a statistical analysis, the contributing area of the initial stream network was defined as $100m^2$, and the resulting stream network was analyzed (Table 5.1). The majority of the study area experienced either consistent flow or no flow, accounting for 99% of the entire site. However, the remaining 1% of the study area experienced flow path fluctuations caused by the DEM modifications. By accounting for these areas, the unusual nLS values observed in the outlying points can be explained as anomalies in the flow path delineations. If these points are excluded, the relationship of slope to nLS output becomes very predictable.

Table 5.1 Summary of the change in flow caused by the uniform slope modifications. The majority of the study area experienced either consistent flow or a lack of flow, and a small percentage (1%) experienced varying flow tendencies.

Flow Description	Area (m^2)	Percent of Total
No Flow	99,950	26.12%
Low Tendency	362	0.09%
.	56	0.01%
.	99	0.03%
.	586	0.15%
.	22	0.01%
.	9	0.00%
.	27	0.01%
.	33	0.01%
.	28	0.01%
Moderate Tendency	12	0.00%
.	23	0.01%
.	140	0.04%
.	33	0.01%
.	13	0.00%
.	11	0.00%
.	477	0.12%
.	163	0.04%
.	72	0.02%
High Tendency	945	0.25%
Consistent Flow	279,560	73.06%
Total:	**382,621 m^2**	**100.00%**

Elevation Data Error

For a Monte Carlo simulation, elevation values were randomly selected within a range of ±7 meters for 25 model runs. The modified DEM was slightly different than the original DEM (Figure 5.4). By selecting the DEM values from an error range, the resulting flow network was highly variable, except for the uppermost regions of the watershed (Figure 5.5). Besides these areas where there was a consistent lack of flow, the majority of the study area experienced some form of fluctuation in the flow tendencies. While flow generally increased in lower portions of the watershed, very few channels experienced flow for every elevation dataset.

Figure 5.4 Sample modification of the DEM during a Monte Carlo simulation, in which each raster cell was assigned the original elevation data ±7 meters.

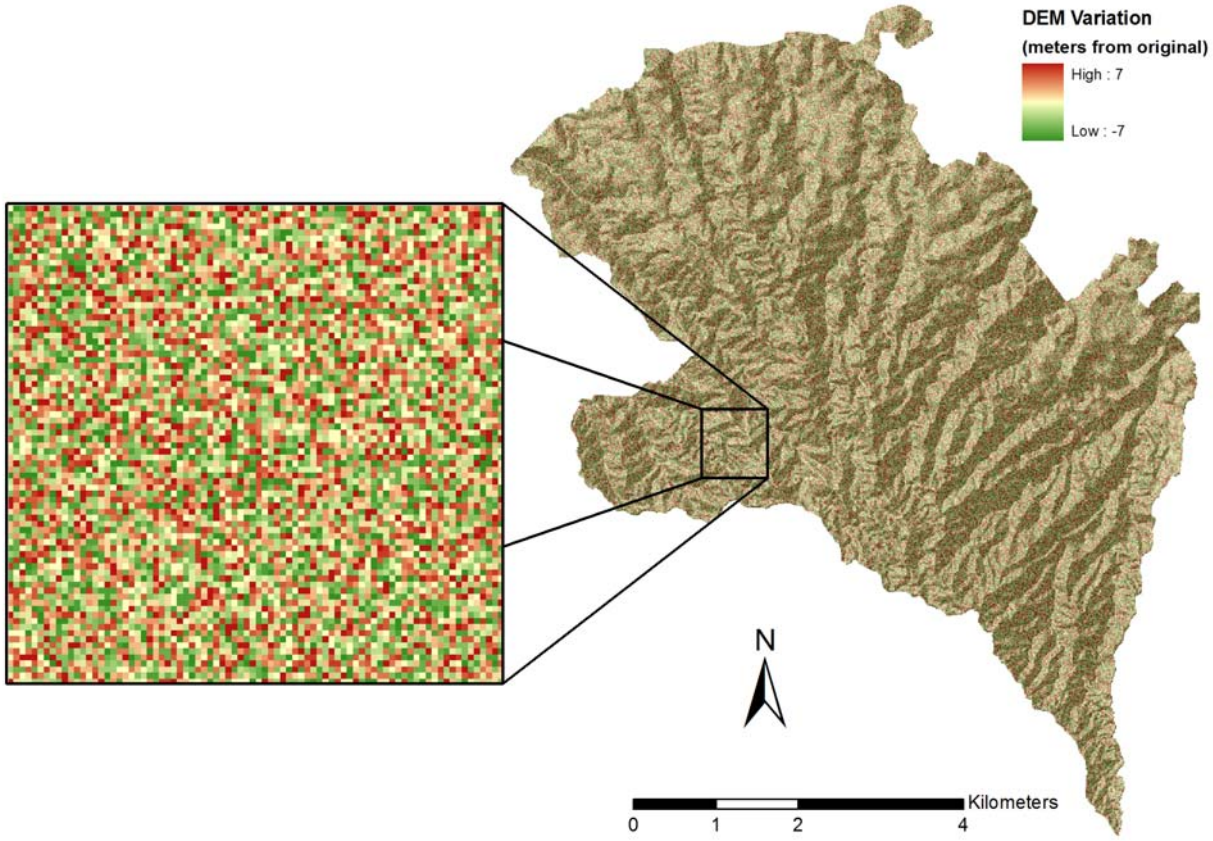

Figure 5.5 Variations in the flow network caused by DEM modification based on DEM error, with flow paths for the original DEM. The majority of the area experienced fluctuations in flow (yellow to red).

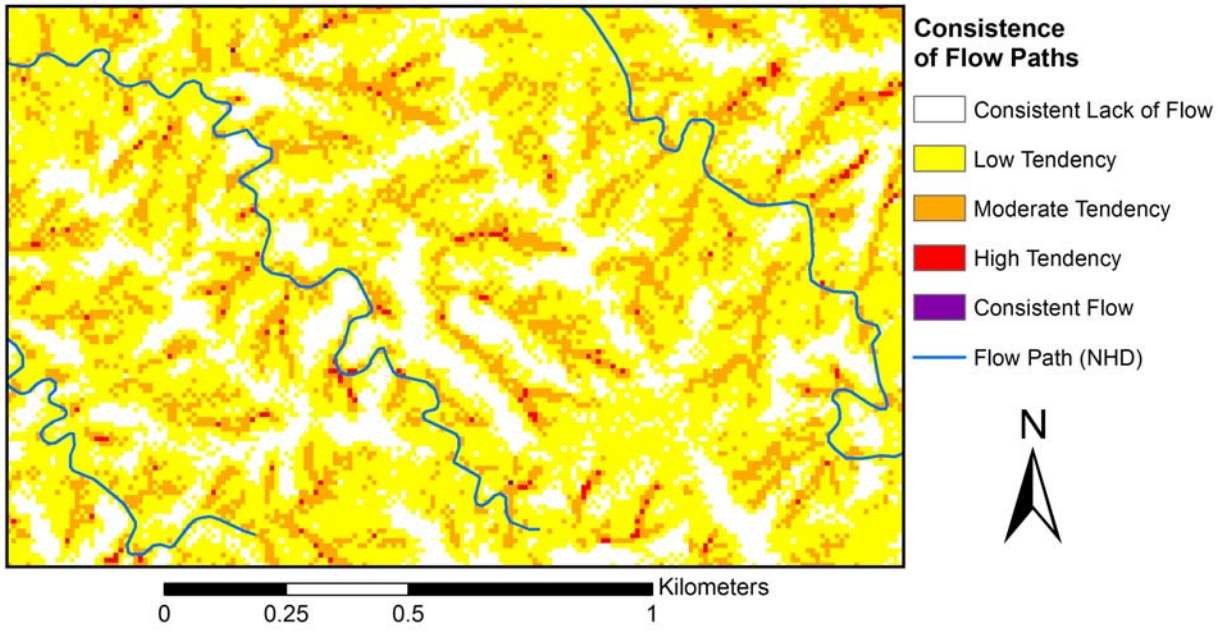

Because DEM error has the potential to cause such significant geographic variations in the flow network, it is important to obtain the most accurate DEM that is available for a study site. While there was a large change in the flow network, this change was less intense in the upstream portions of the watershed, where flow has not accumulated yet (Figure 5.5). Because of this, the error associated with the DEM may have less of an impact on the nLS model, since transitional erosion areas occur primarily in the upstream watersheds. However, accurate elevation data is still vital for accurate nLS output. This analysis, along with the IPP analysis performed on slope, demonstrate the importance of accurate flow paths for the nLS model to operate effectively.

Spatial Arrangement of Landuse/Landcover

Ten LULC maps, based on randomly generated rasters, were created for KTA such that each new raster contained approximately the same area for each of the 14 LULC classes present within the study area. While the total area of each class was similar (Table 5.2), the exact spatial arrangement of individual pixels was varied randomly. An observation point with a large contributing watershed was selected to provide comparisons of the accumulated nLS value after each model run using as input the ten different LULC rasters.

Table 5.2 LULC class and area for ten randomly generated landuse/landcover (LULC) maps, including the resulting accumulated nLS value at a single sample point.

LULC Distribution No.	Percent of Total Area for each Landuse/Landcover lass														Output nLS Value (X 10^{-3})
	Mixed Cliff Communities	*Mixed Grassland*	*Bare Soil*	*Guinea grass*	*Java plum Forest*	*Mixed Alien Grassland*	*Diverse Native Forest*	*Eucalyptus Mixed Forest*	*Ironwood Mixed Forest*	*Christmas berry Forest*	*Strawberry guava Shrubland*	*Disturbed Alien Grasslands*	*Cropland and pasture*	*Roads*	
1	0.01	0.12	0.71	2.90	8.09	15.89	22.38	22.14	15.62	8.17	3.06	0.75	0.13	0.02	217.3
2	0.02	0.17	0.81	3.01	8.06	15.80	22.16	22.25	15.90	7.89	2.98	0.77	0.16	0.02	216.4
3	0.02	0.14	0.74	2.83	8.38	15.81	21.87	22.42	15.91	8.04	2.88	0.79	0.14	0.02	216.7
4	0.03	0.15	0.74	2.87	7.89	15.82	22.10	22.56	15.82	8.22	2.81	0.83	0.13	0.01	217.5
5	0.03	0.11	0.77	2.94	8.04	15.86	21.90	22.19	16.11	8.04	3.05	0.80	0.13	0.01	217.1
6	0.01	0.12	0.78	2.92	8.10	15.71	22.40	22.08	16.00	8.06	2.96	0.75	0.11	0.01	217.0
7	0.02	0.15	0.76	2.90	7.88	15.82	22.32	22.05	16.26	8.15	2.76	0.76	0.18	0.01	217.1
8	0.02	0.12	0.82	2.90	8.15	15.77	22.40	22.27	15.61	8.15	2.89	0.75	0.12	0.02	217.3
9	0.02	0.13	0.75	2.88	8.00	15.62	22.30	22.19	15.82	8.20	3.10	0.85	0.13	0.01	217.5
10	0.02	0.11	0.81	2.85	8.06	15.88	22.30	21.85	16.14	8.11	2.95	0.76	0.14	0.02	216.8

Results show that there may be some effects of modifying the LULC distribution within a watershed (Table 5.2). Examining the nLS equation, it is apparent that the distribution will affect the final output value. For a given LULC distribution, the nLS equation $\sum n_i L_i / \sqrt{S_i}$

becomes $n_1 L_1 / \sqrt{S_1} + n_2 L_2 / \sqrt{S_2} + n_3 L_3 / \sqrt{S_3} + \ldots + n_i L_i / \sqrt{S_i}$. If the LULC distribution is varied such that $n_3 L_1 / \sqrt{S_1} + n_1 L_2 / \sqrt{S_2} + n_1 L_3 / \sqrt{S_3} + \ldots + n_i L_i / \sqrt{S_i}$, the resulting nLS value will not be equal to that of the initial distribution. However, these effects were found to be negligible (±0.3% of the mean nLS value) and some of this difference may be a result of the slight difference in LULC proportions. Because of this, it is apparent that while the LULC distribution does have an impact on the nLS model, it is not as crucial for estimating the nLS output value as the other model parameters, as long as the contributing area at a sample point retains the same general distribution of LULC classes.

Manning's n Parameter

Model sensitivity to variation in Manning's n was assessed using the Monte Carlo technique. Manning's n values were randomly selected within a given range (Table 4.4) for a total of 100 model runs. A sample Manning's n output (Figure 5.6) illustrates the change in the Manning's n distribution. By selecting the Manning's n value from a range, the spatial distribution of the surface roughness coefficients becomes less homogeneous, giving the resulting map a coarse appearance which may better represent natural variation in the actual landscape features, and incorporate some amount of uncertainty in the LULC assessment.

Figure 5.6 Sample distribution of the Manning's roughness coefficient, which was randomly assigned within a defined range for each landuse/landcover class.

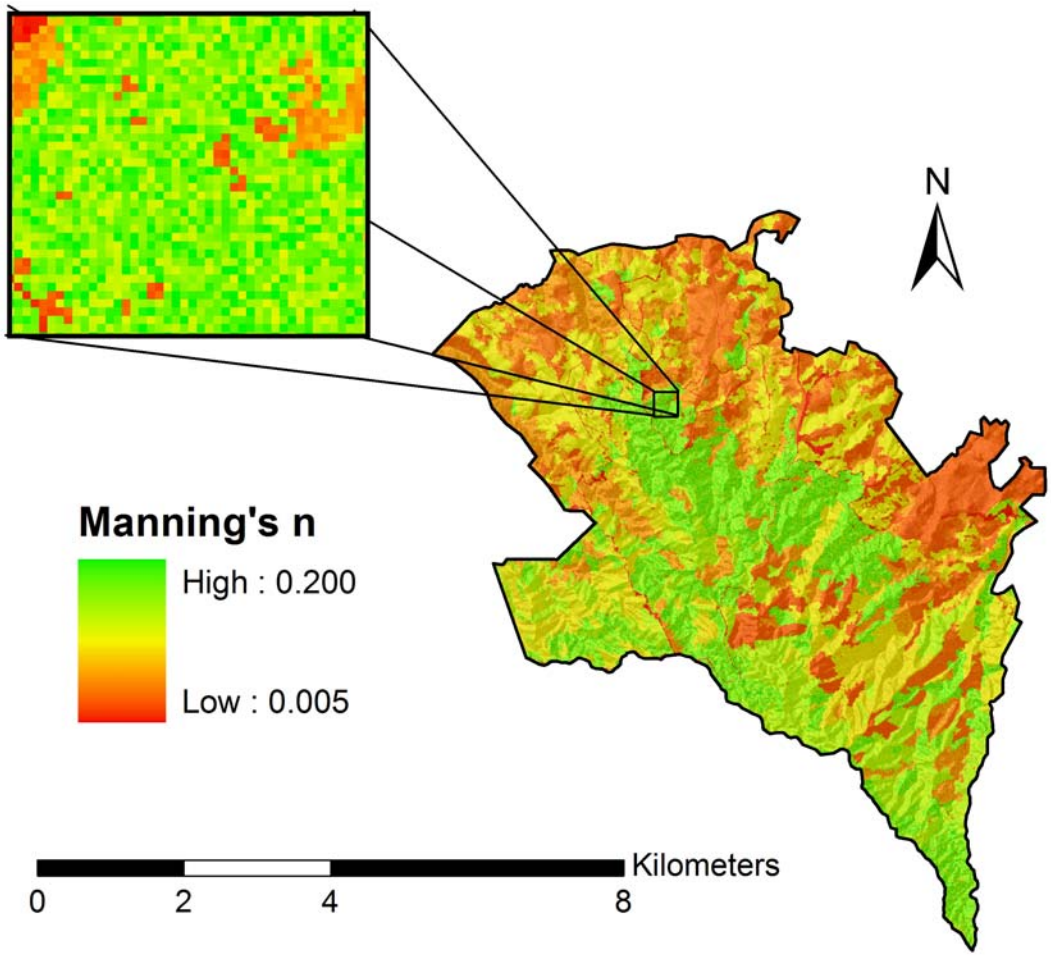

Using a critical nLS threshold value of 100, modifying the Manning's n values had a noticeable effect on the output nLS values (Figure 5.7). For different model runs, the variation in the Manning's n values caused changes in where the critical nLS threshold value was realized. This geographic variability suggests that assigning an accurate Manning's roughness coefficient is vital for accurate model outputs. Because of the significant impact of the roughness coefficient, it may be necessary to adjust the Manning's n value based on seasonal conditions, and more accurate values may need to be obtained for the LULC classes comprising a study area.

Figure 5.7 Shift in output nLS threshold points caused by modifying the uniformity of the Manning's n assignment.

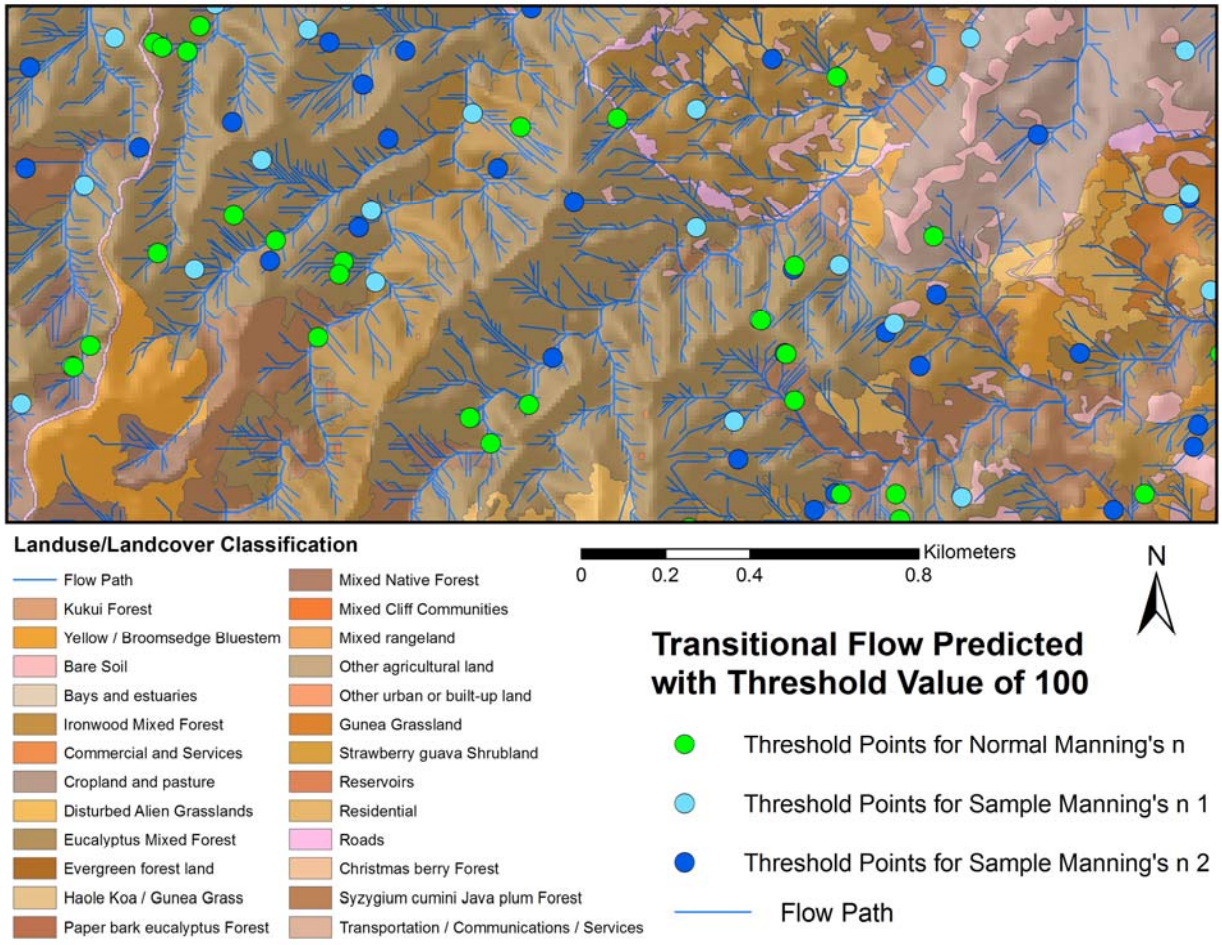

To further analyze the effects of Manning's n, variation in elevation was also examined. To do this, the study area was separated into three zones of varying elevation. The highest elevation zone (436-647m) included regions in the upper watershed with an overall slope of 0.43m/m the middle elevation zone (226-436 m) contained transitional areas with an average slope of 0.45m/m, and the lowest elevation zone (15-225 m) contained the lowest portion of the watershed with an average slope of 0.30m/m. Within each elevation zone, 100 observation points were randomly selected, and the nLS values for those points were extracted for all 100 Monte Carlo simulations. From these values the coefficient of variation was calculated for each

observation point (Figure 5.8). This statistic was calculated by dividing the standard deviation by the mean. The majority of the points had a value of 25% or less, with some exceptions. This indicated that varying Manning's n within a range had an impact on the resulting nLS value, but that impact was not extraordinarily large, and it may be predictable to a certain extent. There were more occurrences of values above 25% for areas within the upper region of the study site, accounting for 6.7% of the total number of points, compared to 3.0% for middle elevations and 2.3% for lowest elevations. In general, the coefficient of variance increased with elevation. The highest elevations had an average value of 30.3, the middle elevations had a value of 16.2, and the lowest elevations had an average value of 11.9. This suggests that areas at higher elevations in the upper watershed create less predictable variations.

Figure 5.8 Coefficient of variation for the nLS output at 300 observation points during the Manning's n Monte Carlo simulation, divided into three elevation zones.

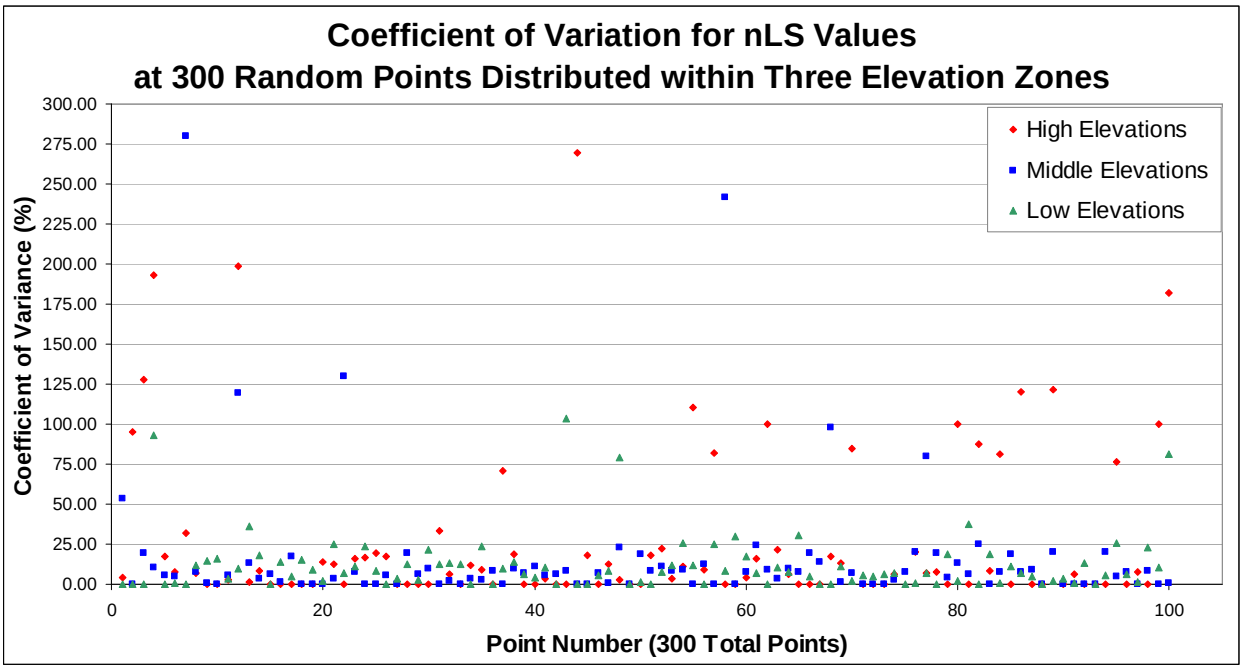

The locations of transitional flow, as indicated by critical threshold points computed by the nLS model, were influenced significantly by adjusting the value of the threshold (Figure 5.9).

Modifying the threshold value caused significant shifts in the location of predicted potential soil erosion. Based on these results, it is evident that selecting an appropriate critical threshold value is vital for obtaining accurate results when applying the nLS model to a given study area.

Figure 5.9 Shift in output points caused by adjusting the critical threshold value for the nLS model.

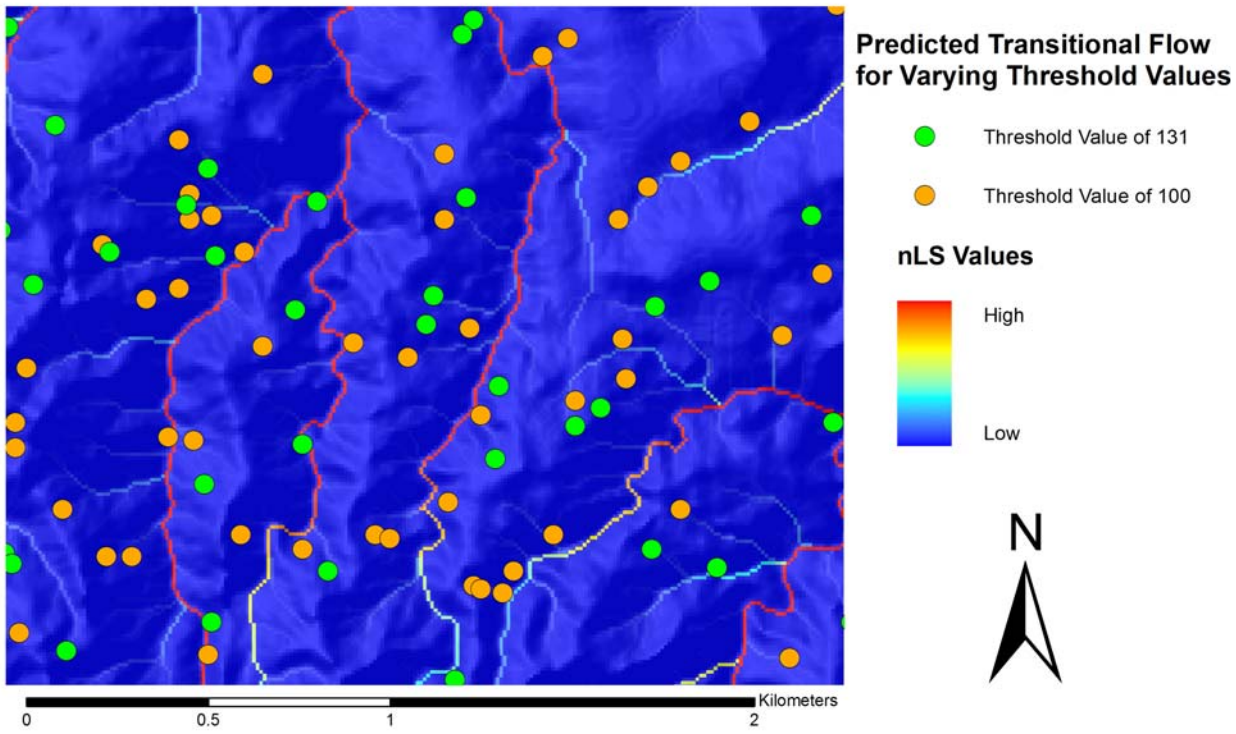

Variation in Model Calculations

The modified version of the nLS model resulted in output values that were noticeably different from the original model (Figure 5.10). In this image, large differences in the two models are shown as purple, while smaller differences are shown as yellow. Threshold values of 100 are shown in red for the alternative model and green for the existing model. From the illustration, it is clear that where the critical threshold is achieved differs according to the model calculation applied. This difference is less dramatic in the upstream portions of the watershed,

but escalates rapidly in the downstream portions, suggesting that proper calculation methods are vital for the accurate predictions of potential erosion sites.

Figure 5.10 Comparison of the existing model, which calculates total accumulated flow lengths, to an alternative model, which calculates the longest flow path.

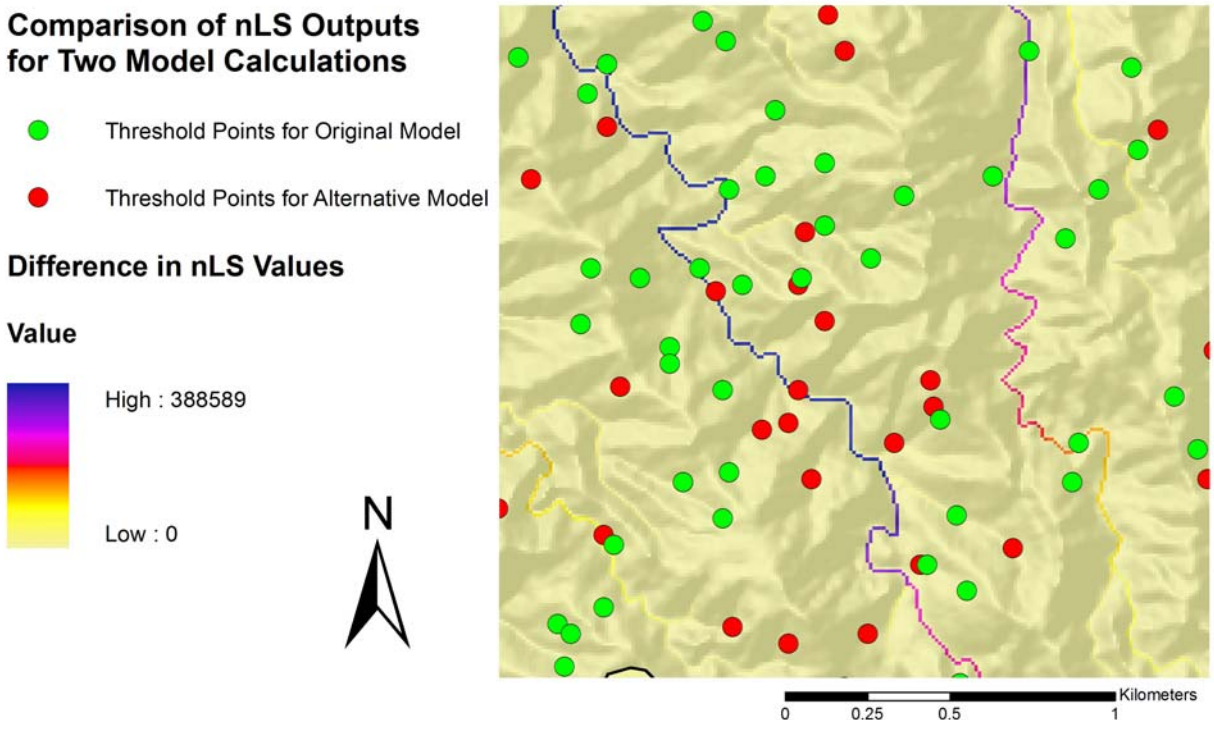

Using a threshold value of 100, the existing model predicts 1367 transition points for the study area, while the alternative form of the model predicts only 1097. Comparing both models at each others threshold points, the existing model had nLS values of 136±5 at points where the alternative model had nLS values of 100. Conversely, the alternative model had nLS values of 523±1000 at points where the alternative model had nLS values of 100. Statistical results of the comparison suggest that the existing nLS model can easily be adjusted to find the threshold locations predicted by the alternative model (Table 5.3).

Table 5.3 Statistical comparison of the two forms of the nLS model. Critical threshold points from each form of the model were compared to nLS values of the other.

	Alternative Model Threshold Points		Existing Model Threshold Points	
	nLS Value for Alternative Model	nLS Value for Existing Model	nLS Value for Existing Model	nLS Value for Alternative Model
Average nLS Value:	100	136	100	523
Maximum Value:	100	159	100	4484
Minimum Value:	100	90	100	0
Median Value:	100	136	100	98
Number of Points:	1097	1097	1367	1367
Standard Deviation:	0	5	0	1000

Study Area Comparisons

Each of the four study areas has unique characteristics that affect nLS model results. In general, the Hawaii study areas have steeper, more mountainous topography than those located in Kansas. In addition, the vegetative conditions for each site created varying effects on the nLS outputs. Using a threshold value of 131 ± 22.6, the total area of potential erosion sites, which was calculated by multiplying the total number of cells by the area of each cell, varied significantly between study areas. However, the percentage of these values with respect to each site's total area was more consistent, falling between 3.5% and 7.5% (Table 5.4).

Table 5.4 Characteristics of potential erosion areas for each study site, as predicted by the nLS model using a threshold value of 100.

	Erosion Area (sq. m)	Area of Potential Erosion as Percent of Total	Average Slope at Erosion Areas (m/m)	Average Manning's n at Erosion Areas
Fort Riley	16,557,500	4.02%	0.060	0.065
Schofield	2,843,200	7.43%	0.324	0.081
Keamuku	3,276,400	3.51%	0.092	0.043
Cheney	11,809,100	4.61%%	0.010	0.045

While the table shows that the average slope and the average roughness coefficient varied, the relationship between these values and the overall characteristics each study site was

more predictable. The average slope of the potential erosion areas was closely related to the average slope of the entire site, following a linear trend (Figure 5.11). Similarly, the average Manning's roughness coefficient was linearly related to the roughness coefficient of the entire site (Figure 5.12). These trends suggest using an equivalent threshold value for varying study sites causes the areas of potential erosion to have characteristics that depend heavily on the study areas' overall conditions. Since this may not be the case, the model may require adjustments to the threshold value to accurately capture the locations of potential erosion sites.

Figure 5.11 Relationship between average slope of the erosion potential areas and that of the entire study area.

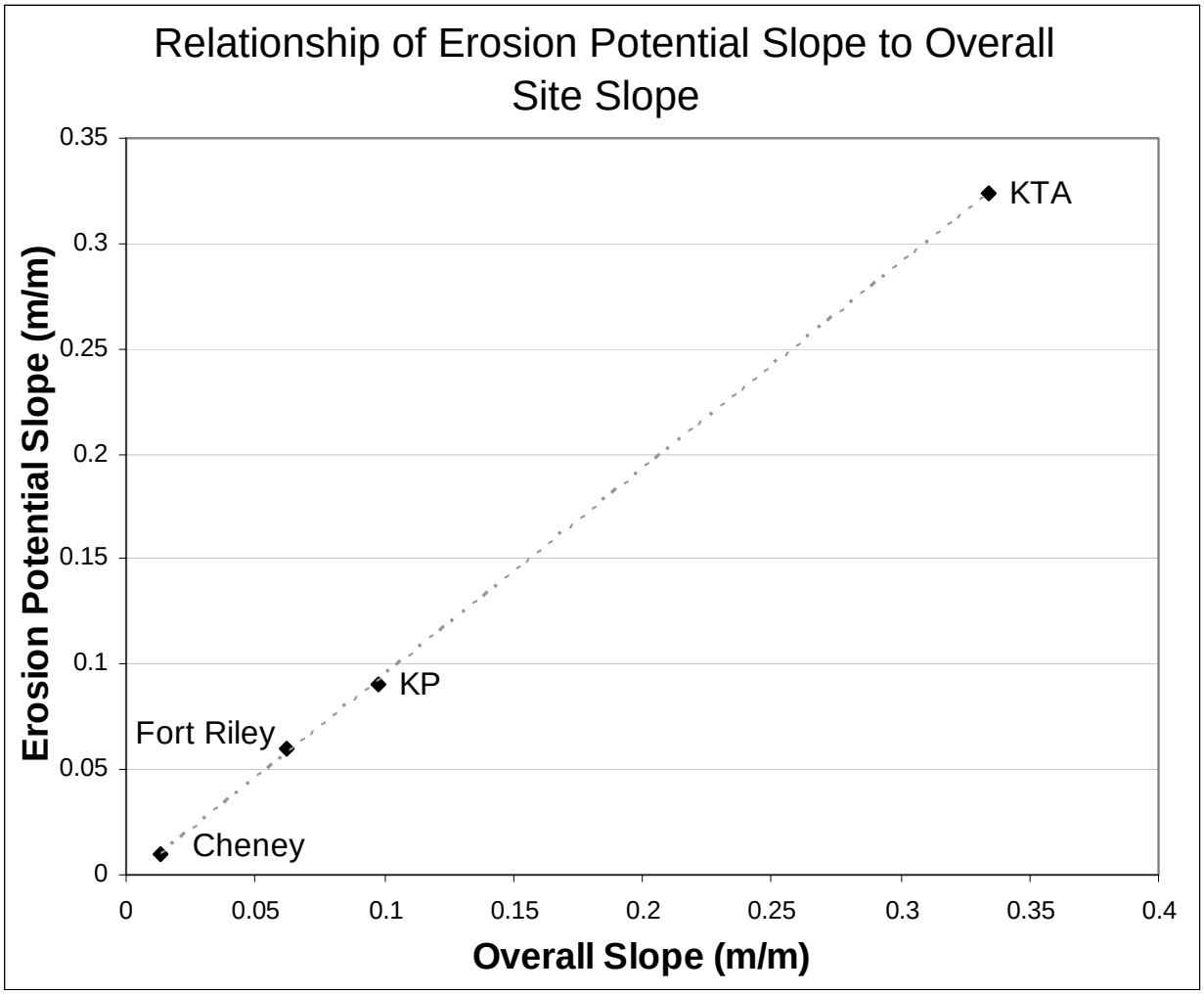

Figure 5.12 Relationship between average Manning's roughness coefficient of erosion potential areas and that of the entire study area.

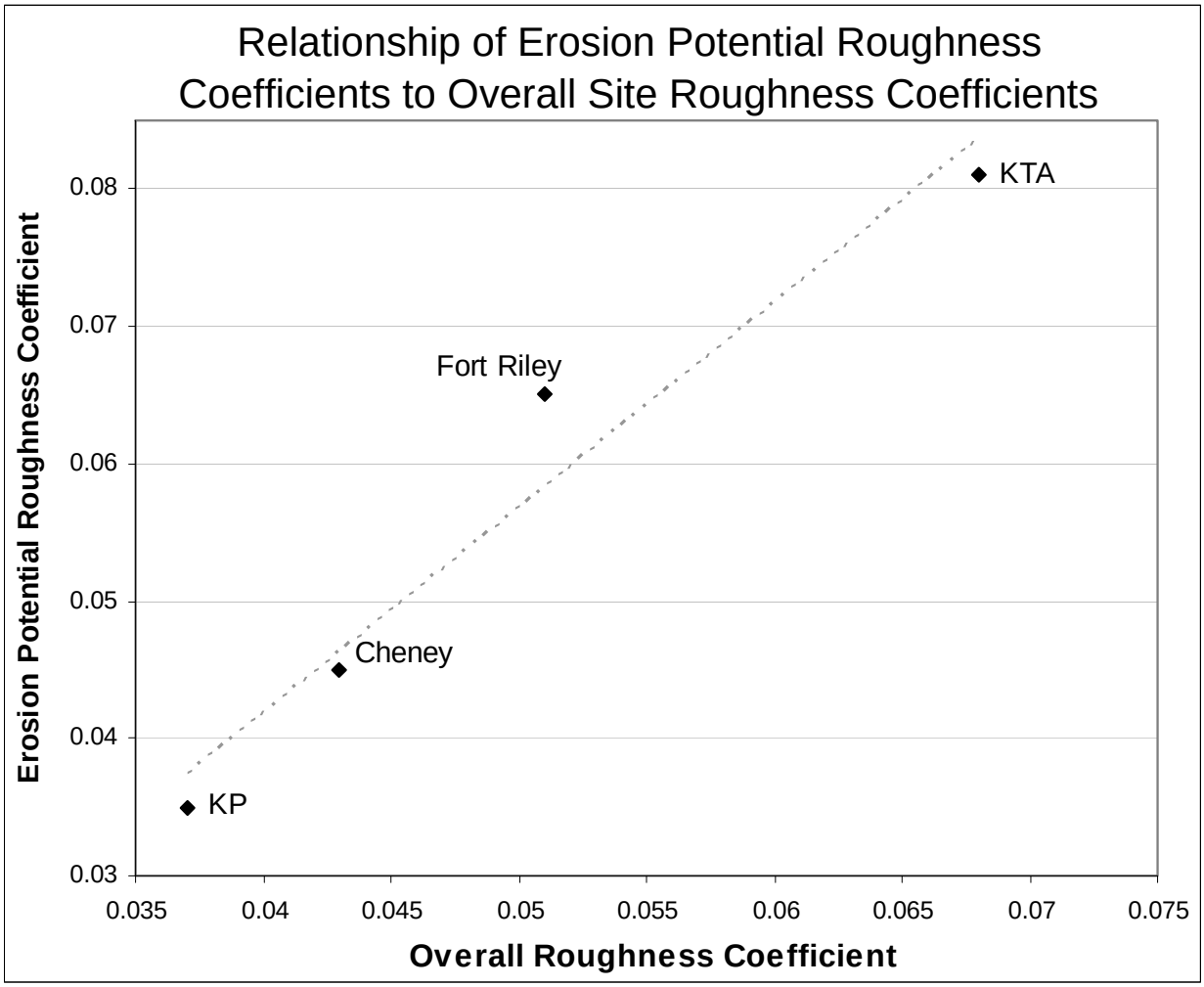

To determine which characteristics of a specific study site will have the biggest impact on predicting potential erosion areas, several comparisons were made. The effects of a study area's overall slope, Manning's roughness coefficient, and drainage density on the predictions of potential erosion sites were examined. For slope, the flatter areas of Fort Riley, PTA, and Cheney seem to follow predictable trend, since increasing slope causes a decrease in the overall prediction of soil erosion potential (Figure 5.13). However, the mountainous terrain of Schofield

creates an unusual outlier, with a much higher area of predicted erosion, as well as a very high slope.

Figure 5.13 Relationship between overall site slope and predicted erosion potential areas, as percent of total area.

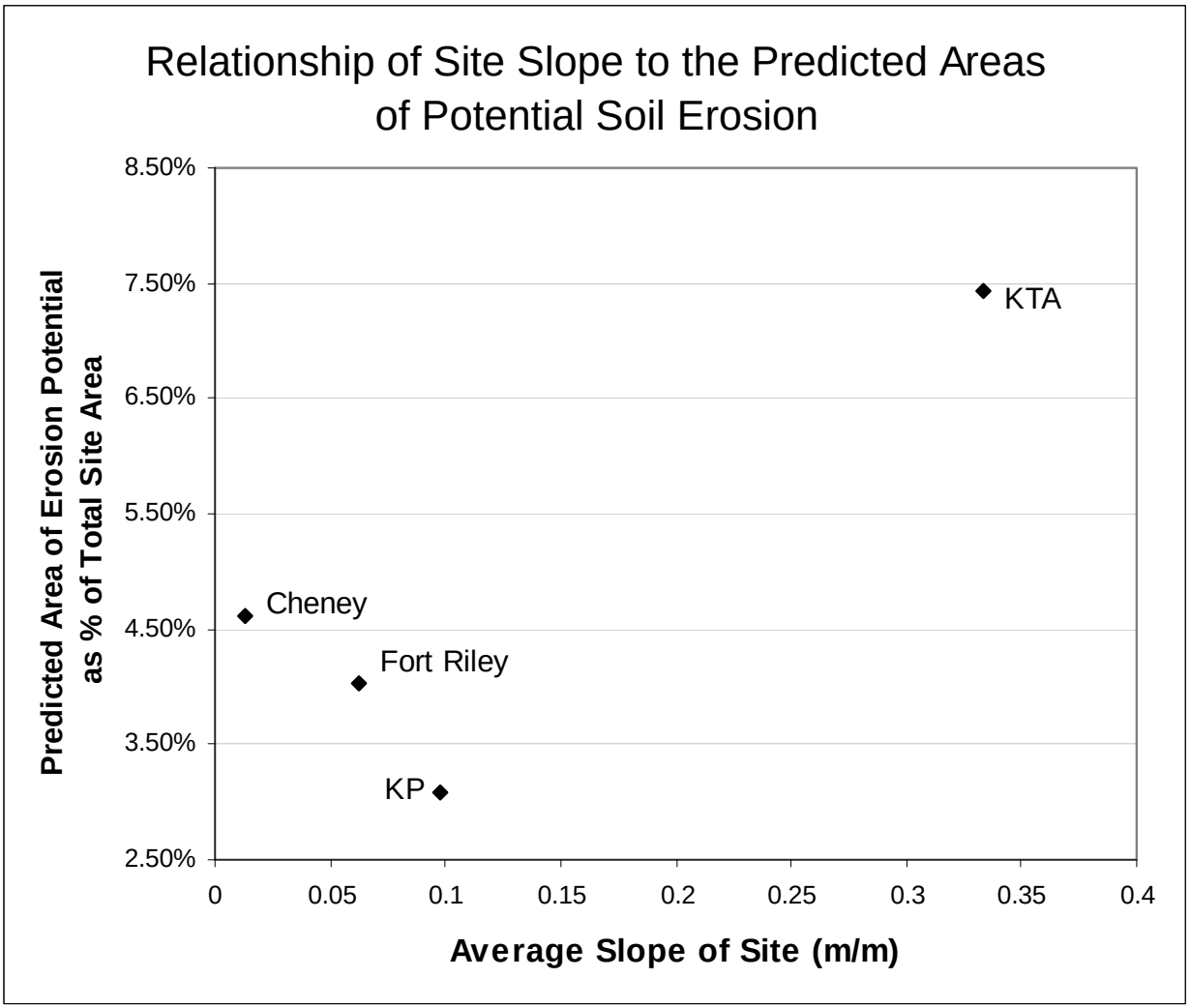

For Manning's roughness coefficient, there is a roughly linear trend indicating an increase in the predicted area of soil erosion potential with increasing overall Manning's roughness coefficient (Figure 5.14). Between Cheney and Fort Riley, however, the trend does not hold. The cause of this difference is unclear.

Figure 5.14 Relationship between overall site roughness coefficient and predicted erosion potential areas, as percent of total area.

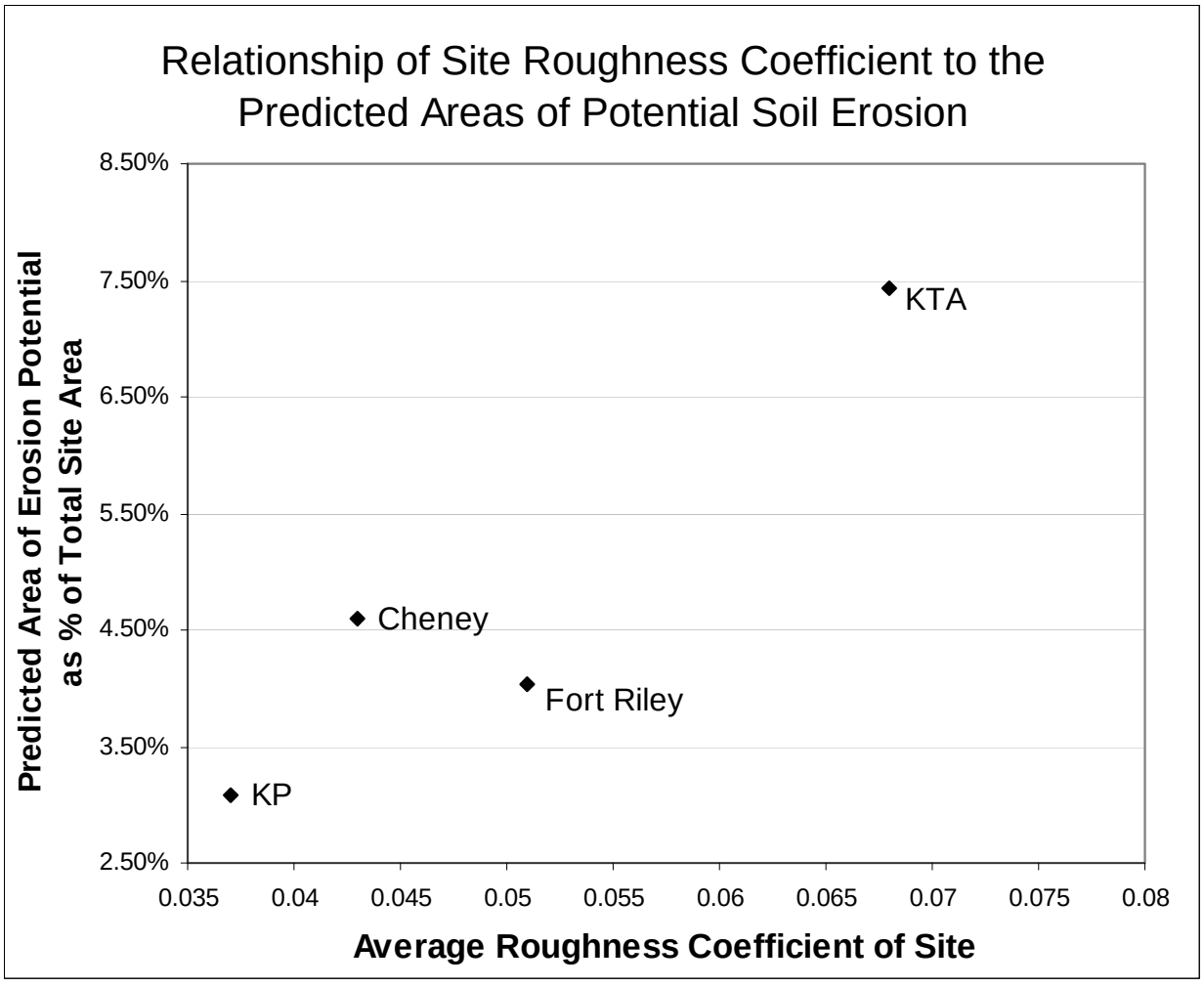

For drainage density, there is also a roughly linear trend indicating an increase in the predicted area of soil erosion potential with increasing overall drainage density (Figure 5.15). Similar to the roughness coefficient, the trend does not hold between Cheney and Fort Riley.

Figure 5.15 Relationship between overall site drainage density and predicted erosion potential areas, as percent of total area.

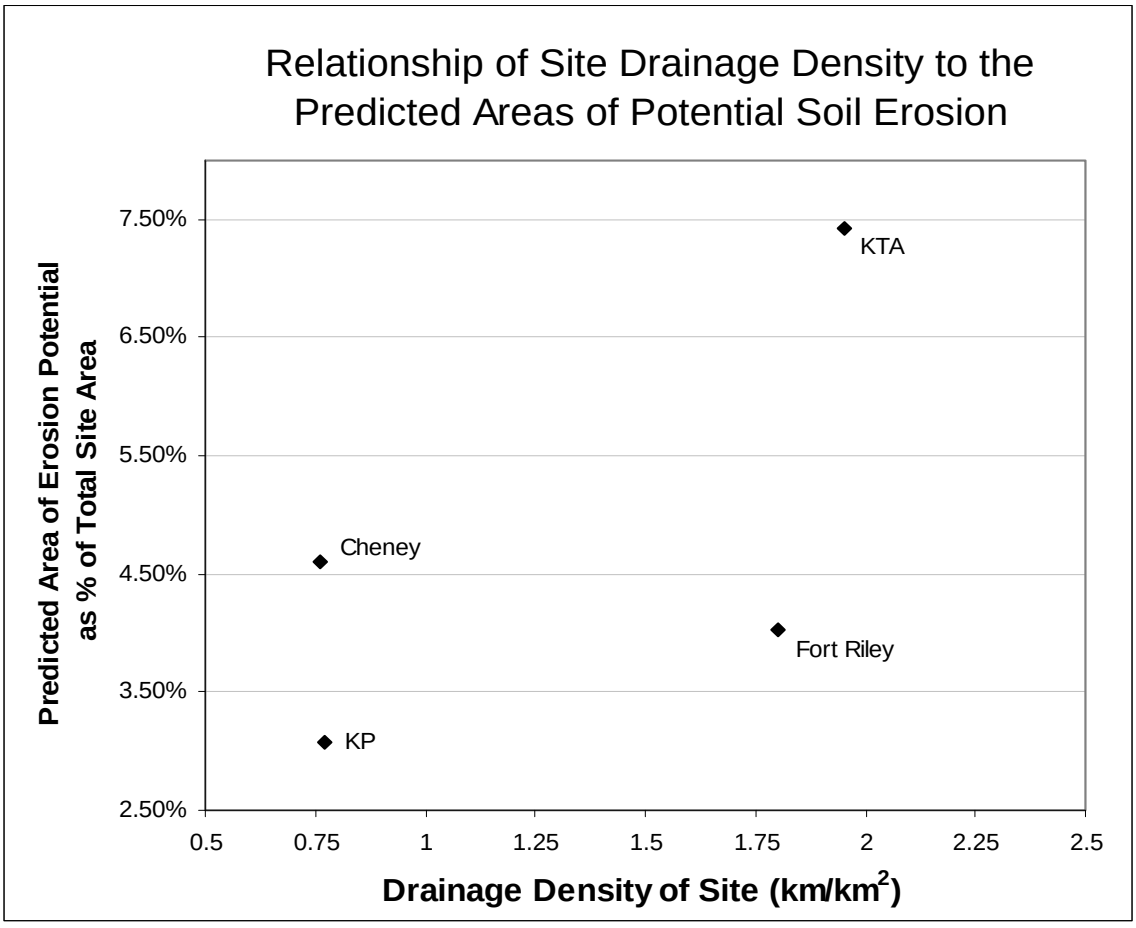

Overall, there seem to be some basic trends formed among sites with varying characteristics. To better understand these trends, it will be necessary to calibrate the model at each site using known gully head locations. In addition, analyzing additional sites will better demonstrate any trends that may exist, providing a more accurate examination of model tendencies.

CHAPTER 6 - Summary and Conclusions

The nLS model was developed as a rapid soil erosion assessment tool for predicting the locations of gully heads in areas of transitional flow (Kim, 2006). The model uses elevation data, landuse/landcover data, and corresponding Manning's roughness coefficients to locate potential areas of transitional flow and where gully heads are likely to form. The goal of this study was to conduct a sensitivity analysis of the nLS model by analyzing the impacts of elevation, LULC, and Manning's coefficient input parameters on model output. In addition, variations in model calculations and threshold parameters were examined.

Overall, each of the model input parameters had unique impacts on the model outputs. In general, the analyses performed on model inputs suggest that slope is more important for the nLS model within study areas that have a steeper terrain. Conversely, Manning's roughness coefficient is more important in study areas with low slopes.

In the IPP analysis of slope, it was determined that adjusting the slope across an entire study area resulted in an output nLS value that corresponds very closely to the slope value of the nLS equation ($nLS = nL/S^{0.5}$). Variation from the equation occurred primarily in lowland areas with low slope values. Based on these results, study areas located in areas of low slope will experience higher variability in the output nLS value, and so accurate LULC data is especially important.

In the analysis of possible DEM error, modifications made to the DEM during a Monte Carlo simulation helped assess the effects of variability in DEM accuracy. It was determined that DEM error has the potential to dramatically alter the calculated flow paths of a study site. In

the uppermost portions of the watershed, the lack of flow accumulation led to areas that consistently lacked any flow paths, regardless of the DEM error. While flow tendencies were generally higher in the lower portions of the watershed, there was significant variation in these flow paths caused by DEM error. Because DEM error has the potential to cause such significant geographic variations in the flow network, it is important to obtain the most accurate DEM that is available for a study site. This analysis, along with the IPP analysis performed on slope, confirm the importance of accurate flow paths for the nLS model to operate effectively.

In the analyzing the LULC distribution, a Monte Carlo simulation was use to assess the effects of variability in the LULC distribution. Results from this analysis show that there are some effects of modifying the LULC distribution within a watershed. However, these effects were relatively small, varying only ±0.3% from the mean output nLS value. While the distribution of the LULC data does have an impact on the nLS model, it is less important than other model parameters, as long as the contributing area for a sample point retains the same general distribution of LULC classes.

In the analysis of Manning's n assignment, a Monte Carlo simulation helped assess the effects of variability in assigning an appropriate roughness coefficient. For different model runs, the variation in the Manning's n values caused changes in where the critical nLS threshold value was realized. This geographic variability suggests that assigning an accurate Manning's roughness coefficient is vital for accurate model outputs. Because of the significant impact of the roughness coefficient, it may be necessary to adjust the Manning's n value based on seasonal conditions, and more accurate values may need to be obtained for the vegetative cover of a study area.

In the analysis of variability for Manning's n, the effect of assigning the roughness coefficients was also examined as a function of elevation. The nLS values at points within three elevation zones revealed that areas in higher regions of the watershed generally have a higher coefficient of variation. In general, the coefficient of variance increased with elevation. This value for the highest, middle, and lowest elevations was 30.3, 16.2, and 11.9, respectively. Of the 38 points that had a high coefficient of variation (above 25%), 20 were located in the uppermost elevation zone, at the top of the watershed. Based on these findings, areas at higher elevations in the upper watershed create less predictable variations in the nLS values.

In the simple IPP analysis of the critical threshold value, modifying the threshold value caused significant shifts in the location of predicted potential soil erosion. This suggests that selecting an appropriate critical threshold value is vital for obtaining accurate results when applying the nLS model to a given study area. It also suggests that the critical threshold value can be used as a simple way of calibrating the model for different study areas.

Varying the calculations used within the model did not indicate any potential to improve model accuracy. By modifying the model to calculate longest flow length rather than accumulated flow length, the overall nLS value was significantly decreased. However, statistical results of the comparison suggest that the original nLS model can easily be adjusted to find the threshold locations predicted by the model developed in this study. Because of these findings

Analysis of the four study sites reveals some basic trends in the nLS model output. First, the characteristics of the predicted potential soil erosion areas depend heavily on the overall site characteristics of the study area. This suggests that the model will need to be calibrated for different ecoregions. For both slope and Manning's n, the relationship between the overall site characteristics and those of potential soil erosion areas is directly proportional. In addition, the

four study areas showed some basic trends relationships between the nLS output and site characteristics including slope, Manning's n, and drainage density. In general, the area of predicted erosion potential, as a percent of the total site area, increased with both roughness coefficient and drainage density. For slope, this value seems to decrease with increasing slope, but KTA creates an outlying point that does not follow this trend. Overall, the results suggest that there are some generalizations that can be made with the nLS model based on a site's conditions, but more study sites need to be included if a stronger relationship is to be determined.

Limitations and Recommendations

The various analyses presented in this study provide useful insight into the potential applications of the nLS model. However, there are many limitations that should be addressed in future studies. As suggested in previous sections, accurate elevation data is important to model performance, and this is especially true in areas with high slope values. While 10-meter DEMs, like those used in the majority of these analyses, have become widely available across the U.S., existing research suggests that finer resolution data would significantly improve the model performance. In addition, accurate classification of the Manning's coefficient with respect to LULC classifications is essential for improving model performance, especially in areas of low slope values (see *Manning's n Parameter*, pg 57). While remote sensing technologies have made detailed LULC classifications increasingly available, updated Manning's coefficients are rare. It may be necessary to obtain more accurate Manning's n values, which could be adjusted to account for seasonal fluctuations in vegetative cover. To test this, it would be necessary to perform additional sensitivity analyses that would better evaluate the Manning's n parameter.

In addition to data accuracy, the effects of temporal variability should be investigated. Erosion is a continuous process that has the potential to substantially modify the topography of

an area. Because of this, frequent acquisition of elevation and LULC data may be required to ensure up-to-date model outputs. On military installations, information on training location, intensity, and timing could be used to predict current and future gully formations. With accurate erosion points, the nLS model can be more precisely calibrated, improving model performance in the future. Other non-hydrologic activities may also need to be considered, including the impacts of civilian movements and animals. Such activities can lead to a loss in vegetative cover, and even modify the flow paths within a study area, which would significantly alter model inputs. A long-term study should be considered to assess the effects of temporal variability associated with these activities.

The model results have been shown to vary in different ecoregions due to the DEM and LULC associated with varying ecoregions (see *Study Area Comparisons*, pg 63). Because of this, it may be necessary to adjust the model, especially the threshold value, for different study areas. While precipitation is not considered in the nLS model, a relationship between the number of gully heads and rainfall does exist (Kim, 2006). This factor could be considered in assessing the model's threshold value. To determine if model adjustments are necessary, future studies should include accurate gully head locations to calibrate the model for a given study site.

References

Abrahams, A.S. and J.F. Atkinson. 1993. Relation between grain velocity and sediment concentration in overland flow. *Water Resources Research* 29(9):3020-3028.

Ayers, P., C. Butler, A. Fiscor, C. Wu, Q. Li, and A. Anderson. 2005. Vehicle impact study, Fort Riley, Kansas, October, 2004. Submitted to ITAM, Fort Riley Military Installation, KS.

Baker, L.A. 1992. Introduction to nonpoint source pollution in the United States and prospects for wetland use. *Ecological Engineering* 1(1-2):1-26.

Bennett, S.J., J. Casalí, K.M. Robinson, K.C. Kadavy. 2000. Characteritics of actively eroding ephemeral gullies in an experimental channel. *Transactions of ASAE* 43(3):641-649.

Chow, V.T. 1959. Open channel hydraulics. McGraw-Hill, New York, NY.

Chytka, J.J., M.J. Webb, A.K.L. Goo, M.T. Morgotta. 2008. Environmental assessment for the use of M117 armored security vehicles at army installations in Hawaii. Submitted to U.S. Army Garrison, HI.

Corwin, D.L. and P.J. Vaughan. 1997. Modeling nonpoint source pollutants in the vadose zone with GIS. *Environmental Science and Technology* 21(8):2157-2175.

Daly, C., W.P. Gibson, G.H. Taylor, G.L. Johnson, and P. Pasteris. 2002. A knowledge-based approach to the statistical mapping of climate. *Climate Research* 22:99-113.

Department of Army. 1988. Environmental effects of Army actions. Army Regulation 200-2. Headquarters, Department of Army, Washington D.C.

Diong, C.H. 1982. Population biology and management of the feral pig (*Sus Scrofa l.*) in Kipahulu Valley, Maui. *Dissertation.* University of Hawaii, Manoa, HI.

Egbert, S.L., D.L. Peterson, A.M. Stewart, C.L. Lauver, C.F. Blodgett, K.P. Price, and E.A. Martinko. 2001, The Kansas GAP land cover map: final report. Kansas biological survey report no. 98. University of Kansas, Lawrence, KS.

Ferreira, V.A., G.A. Weessies, D.C. Yoder, G.R. Foster, and K.G. Renard. 1995. The site and condition specific nature of sensitivity analysis. *Journal of Soil and Water Conservation* 50(5):493-497.

Fiener, P., G. Govers, and K. Van Oost. 2008. Evaluation of a dynamic multi-class sediment transport model in a catchment under soil-conservation agriculture. *Earth Surface Processes and Landforms* 33:1639-1660.

Flanagan D.C., and M.A. Nearing. 1995. USDA water erosion prediction project: hillslope profile and watershed model documentation. National Soil Erosion Research Laboratory Report 10. USDA-ARS NSERL: West Lafayette, IN.

Gassman, P.W., M.R. Reyes, C.H. Green, and J.G. Arnold. 2007. The Soil and Water Assessment Tool: Historical Development, Applications, and Future Research Directions. *Transactions of the ASABE* 50(4):1211-1250.

Gatto, L. W., 2001. Overwinter changes to vehicle ruts and natural rills and effects on soil erosion potential. In: D.E. Stott, R.H. Mohtar and G.C. Steinhardt (eds). Sustaining the Global Farm. Proc. 10th ISCO Conference 1999:472-475.

GDSI (Geographic Decision Systems International). 1995. Hawaii Statewide GIS Program, Watershed Unit Boundary Lines and Attributes. Hawaii State Office of Planning. Honolulu, HI.

Gesch, D., M. Oimoen, S. Greenlee, C. Nelson, M. Steuck, and D. Tyler. 2002. The National Elevation Dataset. *Photogrammetric Engineering and Remote Sensing* 68(1):5-11.

Goodchild, M.F., B.O. Parks, and L.T. Steyaert. 1993. Environmental modeling with GIS. Oxford University Press. New York, NY.

Gordon, L., S.J. Bennett, R.L. Bingner, F. Theurer, and C.V. Alonso. 2006. REGEM: The revised ephemeral gully erosion model. In: Proceedings of the 8th Federal Interagency Sedimentation Conference, Reno, Nevada.

Jaber, F.H. and R.H. Mohtar. 2002. Dynamic time step for one-dimensional overland flow kinematic wave solution. *Journal of Hydrologic Engineering* 7(1):3-11.

Jantz, D.R., R.F. Harner, H.T. Rowland, and D.A. Gier. 1975. Soil Survey of Riley County and Part of Geary County, Kansas. USDA, Soil Conservation Service, Washington D.C.

Jetten, V., J. Boiffin, A.P. De Roo. 1996. Defining monitoring strategies for runoff and erosion studies in agricultural catchments: a simulation approach. *European Journal of Soil Science* 47:579–592.

Jetten, V., G. Govers, R. Hessel. 2003. Erosion models: quality of spatial predictions. *Hydrological Processes* 17:877–900.

Kim, I.J. 2006. Identifying the roles of overland flow characteristics and vegetated buffer systems for nonpoint source pollution control. *Dissertation.* Kansas State University, Manhattan, KS.

Laguna, A. and J.V. Giraldez. 1993. The description of soil erosion through a kinematic wave model. *Journal of Hydrology* 145:65-82.

Lal, R. 1994. Soil erosion research methods, (second ed.). Soil Water Conservation Society. St Luci Press, Delray Beach, FL.

Liu, K., P. Ayers, H. Howard, and A. Anderson. 2007. Influence of turning radius on military vehicle induced rut formation. Proceedings of the Joint North America, Asia-Pacific ISTVS Conference and Annual Meeting of the Japanese Society for Terramechanics, Fairbanks, AK.

Livingston, E.H. 2000. Lessons learned about successfully using infiltration practices. Proceedings of the National Conference on Tools for Urban Water Resources Management and Protection, Chicago, Illinois.

Ma, L., J.C. Ascough II, L.R. Ahuja, M.J. Shaffer, J.D. Hanson, and K.W. Rojas. 2000. Root Zone Water Quality Model sensitivity analysis using Monte Carlo simulation. *Transactions of ASAE* 43(4):883-895.

McCuen, R.H. and J.M. Spiess. 1995. Assessment of kinematic wave time of concentration. *Journal of Hydrologic Engineering* 121(3):256-266.

Merritt, W.S., R.A. Letcher, and A.J. Jakeman. A review of erosion and sediment transport models. 2003. *Environmental Modeling and Software* 18:761–799.

Milchunas, D.G., K.A. Schultz, and R.B. Shaw. 1999. Plant community response to disturbance by mechanized military maneuvers. *Journal of Environmental Quality* 28:1533-1547.

Miller, S. and A. Holt. 1992. The Alien pest species invasion in Hawaii: background study and recommendations for interagency planning. The Nature Conservancy of Hawaii, Honolulu, HI and the Natural Resources Defense Council, New York, NY.

Morgan, R.P.C., J.N. Quinton, R.E. Smith, G. Govers, J.W.A. Poesen, K. Auerswald, G. Chisci, D. Torri, and M.E. Styczen. 1998. The European soil erosion model (EUROSEM): a dynamic approach for predicting sediment transport from fields and small catchments. *Earth Surface Processes and Landforms* 23:527-544.

Mostaghimi, S., S.W. Park, R.A. Cooke, and S.Y. Wang. 1997. Assessment of management alternatives on a small agricultural watershed. *Water Resources* 31(8):1867-1878.

Nearing, M.A., L. Deer-Ascogh, and J.M. Laflen. 1990. Sensitivity analysis of the WEPP hillslope profile erosion model. *Transactions of ASAE* 33(3):839-849.

Neitsch, S.L., J.G. Arnold, J.R. Kiniry, J.R. Williams, and K.W. King. 2002. Soil and Water Assessment Tool Theoretical Documentation, version 2000. GSWRL Report 02-01, BRC Report 02-05, TR-191. Texas Water Resources Institute, College Station, TX.

NOAA/NLCD. National environmental satellite, data, and information service. Available online at http://www.ncdc.noaa.gov Accessed Aug 29, 2009.

Novotny, V. 2003. Water quality: diffuse pollution and watershed management (second ed.). John Wiley and Sons, Inc., New York, NY.

NRCS. 2001. Conservation practice standard: diversion. Available online at: ftp://ftp-fc.sc.egov.usda.gov/NHQ/practice-standards/standards/362.pdf Accessed Jan 22, 2009.

NRCS. 2002. Conservation practice standard: dike. Available online at: ftp://ftp-fc.sc.egov.usda.gov/NHQ/practice-standards/standards/356.pdf Accessed Jan 22, 2009.

NRCS. 2003. Conservation practice standard: vegetative barrier. Available online at: ftp://ftp-fc.sc.egov.usda.gov/NHQ/practice-standards/standards/601.pdf Accessed Jan 20, 2009.

NRCS. 2007. Conservation practice standard: critical area planting. Available online at: ftp://ftp-fc.sc.egov.usda.gov/NHQ/practice-standards/standards/342.pdf Accessed Jan 20, 2009.

NRCS. 2008. Conservation practice standard: terrace. Available online at: ftp://ftp-fc.sc.egov.usda.gov/NHQ/practice-standards/standards/600.pdf Accessed Jan 22, 2009.

NRCS. Web soil survey. Soil survey staff, United States Department of Agriculture. Available online at http://websoilsurvey.nrcs.usda.gov Accessed August 15, 2009.

O'Callaghan, J.F. and D.M. Mark. 1984. The extraction of drainage networks from digital elevation data. *Computer Vision, Graphics, and Image processing* 28:323-344.

Omernik, J. M. 1995. Ecoregions: a spatial framework for environmental management. In: W.S. Davis and T.P. Simon (eds.). Biological assessment and criteria: tools for water resource planning and decision making. Lewis Publishers, Boca Raton, FL.

Pope, L.M. and C.R. Milligan. 2002. Sources and concentrations of phosphorus in the Cheney Reservoir watershed, south-central Kansas. USGS fact sheet 010–02. Lawrence, KS.

Quinton J. 1997. Reducing predictive uncertainty in model simulations: a comparison of two methods using the European soil erosion model (EUROSEM). *Catena* 30:101-117.

Quist, M.C., P.A. Fay, C.S. Guy, A.K. Knapp, and B.N. Rubenstein. 2003. Military training effects on terrestrial and aquatic communities on a grassland military installation. *Ecological Applications* 13(2):432-442.

Ragan, R.M. and J.O. Duru. 1972. Kinematic wave nomograph for times of concentration. *Journal of Hydrologic Engineering* 98(10):1765-1771.

Ricketts, T.H., Eric Dinerstein, D. Olson, C. Loucks, W. Eichbaum, D. DellaSalla, K.Kavanagh, P. Hedao, P. Hurley, K. Carney, R. Abell, and S. Walters. 1999. Terrestrial ecoregions of North America: a conservation assessment. Island Press, Washington, D.C.

Rockers, J.J., I. Ritcliff, L.W. Doed, and E.F. Bouse. 1966. Soil survey of Reno County, Kansas: USDA, Soil Conservation Service, Washington D.C.

Singh, V. P. 2001. Kinematic wave modeling in water resources: a historical perspective. *Hydrological Processes.* 15(4):671-706.

Smith, R.E., D.C. Goodrich, D.A. Woolhiser, and C.L. Unkrich. 1995. KINEROS – a kinematic runoff and erosion model. In: V.P. Singh (ed.). Computer models of watershed hydrology. Water Resources Publications, Highlands Ranch, CO.

SRGI (Sustainable Resources Group International, Inc.). 2009. Erosion monitoring and auditing project for the U.S. Army Kahuku Training Area (KTA), Oahu, Hawaii. Submitted to U.S. Army Garrison, HI and ITAM, Schofield Barracks, HI.

Tiscareno-Lopez, M., V.L. Lopes, J.J. Stone, and L.J. Lane. 1993. Sensitivity analysis of the WEPP watershed model for rangeland and applications I: hillslope processes. *Transactions of ASAE* 36(6):1659-1672.

TTI (Tetra Tech, Inc.). 2004. Final environmental impact statement: transformation of the 2nd Brigade, 25th Infantry Division (L) to a stryker brigade combat team in Hawai'i. Submitted to the Department of the Army, Office of the Secretary of the Army, Washington D.C. and the U.S. Army Corps of Engineers, Honolulu Engineer District, Fort Shafter, HI.

US Army, Hawaii and 25th Infantry Division. 2001. Integrated natural resources management plan 2002-2006 and environmental assessment: Oahu training lands. Headquarters, U.S. Army Garrison, HI.

USEPA. 2002. National water quality inventory: 2000 report to congress. EPA-841-F-02-003. Office of Water, Washington D.C.

USEPA. 2003. National management measures to control nonpoints source pollution from agriculture. EPA 842-B-03-004. Office of Water, Washington D.C.

USEPA. 2004. National water quality inventory. Available online at: http://www.epa.gov/owow/305b/2004report Accessed Jun 29, 2009.

Veihe, A., and J. Quinton. 2000. Sensitivity analysis of EUROSEM using Monte Carlo simulation I: hydrological, soil and vegetation parameters. *Hydrological Processes* 14:915-926.

Veith, T.L., M.L. Wolfe, and C.D.Heatwole. 2003. Development of optimization procedure for cost-effective BMP placement. *Journal of the American Water Resources Association* 39(6):1331-1343

Verro. R., M. Calliera, G. Maffioli, D. Auteri, S. Sala, A. Finizio, and M. Vighi. 2002. GIS-based system for surface water risk assessment of agricultural chemicals methodological approach (1). *Environmental Science and Technology* 36(7):1532-1538

Ward, A.D. and S.W. Trimble. 2003. Environmental hydrology (second ed.). Lewis Publishers, New York, NY.

Wedwick, S., B. Lakhani, J. Stone, P. Waller, and J. Artiola. 2001. Development and sensitivity analysis of the GLEAMS-IR model. *Transactions of the ASAE* 44(5): 1095-1104.

Willgoose, G. and G. Kuczera. 1994. Estimation of subgrid kinematic wave parameters for hillslopes. *Hydrological Processes* 9:469-482.

Wong, T.S.W. 2005. Assessment of time of concentration formulas for overland Flow. *Journal of Irrigation and Drainage Engineering* 131(4):383-387.

Wong, T.S.W. and C.N. Chen. 1999. Time of concentration formula for sheet flow of varying flow regime. *Journal of Hydrologic Engineering* 2(3):136-139.

Zerihun, D., J. Feyen, and J.M. Reddy. 1996. Sensitivity analysis of furrow-irrigated performance parameters. *Journal of Irrigation and Drainage Engineering*. 122(1):49-57.

Zhang, W. and D. Montgomery. 1994. Digital elevation model grid size, landscape representation, and hydrologic simulations. *Water Resources Research* 30(4):1019-1028.

Appendix A - Illustrations of Models used in nLS Analyses

The following diagrams illustrate the flow of model calculations and processes within each model. Each diagram is taken directly from ArcGIS 9.3 ModelBuilder. Within these images, the flow of model processing moves from left to right. The blue circles represent input values, the yellow rectangles represent model processes, and the green circles represent derived data.

Advanced nLS Model

The complete version of the nLS model includes mathematical conversions, as well as the extraction of threshold values (Figure A.1). Inputs for the model are a DEM, a LULC raster, Manning's n lookup table, and the nLS threshold range. Outputs for the model are nLS threshold points and an nLS raster for the entire study area. More advanced versions of the model have also been developed to make the model more user-interactive, but these have been excluded from this study.

Figure A.1 Complete nLS model, which uses elevation and landuse/landcover data to locate areas of potential soil erosion.

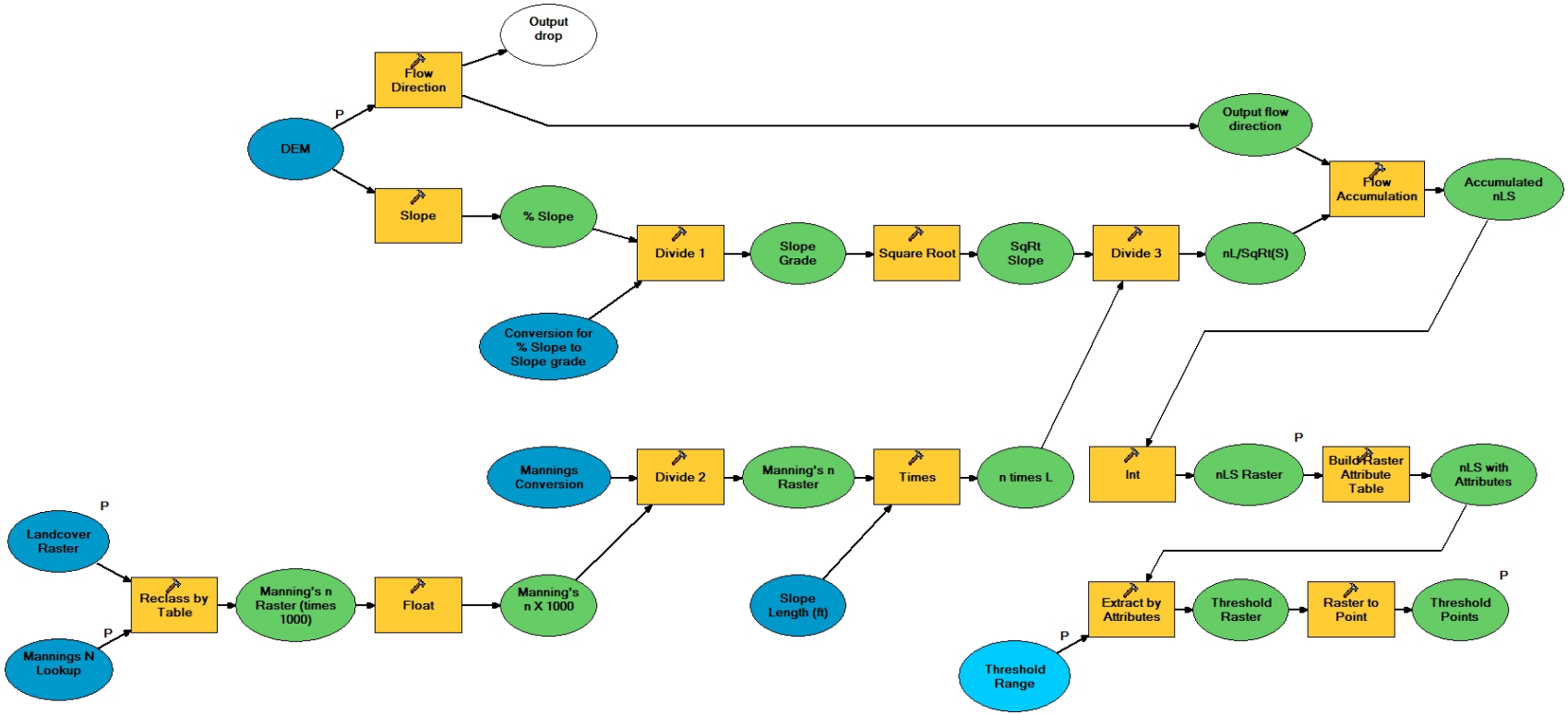

Slope Sensitivity Analysis

To analyze the impacts of slope, a model was developed that modified the elevation values by increments from 10% to 200% of the original landscape (Figure A.2). Inputs and outputs for the model are identical to those of the advanced model.

Figure A.2 Modified nLS model used for slope sensitivity, which modifies the elevation from 10% to 200% of the original.

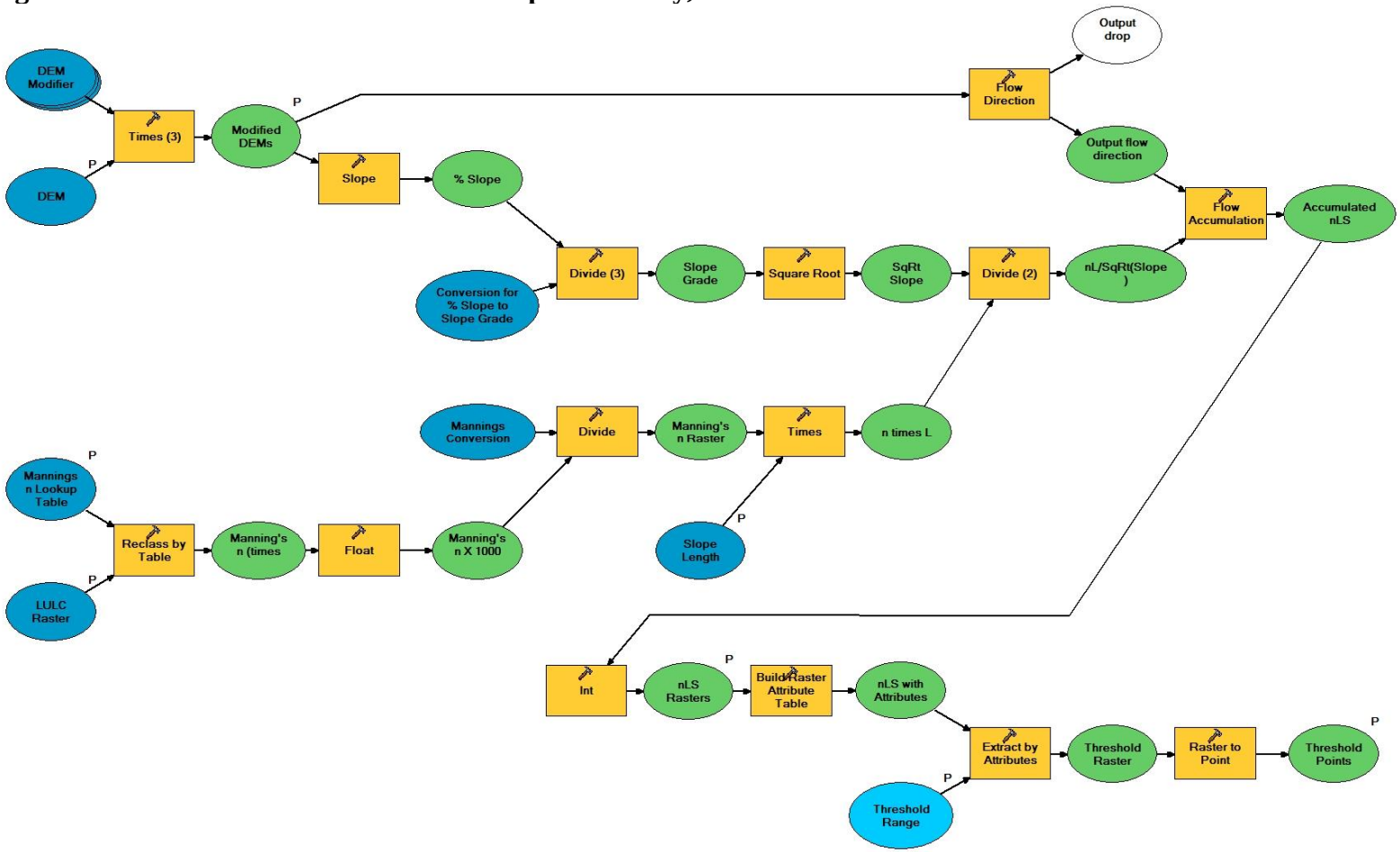

Flow Variations within Slope Sensitivity and DEM Error Analyses

A model was developed for evaluating the impacts of elevation modification on flow paths (Figure A.3). For each modified DEM the flow paths were calculated and summarized in an output raster. Inputs for the model are the modified DEMs, while the output is a raster that summarized the change in flow paths (Figure 5.3).

Figure A.3 Model used for examining inconsistent flow paths.

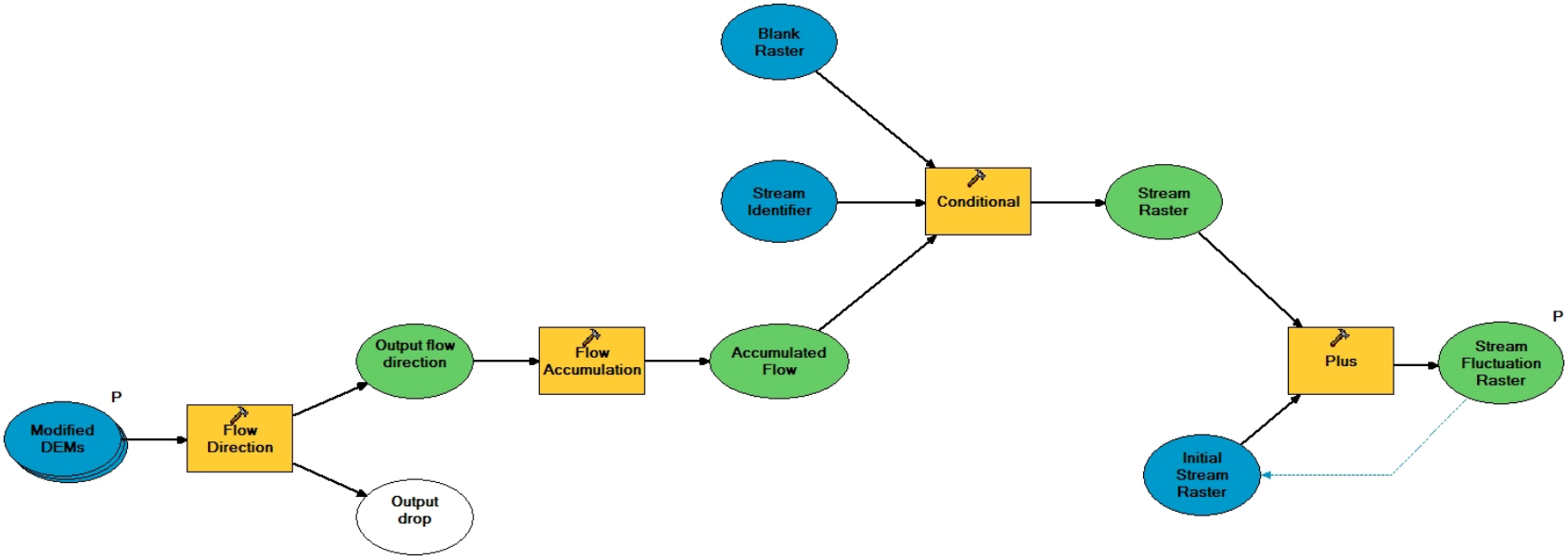

Landuse and Landcover Distribution Analysis

A model was developed for randomly distributing the LULC while retaining the basic composition of LULC types (Figure A.4). Inputs for the model are a DEM, a folder workspace for the random LULC rasters, and a Manning's n lookup table. Outputs for the model include the nLS threshold points and the nLS raster.

Figure A.4 Modified nLS model used for analyzing landuse/landcover distribution by randomly assigning a LULC.

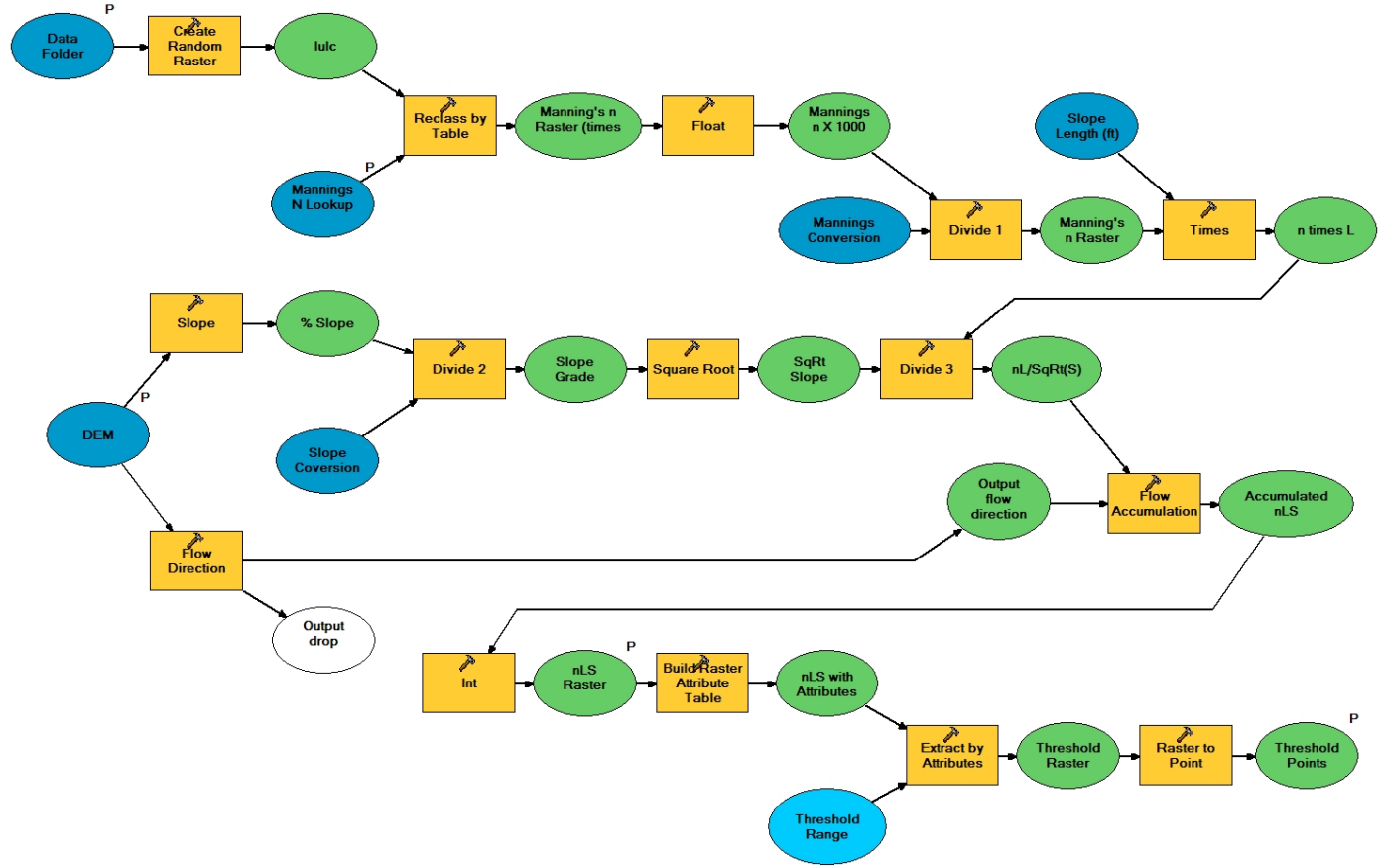

Manning's n Sensitivity Analysis

A model was developed that performs a Monte Carlo simulation by repeatedly varying the Manning's n for each LULC type (Figure A.5). Inputs are a LULC raster, a flow direction raster derived from the DEM, a workspace folder, a flow length value (equal to the DEM resolution), a raster of $\sqrt{S}$ derived from the DEM, a threshold range, a raster representing the extent of the study area, and the number of model iterations. Outputs are the nLS threshold points and the nLS raster.

Figure A.5 Modified nLS model used for the sensitivity analysis of Manning's n uniformity.

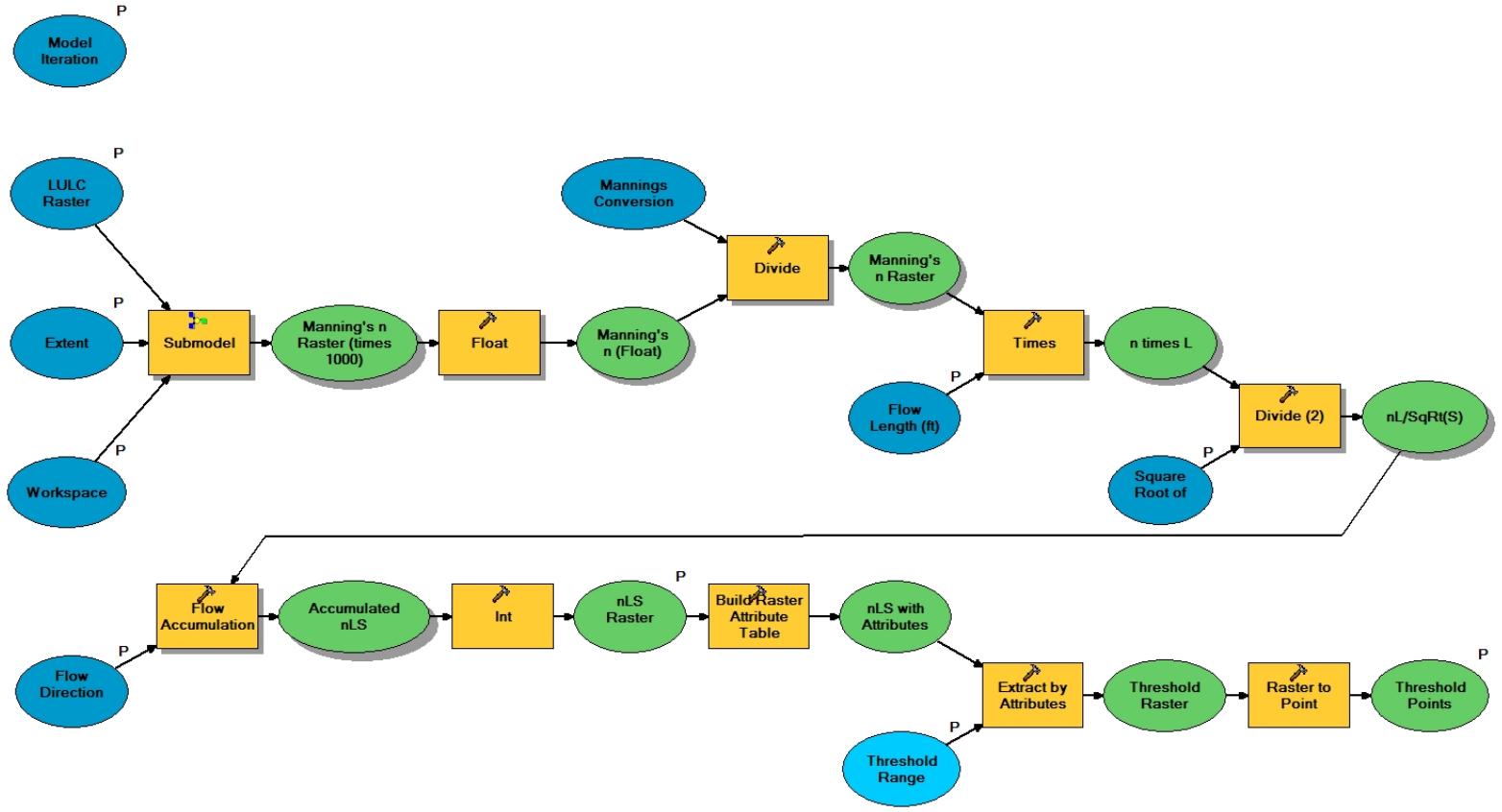

Manning's n Submodel

A submodel (Figure A.6) was developed to be used within the sensitivity analysis for Manning's n. Each LULC type was assigned a random Manning's n value within a preset range. Inputs include the LULC raster, a workspace folder, and a raster representing the extent of the study area. The output is the Manning's n raster.

Figure A.6 Submodel used within the Manning's n sensitivity analysis to assign Manning's n values to each area.

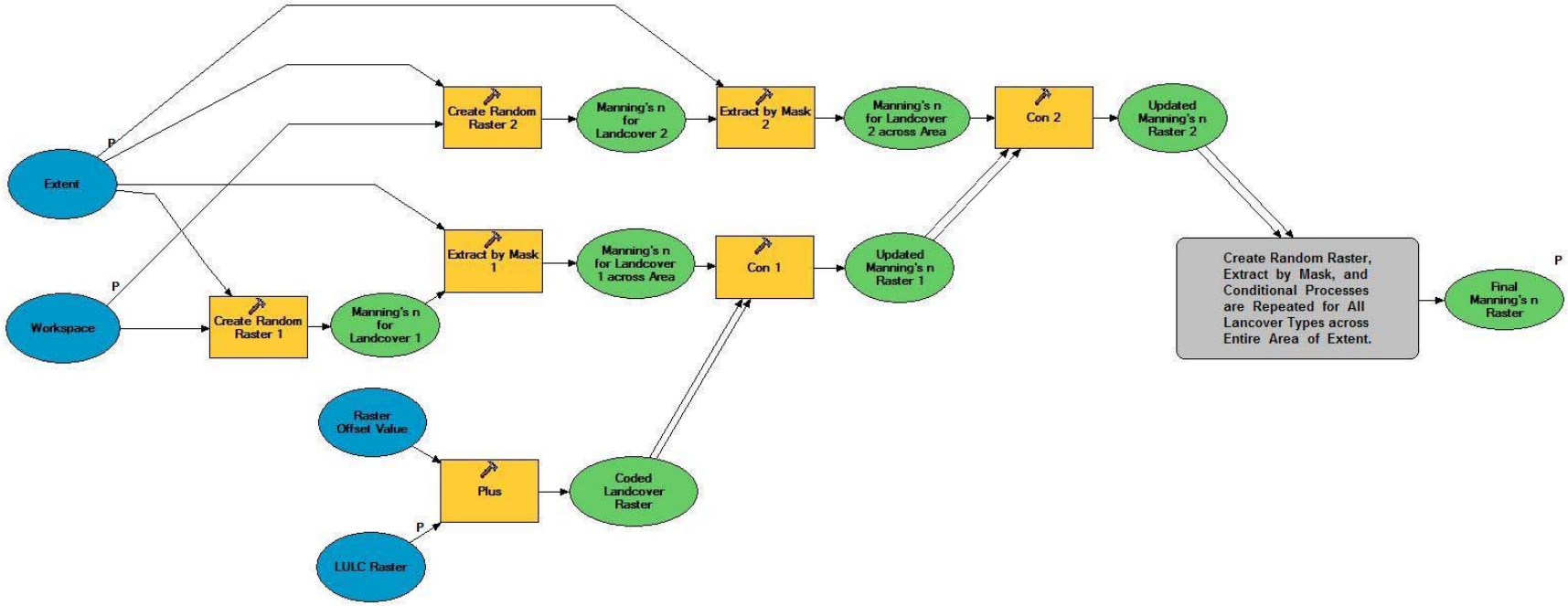

Variation in Model Calculations

A model was developed for analyzing the effects of varying calculations within the nLS model (Figure A.7). The model calculates the average Manning's n and Slope for the contributing watershed at each point in the study area. Inputs are a DEM, a Manning's n raster, the flow length (equal to raster resolution), and a threshold range. Outputs are the nLS raster and threshold points.

Figure A.7 Modified nLS model with alternative calculations, which calculates nLS using longest flow length.

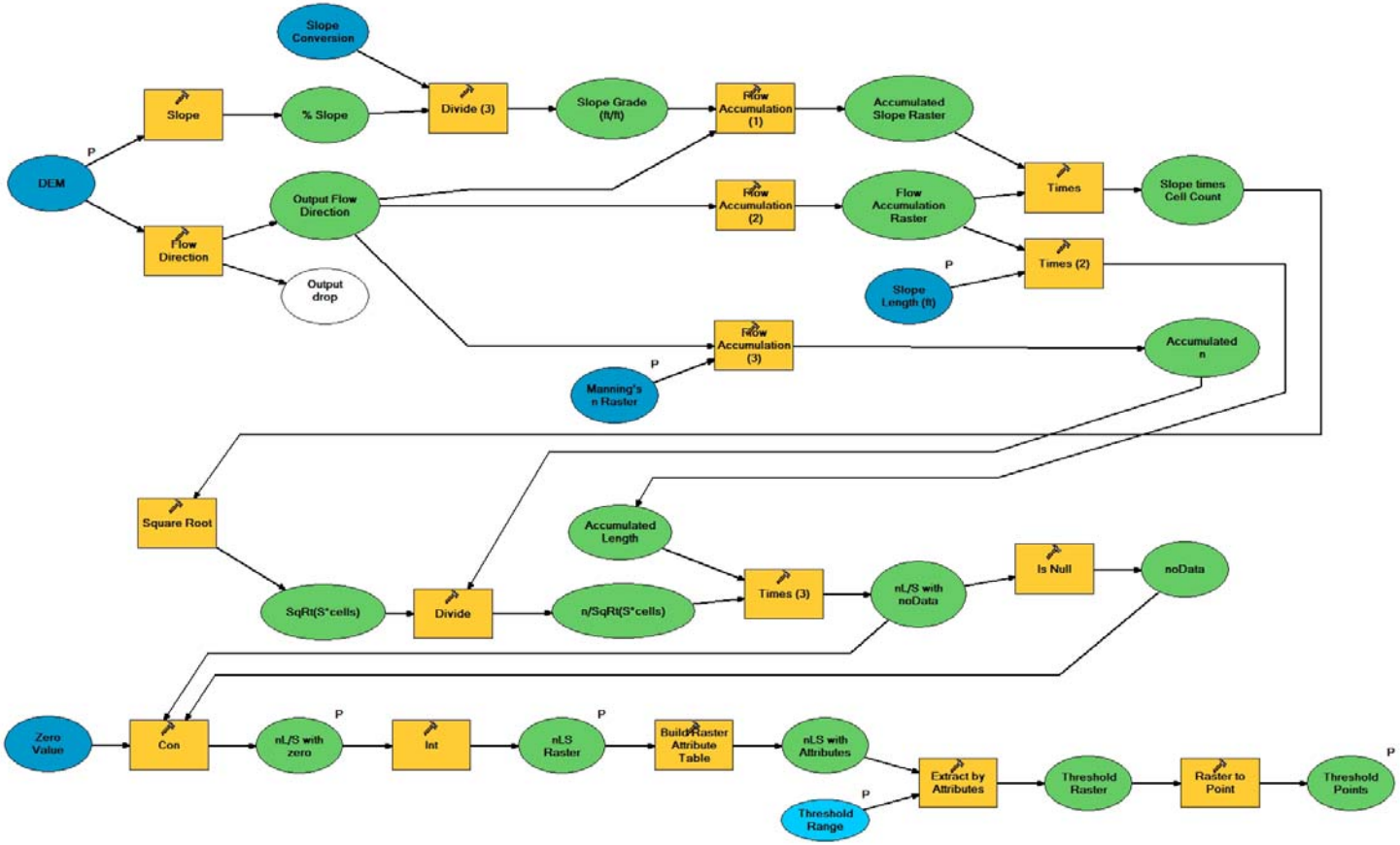

Appendix B - ArcGIS Tool Descriptions

A variety of tools were used within the GIS analyses of this study. A summary of these tools is given below (Table B.1). All information was taken from the ArcGIS Desktop 9.3 Help website (http://webhelp.esri.com/arcgisdesktop/9.3/).

Table B.1 Summary of GIS tools used within analyses

Slope Identifies the rate of maximum change in z-value from each cell. Slope is the rate of maximum change in z-value from each cell. The range of slope values in degrees is 0 to 90. For percent rise, the range is 0 for near infinity. A flat surface is 0 percent, a 45 degree surface is 100 percent, and as the surface becomes more vertical, the percent rise becomes increasingly larger. If the center cell in the immediate neighborhood (3 x 3 window) is NoData, the output is NoData. If any neighborhood cells are NoData, they are assigned the value of the center cell; then the slope is computed. The use of a z-factor is essential for correct slope calculations when the surface z units are expressed in units which are different from the ground x,y units. *Parameters*: input surface raster, output slope raster, measurement units (degree or percent rise), z-factor
Flow Direction Creates a raster of flow direction from each cell to its steepest downslope neighbor. The output of the Flow Direction tool is an integer raster whose values range from 1 to 255. If a cell is lower than its eight neighbors, that cell is given the value of its lowest neighbor, and flow is defined toward this cell. If multiple neighbors have the lowest value, the cell is still given this value, but flow is defined with one of the two methods explained below. This is used to filter out one-cell sinks, which are considered noise. If a cell has the same change in z-value in multiple directions and is not part of a sink, the flow direction is assigned with a lookup table defining the most likely direction. For adjacent cells, this is analogous to the percent slope between cells. Across a flat area, the distance becomes the distance to the nearest cell of lower elevation. The result is a map of percent rise in the path of steepest descent from each cell. When using the NORMAL option, a cell at the edge of the surface raster will flow toward the inner cell with the steepest drop in z-value. If the drop is less than or equal to zero, the cell will flow out of the surface raster. *Parameters*: input surface raster, output direction raster, flow at edge cells (normal or forced), optional output drop raster
Flow Accumulation Creates a raster of accumulated flow to each cell. The result of Flow Accumulation is a raster of accumulated flow to each cell, as determined by accumulating the weight for all cells that flow into each downslope cell. Cells of undefined flow direction will only receive flow; they will not contribute to any downstream flow. A cell is considered to have an undefined flow direction if its value in the input flow direction raster is anything other than 1, 2, 4, 8, 16, 32, 64, or 128. The accumulated flow is based on the number of cells flowing into each cell in the output raster. The current processing cell is not considered in this accumulation. Output cells with a high flow accumulation are areas of concentrated flow and can be used to identify stream channels. Output cells with a flow accumulation of zero are local topographic highs and can be used to identify ridges. If the input flow direction raster is not created with the Flow Direction command, there is a chance that the defined flow could loop. If the flow direction does loop, Flow Accumulation will go into an infinite loop and never finish. *Parameters*: input flow direction raster, output flow accumulation raster, optional input weight raster, output type (float or integer)

Table B.1 Summary of GIS tools (continued)

Reclass by Table Reclassifies or changes the values of the input cells of a raster using a remap table. The input raster must have valid statistics. The 'from value field', 'to value field', and 'output value field' are the field names in the table that define the remapping. The remap table can be an INFO table, a .dbf file, an Access table, or a text file. The values in the from and to fields can be any numerical item. The assignment values in the output field must be integers. Values in the from field for .dbf, INFO and Geodatabase tables do not need to be sorted. For text-file based tables, they must be sorted in ascending order. The values should not overlap in either case. The output raster will always be of integer type. *Parameters*: input raster, input reclassification table, table field holding beginning range value, table field holding ending range value, table field holding new value, output reclassified raster, missing value option (reclass as data or nodata)
Build Raster Attribute Table Adds a raster attribute table to a raster dataset or updates an existing one. If you want to delete an existing table and create a new one, check the Overwrite check box. A new raster attribute table will be created. If you have an existing table and you do not check the Overwrite check box, the table will be updated. No fields will be deleted, but the values in the table will be up-to-date. It is not possible to build a raster attribute table for a raster dataset that is a pixel type of 32-bit floating point. *Parameters*: input raster, overwrite option (none or overwrite existing attribute tables)
Extract by Attributes Extracts the cells of a raster based on a logical query. If the Where clause evaluates to true, the original input value is returned for the cell location. If the Where clause evaluates to false, the cell location is assigned NoData. If the input raster is integer, the output raster will be integer. If the input raster is floating point, the output raster will be floating point. If the input raster is floating point, the query must reference Value. Any extra items (other than Value and Count) of the input raster are dropped for the output raster. If an item other than Value of Input raster is specified in the Where clause, the original input value is returned for the cell location. *Parameters*: input raster, output point features, raster value field
Raster to Point Converts a raster dataset to point features. For each cell of the input raster dataset, a point will be created in the output feature class. The points will be positioned at the centers of cells that they represent. The NoData cells will not be transformed into points. The input raster can have any cell size and may be any valid raster dataset. The feature output is assumed to be a shapefile. The Field parameter allows you to choose which column in the raster dataset will become an attribute in the output point file. The column containing the cell values (VALUE) will become a column with the heading Grid_code in the attribute table of the output feature class. *Parameters*: input raster, overwrite option (none or overwrite existing attribute tables)
Square Root Calculates the square root of cells in a raster. Output values are always floating point, regardless of the input values. Input values must be greater than or equal to zero. If they are not, the output will be NoData. A number can be used as an input; however, the cell size and extent must first be set in the environment. *Parameters*: input raster, output raster
Divide Divides the values of two rasters on a cell-by-cell basis. The order of input is relevant for Divide. When a number is divided by zero, the output result is NoData. If both inputs are integers, Divide performs an integer division, and the output result is an integer. For example, if 3 is divided by 2, the output is 1. If either input is of floating-point type, Divide performs a floating-point division, and the result is a floating-point value. For example, if 3 is divided by 2.0, the output is 1.5. A number can be used as an input; however, the cell size and extent must first be set in the environment. *Parameters*: input numerator raster or constant, input denominator raster or constant, output raster

Table B.1 Summary of GIS tools (continued)

Times Multiplies the values of two rasters on a cell-by-cell basis. The order of input is irrelevant in the multiplication expression. If both inputs are integers, the output values will be integer; otherwise, the output values will be floating point. A number can be used as an input; however, the cell size and extent must first be set in the environment. *Parameters*: input first raster or constant, input second raster or constant, output raster
Float Converts each cell value of a raster into a floating-point representation. Input values are integers and can be positive or negative. If floating-point values are input, the output will be the same as the input. A number can be used as an input; however, the cell size and extent must first be set in the environment. *Parameters*: input raster, output floating-type raster
Int Converts each cell value of a raster to an integer by truncation. Integer rasters cannot have values larger than 2,147,483,647 (maximum size determined by 231 – 1), or smaller than -2,147,483,648 (minimum size determined by 231). If Int is used on a floating-point raster in which any value is outside this range, all of the cells in the resulting raster will be NoData. Input values should be floating point and can be either positive or negative. A constant (number) can be used as an input; however, the cell size and extent must first be set in the environment.Storing categorical (discrete) data as an integer raster will use significantly less disk space than the same information stored as a floating-point raster. Whenever possible, it is recommended to convert floating-point rasters to integer with the Int function. *Parameters*: input raster, output integer-type raster
Con Performs a conditional if/else evaluation on each of the input cells of an input raster. If either the true raster or optional false raster is floating point, the output raster will be floating point. If both the true expression and optional false raster are integer, the output raster will be integer. If the evaluation of the expression is nonzero, it is treated as True. If no input false raster or constant is specified, NoData will be assigned to those cells that do not result in True from the expression. If NoData does not satisfy the expression, it does not receive the value of the input false raster; it remains NoData. The maximum length of the expression is 4096 characters. *Parameters*: input conditional raster, input raster or constant for true test, input raster or constant for false test, output raster, selective SQL expression